



University of  
**Nottingham**

UK | CHINA | MALAYSIA

# Cosmological Consequences of Coupled Quintessence

Finlay H. Noble Chamings

Thesis submitted to the University of Nottingham  
for the degree of Doctor of Philosophy

September 2019

*I think perhaps the most important problem is that we are trying to understand the fundamental workings of the universe via a language devised for telling one another when the best fruit is.*

—Terry Pratchett

Chapter 3 of this thesis contains material from the following paper:

F. Noble Chamings, A. Avgoustidis, E. J. Copeland, A. M. Green, B. Li. ‘Early dark energy constraints on growing neutrino quintessence cosmologies’ *Physical Review*, vol. D100, p. 043525, 2019. DOI: 10.1103/PhysRevD.100.043525. arXiv: 1904.00884 [astro-ph.CO].

Chapter 4 contains material currently in preparation for publication.

**Supervisors:** Prof. Edmund J. Copland  
Prof. Anne M. Green  
Dr. Anastasios Avgoustidis

**Examiners:** Prof. Carsten van de Bruck (*University of Sheffield*)  
Dr. Adam Moss (*University of Nottingham*)

**Submitted:** 25 September 2019

**Examined:** 1 November 2019

**Final version:** 20 November 2019

This thesis is dedicated to Richard Paul Astley, to whose 1987 hit 'Never gonna give you up' I have listened literally thousands of times while working on my PhD (I have it on as I write these words as a matter of fact). I don't know how I could have done it without you, Rick.



# Abstract

Understanding the cause of the observed accelerating expansion of the universe is one of the most pressing problems in cosmology. To this end, I investigate two classes of dark energy models and their cosmological implications. These comprise growing neutrino quintessence, in which dark energy is coupled to the neutrinos, and models in which dark energy interacts with dark matter via a pure momentum coupling.

The standard model of cosmology,  $\Lambda$ CDM, is introduced, along with the issues it faces that motivate the study of alternatives. I also describe the various sources of cosmological data which provide the basis for stringent tests to be carried out on cosmological models. Following this I discuss a class of alternatives to  $\Lambda$ CDM known as dynamical dark energy, with a focus on quintessence and interacting dark energy.

Having discussed the necessary motivation and background, I proceed to present a study of growing neutrino quintessence cosmologies. Working at the level of the background equations of motion in the Einstein frame I carry out an analytic calculation finding important disagreement with previous results. Numerical evolution of the same equations yields constraints on growing neutrino quintessence cosmologies from the lack of observation of early dark energy in the Planck Collaboration analysis of cosmic microwave background data. I also perturb the equations of motion to linear order in a frame in which the strength of gravity and the particle masses depend on the dark energy field, with a view to gaining a more detailed understanding of the model behaviour.

The focus then turns to models in which dark energy interacts with dark matter via a pure momentum coupling. I review previous work which has found such models to be capable of easing tensions between early and late probes of structure formation and present an analytic argument as to why this behaviour occurs. I broaden the analysis by considering a range of coupling functions and potentials, finding that structure growth suppression is present for rather generic choices. In particular, a steeper potential can increase the suppression, without giving rise to an unrealistically small present-day expansion rate provided the coupling parameter is sufficiently large.

Both models prove promising in addressing some of the outstanding issues with our current understanding of cosmology, and the present analysis provides improved prospects for constraining or detecting these types of dark energy in future studies.

# Acknowledgements

First, and most importantly, I would like to thank my supervisors Ed, Anne, and Tasos. I could not have wished for more helpful, supportive or, for that matter, numerous supervisors. I very much appreciate the time and effort you have all spent on this, your patience, your expertise, and your support. Thank you all very much. I am very grateful to Baojiu Li, whose help modifying CAMB was invaluable, and to Alkistis Pourtsidou, without whose kind advice the work in Chapter 4 would have been a non-starter. In particular, thank you both for letting me use your modified versions of the codes.

Thanks also go to my other colleagues, who have helped with this thesis in ways ranging from answering my stupid questions about cosmology, to listening to me complain about whatever particular problem I'm currently stuck on. In particular, thanks to Tom, whom I have bombarded with more questions than anybody (and, incidentally, who has been the best house-mate I could have wished for), and to Daniela, who has repeatedly gone above and beyond in welcoming my questions, and providing more comprehensive and comprehensible explanations than I would have imagined possible.

I would like to thank the many people who have helped me in a non-academic way during my time here, but I'm afraid you are too many to name. Thank you to my office-mates, to the CAPT occupants more generally, to the Wednesday climbers, to the former residents of Cloister House, to the Movie Night attendees, to the jugglers, to the non-Nottingham people who have caused me to continue funding the Great British rail network, to the band, to the second band, to the wing chun society. I know I said I wouldn't name people, but I must single out both Jake and Charutha, my office comrades for the duration of our PhDs<sup>1</sup>. You have improved my life in so many ways.

I also want to thank my parents, without whom I would not have been able to do this (nor anything else, for that matter). In particular, I am eternally grateful to Mum for bribing me with actual money to learn to touch type when I was a child. This thesis contains 340 minutes-worth of words at my current rate of typing, and while admittedly it took me rather longer than 340 minutes to write, I'm sure it would have been a true misery to type by 'hunt and peck'. On the subject of family, thanks also to Callum, for generally being great.

Finally, I would like to thank the universities of Cambridge, Edinburgh, Lancaster, Durham, Liverpool, Sheffield, Glasgow, and Manchester for rejecting my PhD applications. I've had a great time in Nottingham and I wouldn't change a thing.

---

<sup>1</sup>with the exception of right at the end of mine, since you both had the effontery to complete your PhDs rather more promptly than I was able to...

# Conventions

In this thesis I adopt the following conventions unless stated otherwise. The space-time metric has a ‘mostly plus’ signature,  $(-+++)$ . Greek indices run from 0 to 3, with the 0th index corresponding to time and the other three corresponding to space; Latin indices run from 1 to 3. I work in natural units in which  $c = \hbar = 1$ . All logarithms in this thesis are natural logarithms and are denoted by ‘log’.

When discussing Friedmann–Lemaître–Robertson–Walker space-times I assume zero spatial curvature. The scale factor is normalised such that  $a = 1$  at the present epoch. Barred quantities, for example  $\bar{\chi}$ , refer to spatial averages;  $\bar{\chi}$  is homogeneous and depends only on time. Occasionally I use bars for other purposes; in those cases I will make this clear.

I employ various notations for differentiation. Partial differentiation of a variable  $\phi$  with respect to the space-time co-ordinate  $x^\mu$  is denoted by  $\partial_\mu\phi \equiv \partial\phi/\partial x^\mu$ . Covariant derivatives are denoted by  $\nabla_\mu$ . In Chapter 3 I use subscript comma notation to refer to partial differentiation with respect to spatial co-ordinates by, for example,  $\Psi_{,i} \equiv \partial\Psi/\partial x^i$ . In all other instances of subscript comma notation the symbol in the subscript is the variable being differentiated with respect to, for example  $V_{,\phi} \equiv dV/d\phi$  for a function  $V(\phi)$ . Differentiation of a dynamical quantity with respect to physical time is denoted by subscript comma notation as above. Differentiation with respect to conformal time,  $\tau$ , is denoted by a dot as follows:  $\dot{\phi} \equiv d\phi/d\tau$ . Differentiation with respect to the natural logarithm of the scale factor,  $N \equiv \log(a)$ , is denoted by a prime as follows:  $\phi' \equiv d\phi/dN$ .

Where there exist multiple correct forms of the pluralisation of a noun, I choose to adopt the form closest to the common conventions in the English language, as opposed to the plural inherited from the language from which the noun was borrowed, even if the latter is the more common choice in scientific writing. For example, while ‘supernovas’ and ‘supernovae’ are both found in the dictionary, I shall favour the English-style ‘supernovas’ at the expense of the Latin-inspired ‘supernovae’.

# Abbreviations

<b>CDM</b>	Cold dark matter
<b>CMB</b>	Cosmic microwave background
<b>GNQ</b>	Growing neutrino quintessence
<b>MACHO</b>	Massive compact halo object
<b>MCMC</b>	Markov chain Monte Carlo
<b>PBH</b>	Primordial black hole
<b>SZ</b>	Sunyaev–Zel’dovich
<b>TRGB</b>	Tip of the red-giant branch
<b>WIMP</b>	Weakly interacting massive particle

# List of Figures

1.1	CMB power spectrum . . . . .	12
1.2	2dF Galaxy Redshift Survey . . . . .	15
1.3	Evolution of cosmological fluids . . . . .	18
1.4	Early- and late-universe measurements of the Hubble constant . . . . .	21
3.1	GNQ $\phi$ evolution . . . . .	60
3.2	GNQ $w_\phi$ evolution . . . . .	61
3.3	GNQ $\Omega_\phi$ evolution . . . . .	61
3.4	Early dark energy constraint on $\kappa$ . . . . .	62
3.5	Comparison between constant and varying $k^2(\phi)$ . . . . .	64
3.6	GNQ $\phi$ evolution for inverse power-law potential . . . . .	65
3.7	GNQ $\Omega_\phi$ evolution for inverse power-law potential . . . . .	66
3.8	Ratio $\Omega_\phi/\Omega_\nu$ relationship to coupling . . . . .	67
4.1	Structure growth suppression for Type 3 coupling with $n = 0$ . . . . .	86
4.2	Scaling of $\dot{\phi}$ with $\beta_0$ . . . . .	87
4.3	CDM velocity divergence dependence on $\beta_0$ . . . . .	89
4.4	Scalar field perturbation dependence on $\beta_0$ . . . . .	90
4.5	Scalar field energy density evolution for Type 3 coupling with $n = 0$ . . . . .	92
4.6	CDM density contrast terms evolution for Type 3 coupling with $n = 0$ . . . . .	95
4.7	Matter power spectrum for Type 3 coupling with $n = 0$ . . . . .	96
4.8	$\dot{\phi}$ evolution for various Type 3 couplings . . . . .	100
4.9	Scalar field perturbation dependence on $\beta_{n-2}$ . . . . .	102
4.10	CDM velocity divergence dependence on $\beta_{n-2}$ . . . . .	103
4.11	Matter power spectrum for various Type 3 couplings . . . . .	104
4.12	Structure growth suppression for various Type 3 couplings . . . . .	105
4.13	Structure growth suppression for different slopes of the scalar field potential . . . . .	108
4.14	Hubble constant for different slopes of the scalar field potential . . . . .	109

## LIST OF FIGURES

---

4.15	Scalar field energy density evolution for different Type 3 couplings and potentials . . . . .	110
4.16	CDM velocity divergence evolution for different slopes of the scalar field potential . . . . .	111
4.17	Evolution of $\dot{\phi}$ for double exponential potentials with and without a Type 3 coupling . . . . .	113

# Contents

<b>1</b>	<b>Introduction</b>	<b>1</b>
1.1	Einstein field equations . . . . .	2
1.1.1	Cosmological constant . . . . .	3
1.2	Cosmological solutions . . . . .	4
1.3	Energy content of the universe . . . . .	5
1.4	The expanding universe . . . . .	7
1.5	Cold dark matter . . . . .	9
1.6	Precision cosmology . . . . .	11
1.6.1	Cosmic microwave background . . . . .	11
1.6.2	Cosmic inflation . . . . .	12
1.6.3	Large-scale structure . . . . .	14
1.6.4	Numerical simulations . . . . .	16
1.7	Problems with $\Lambda$ CDM . . . . .	16
1.7.1	Theoretical problems . . . . .	16
1.7.2	Observational problems . . . . .	20
1.8	Beyond $\Lambda$ CDM . . . . .	23
<b>2</b>	<b>Dynamical dark energy</b>	<b>25</b>
2.1	Introduction . . . . .	25
2.2	Quintessence . . . . .	26
2.3	Interacting dark energy . . . . .	29
2.4	Growing neutrino quintessence . . . . .	33
2.5	Summary . . . . .	38
<b>3</b>	<b>Growing neutrino quintessence</b>	<b>40</b>
3.1	Introduction . . . . .	40
3.2	Equations of motion . . . . .	42
3.2.1	Conformal frames . . . . .	44
3.3	Approximate analytic solutions . . . . .	48
3.3.1	Exponential potential . . . . .	48

3.3.2	Inverse power-law potential . . . . .	55
3.4	Numerical background evolution . . . . .	58
3.4.1	Exponential potential . . . . .	59
3.4.2	Inverse power-law potential . . . . .	63
3.4.3	Coupling function . . . . .	65
3.5	Perturbative analysis . . . . .	66
3.6	Discussion . . . . .	71
<b>4</b>	<b>Type 3 interacting dark energy</b>	<b>74</b>
4.1	Introduction . . . . .	74
4.2	Cosmic Linear Anisotropy Solving System . . . . .	77
4.2.1	Equations of motion . . . . .	78
4.2.2	Boltzmann equation . . . . .	80
4.2.3	Implementation in CLASS . . . . .	82
4.2.4	Type 3 modification . . . . .	83
4.3	Semi-analytic explanation of structure growth suppression . . . . .	85
4.3.1	Effect of the coupling on the background evolution of the scalar field . . . . .	86
4.3.2	Effect of the coupling on the CDM velocity divergence . . . . .	88
4.3.3	Effect of the coupling on the CDM density contrast . . . . .	90
4.3.4	Effect of the coupling on the matter power spectrum . . . . .	95
4.4	Generalisation of the coupling . . . . .	97
4.4.1	Effect of the coupling on the scalar field evolution . . . . .	98
4.4.2	Effect of the coupling on the metric perturbation . . . . .	100
4.4.3	Effect of the coupling on the CDM velocity divergence . . . . .	100
4.4.4	Summary . . . . .	104
4.5	The role of the scalar field potential . . . . .	105
4.5.1	Field redefinition relating potential and coupling . . . . .	106
4.5.2	Effect of changing the slope of a single exponential potential . . . . .	107
4.5.3	Double exponential potentials . . . . .	111
4.6	Discussion . . . . .	112
<b>5</b>	<b>Conclusions</b>	<b>117</b>

# Chapter 1

## Introduction

Questions regarding the origin and development of the universe in which we find ourselves have intrigued, fascinated, and frustrated humanity for longer than anybody has been keeping track. The past century, and especially the past few decades, have seen this ancient subject mature into a rigorous scientific discipline that now provides us with the tools to build a robust, quantitative understanding of the cosmos. At the centre of this understanding is the theory of gravity, by far the weakest of the four fundamental forces, but nevertheless the one which dominates the behaviour of the universe on large scales due to its infinite range and the fact that, unlike electromagnetism, contributions to gravity can only accumulate and never cancel out. For the past century the leading theory of gravity has been Einstein's general theory of relativity. I introduce this theory in Section 1.1 and discuss how it can be applied to the universe as a whole in Section 1.2.

General relativity describes the way in which matter (and other sources of energy and momentum) affects the curvature of space-time and in turn how the curvature of space-time affects the motion of matter. In cosmology, the various contributions to the universe's energy density dilute in different ways as the universe expands while also driving that expansion through their gravitational effects. I introduce the basic idea behind this relationship in Section 1.3 and discuss the history of the universe's expansion in Section 1.4.

Excitingly, it has been convincingly demonstrated that the various kinds of matter contained in the Standard Model of particle physics are not able to explain the details of the universe's evolution which we are now able to observe. Indeed, such matter constitutes only 5% of the total energy density of the universe. 25% is believed to be an exotic form of matter called cold dark matter, which I introduce in Section 1.5. The remaining 70% is called dark energy and is even less well understood than dark matter. Dark energy is most commonly described by a cosmological constant, introduced in Section 1.1.1, but it can also be described by a dynamical

field which evolves as the universe expands and is able to vary in space. This latter approach will be discussed in some detail in Chapter 2 and is the subject of the research that has gone into Chapters 3 and 4.

The incredible discoveries that have been made in the field of cosmology would not have been possible without large amounts of high-quality cosmological data and sophisticated computational and statistical methods for the analysis of that data. Two of the most important sources of cosmological data are the background radiation left over from the hot, dense early universe, and the distribution of galaxies, galaxy clusters, and even larger structures that form in the late universe. These features, and approaches to measure and interpret them, are discussed in Section 1.6. In that section I also introduce inflation, the process believed to have provided the seeds that grew into the cosmological features that attract such careful study.

Despite this remarkable recent progress, the standard model of cosmology retains several important question marks. The most obvious of these is perhaps that we do not have a full understanding of what the dark sector of the universe is even made of, but the subtler problems are no less worrying. In Section 1.7 I discuss theoretical difficulties in explaining the small size of the cosmological constant, the apparently improbable coincidence of the very similar densities of matter and dark energy in the present epoch, the as-yet unsuccessful search for dark matter, and disagreements between early- and late-universe measurements when  $\Lambda$ CDM is assumed. The various problems with the current paradigm motivate the study of alternatives; these are mentioned briefly in Section 1.8. I end this chapter with an outline for the rest of the thesis.

## 1.1 Einstein field equations

Gravitational interactions are central to any attempt to understand the evolution of the universe and its contents, so we will begin our discussion of the standard model of cosmology by introducing the theory of gravity upon which it is built. In Einstein's general theory of relativity [1], the gravitational force results from the motion of particles along the geodesics of curved space-time. This curved space-time is represented by a metric  $g_{\mu\nu}$  whose dynamics are described by the Einstein field

equations<sup>2</sup>:

$$R_{\mu\nu} + \frac{1}{2}Rg_{\mu\nu} = \frac{1}{M_{\text{P}}^2}T_{\mu\nu}, \quad (1.1)$$

where  $R_{\mu\nu}$  and  $R$  are the Ricci tensor and scalar respectively (built from the metric tensor and its derivatives) and  $T_{\mu\nu}$  is the energy–momentum tensor, which contains information on the matter content of the space-time under consideration.  $M_{\text{P}}$  is the reduced Planck mass:  $M_{\text{P}} = (8\pi G)^{-1/2}$ , where  $G$  is the gravitational constant. The combination  $R_{\mu\nu} + (1/2)Rg_{\mu\nu}$  is known as the Einstein tensor.

The divergence of the Einstein tensor is equal to zero by geometric identities called the Bianchi identities. This immediately means that  $\nabla_{\mu}T_{\nu}^{\mu} = 0$ , which corresponds to conservation of energy and momentum.

General relativity can also be defined at the level of the action. The Einstein–Hilbert action is given by:

$$S = \int d^4x \sqrt{-g} \left( \frac{M_{\text{P}}^2}{2} R + \mathcal{L}_{\text{m}} \right), \quad (1.2)$$

where  $\mathcal{L}_{\text{m}}$  contains the non-gravitational part of the action. Varying Eq. (1.2) with respect to the metric  $g_{\mu\nu}$  yields Eq. (1.1), where

$$T_{\mu\nu} \equiv \frac{-2}{\sqrt{-g}} \frac{\delta \sqrt{-g} \mathcal{L}_{\text{m}}}{\delta g^{\mu\nu}}. \quad (1.3)$$

### 1.1.1 Cosmological constant

The simplest modification one can make to Eq. (1.1) is to introduce a constant term proportional to the metric tensor  $g_{\mu\nu}$ . This modification, known as a cosmological constant, maintains the symmetries of the equations, which I have not discussed here, but are discussed in detail in Ref. [2]. Einstein introduced a term  $\Lambda g_{\mu\nu}$  to the Einstein tensor, with the goal of creating static cosmological solutions. It is now known that the universe is not static but is expanding, so the cosmological constant was removed again, with Einstein reportedly calling it his greatest mistake. However, as will be discussed in Section 1.4, the universe’s expansion is accelerating, which motivates the reintroduction of a cosmological constant. Rather than thinking of it

---

<sup>2</sup>The material in this and the two following sections can be found in any introductory textbook or lecture course on general relativity and cosmology. In particular, the reader is referred to Section 8 of Ref. [2].

as a modification to the Einstein tensor, the cosmological constant is often considered a term in the energy–momentum tensor, where it plays the role of the energy density of the vacuum, a source of energy even in the absence of matter and radiation.

## 1.2 Cosmological solutions

There are three broad methods by which the Einstein field equations can be solved. These are: the assumption of a highly symmetric system such that an exact analytic solution may be found (see Ref. [3] for a detailed treatment); perturbation theory, in which an exact solution is expanded upon by deviations that are assumed to be small (see, for example, Ref. [4] for a review); and by employing numerical methods, where analytic solutions cannot be obtained, normally involving resource-intensive computational tools (see Ref. [5] for a review). For cosmological solutions we start with the first of these methods, employing the so-called cosmological principle. The cosmological principle states that the universe is homogeneous and isotropic when viewed on very large scales<sup>3</sup>. The Friedmann–Lemaître–Robertson–Walker metric is an exact solution to the Einstein field equations that satisfies the cosmological principle. The most general form of this metric is given by:

$$ds^2 = g_{\mu\nu}dx^\mu dx^\nu = -dt^2 + a(t)^2 d\Sigma^2, \quad (1.4)$$

where  $x^\mu$  are the four space-time co-ordinates,  $\Sigma$  are the co-ordinates of a three-dimensional space of uniform curvature and  $a(t)$  is the scale factor, in which all the space-time dependence of the metric is contained. The scale factor describes the size of the universe, normalised such that  $a = 1$  in the present epoch. The space described by  $\Sigma$  can have positive, negative or zero curvature. This is sometimes parametrised in the following way:

$$d\Sigma^2 = \frac{dr^2}{1 - kr^2} + r^2(d\theta^2 + \sin^2\theta d\phi^2), \quad (1.5)$$

where  $r$ ,  $\theta$ , and  $\phi$  are spherical polar co-ordinates and  $k$  is the curvature constant, which parametrises the spatial geometry. Recent observations find the universe is very close to being spatially flat [6], so hereafter I shall make this assumption and

---

<sup>3</sup>The extent to which this is a valid approximation for the universe in which we live is discussed in Section 1.6.

set  $k = 0$ .

The evolution of the scale factor can be found by solving the Einstein field equations where we assume that the energy–momentum tensor consists of a homogeneous, isotropic perfect fluid with a known equation of state, given by

$$T_{\mu}^{\nu} = \begin{pmatrix} -\rho(t) & 0 & 0 & 0 \\ 0 & p(t) & 0 & 0 \\ 0 & 0 & p(t) & 0 \\ 0 & 0 & 0 & p(t) \end{pmatrix}, \quad (1.6)$$

where  $\rho$  is the density of the fluid and  $p$  is its pressure. The equation of state is defined by  $w \equiv p/\rho$ . With the metric tensor given by Eq. (1.4) and the energy–momentum tensor given by Eq. (1.6), one can show that the Einstein field equations simplify to the Friedmann equations, given by:

$$H^2 = \frac{\rho}{3M_{\text{P}}^2}, \quad (1.7)$$

and

$$H_{,t}^2 = -\frac{1}{2M_{\text{P}}^2}(\rho + p), \quad (1.8)$$

where  $H \equiv a_{,t}/a$  is the Hubble parameter and subscript comma notation denotes differentiation. There is a third equation that it is convenient to introduce here, which is the continuity equation:

$$\rho_{,t} + 3H(\rho + p) = 0, \quad (1.9)$$

which is simply  $\nabla^{\mu}T_{\mu\nu} = 0$  for the case of a homogeneous, isotropic perfect fluid. Note that only two of Eqs. (1.7) to (1.9) are independent. It is often convenient to choose to work with Eqs. (1.7) and (1.9) as they contain only first derivatives with respect to time.

### 1.3 Energy content of the universe

The universe can be modeled as consisting of three different types of fluid: matter, radiation, and dark energy. For the purposes of this thesis, matter is any fluid with

an equation of state of  $w_m = 0$ , radiation is any fluid with  $w_r = 1/3$ , and dark energy is any fluid with  $w_{\text{DE}} < -1/3$ . For now we will restrict ourselves to  $w_{\text{DE}} = -1$ , which is the equation of state of a cosmological constant as introduced in Section 1.1.1. Physically, a fluid consisting of massive particles moving at speeds much less than the speed of light, such that  $\langle v^2 \rangle \ll 1$ , will have  $w \approx 0$ , and a fluid consisting of massless particles (which necessarily move at the speed of light) is described by  $w = 1/3$ . Such species are often called non-relativistic and relativistic respectively. Various physical mechanisms for obtaining a negative equation of state are discussed in Chapter 2. For a given equation of state, Eq. (1.9) can be used to find the evolution of the energy density as a function of the scale factor:

$$\rho_m(a) = \rho_{m0}a^{-3}, \quad (1.10)$$

$$\rho_r(a) = \rho_{r0}a^{-4}, \quad (1.11)$$

and

$$\rho_{\text{DE}}(a) = \rho_{\text{DE}0}, \quad (1.12)$$

where the subscript 0 denotes the present epoch. The above relations imply that these three species evolve at different rates as the universe expands, and hence different cosmological epochs will be characterised by the domination of different species. In particular, for appropriate values of  $\rho_{m0}$ ,  $\rho_{r0}$ , and  $\rho_{\text{DE}0}$ , an expanding universe undergoes first a period of radiation domination, followed by a period of matter domination since  $\rho_r$  falls more quickly than  $\rho_m$ , and finally a period of dark energy domination as  $\rho_m$  and  $\rho_r$  both fall below  $\rho_{\text{DE}}$ . As discussed later, our own universe's history follows such a progression.

Not only do the energy densities of the contents of the universe depend on the expansion, but the rate of expansion also depends on the contents, as given by Eq. (1.7). For a universe that contains only one of the three fluids considered above, Eq. (1.7) can be exactly solved. One obtains  $a(t) \propto t^{1/2}$ ,  $a(t) \propto t^{2/3}$  and  $a(t) \propto \exp(H_0 t)$  for a universe containing only radiation, matter or dark energy respectively.  $H_0$  is the present-day value of the Hubble parameter and is known as the Hubble constant. These expressions can also serve as approximate solutions for a universe which contains all three species but is temporarily dominated by only one.

A convenient quantity when discussing the energy content of the universe is the critical density, which is defined by

$$\rho_{\text{crit}} = 3M_{\text{p}}^2 H^2. \quad (1.13)$$

A spatially flat universe has a total energy density equal to the critical density. We can now introduce the density parameters  $\Omega_i$ , defined by

$$\Omega_i = \frac{\rho_i}{\rho_{\text{crit}}}, \quad (1.14)$$

for each species  $i$ . For a spatially flat universe,  $\Omega_i$  is the fraction of the universe's energy density accounted for by species  $i$ . For a flat universe containing matter, radiation, and dark energy, the Friedmann equation, Eq. (1.7), becomes

$$1 = \Omega_{\text{m}}(a) + \Omega_{\text{r}}(a) + \Omega_{\text{DE}}(a). \quad (1.15)$$

## 1.4 The expanding universe

The fact that the universe is expanding has been known for around a century. In the 1910s, Vesto Slipher published work showing that the spectrums of distant galaxies were redshifted, implying that they are receding from us [7, 8]. In the 1920s, Alexander Friedmann and Georges Lemaître independently provided a theoretical understanding of the expansion of the universe by means of solving the Einstein field equations [9, 10]. In 1929, Edwin Hubble confirmed the expansion, and demonstrated that the velocity inferred from the redshift of the galaxies was proportional to their distance from us, inferred from the observed luminosity of ‘standard candles’ such as supernovas and Cepheid variables [11]. This is known as ‘Hubble’s Law’ and it can be expressed as  $v = H_0 r$ , where  $v$  and  $r$  are the relative velocity and separation of a pair of galaxies, and the constant of proportionality  $H_0$  is the Hubble constant introduced earlier. Since Edwin Hubble’s rough measurement of the Hubble constant, efforts have been ongoing to measure the expansion rate of the universe as accurately as possible. This is a particularly interesting question because different methods of inferring  $H_0$  give results that are in tension with one another. I review the various approaches and the values of  $H_0$  they give in Section 1.7.2.

As well as measuring the present-day rate of expansion, it is of interest to cosmologists to understand the expansion history. As mentioned in Section 1.3, the expansion history can help us understand what the universe is composed of. In 1998 it was convincingly demonstrated that the expansion of the universe is accelerating [12, 13], a discovery that won Adam Riess, Brian Schmidt, and Saul Perlmutter the Nobel Prize in physics in 2011. Such acceleration is not possible in a matter- or radiation-dominated universe, but it can occur in a universe dominated by a fluid with equation of state  $w < -1/3$ , such as dark energy. If the dark energy is assumed to take the form of a cosmological constant then the density parameters of matter and dark energy can be inferred as  $\Omega_{m0} = 0.315 \pm 0.007$  [6] and  $\Omega_{\Lambda0} \approx 1 - \Omega_{m0}$ . (The contribution to the overall energy density from radiation is very small,  $\mathcal{O}(10^{-4})$ , in the present epoch.)

As the universe expands, its temperature drops, meaning that the universe in the past was hotter and denser than it is today. The very early part of the universe's evolution is known as the 'hot big bang'. As the universe expands and cools, its changing temperature gives rise to various different physical processes. An important transition occurred at a temperature of around 3000 K, before which the universe was opaque to photons due to a very high Thompson scattering rate with free electrons. Once the temperature was sufficiently low as to allow the formation of neutral hydrogen (a process known as recombination), the number of free electrons and hence the Thompson scattering rate dropped rapidly, causing the photons to decouple from the baryonic matter<sup>4</sup> and pass freely through the universe. This gives rise to the cosmic microwave background radiation, which is discussed in Section 1.6. Earlier still, big bang nucleosynthesis took place at a temperature of around  $10^9$  K, in which light nuclei such as deuterium and helium were able to form and remain stable. Continuing further back in time before nucleosynthesis, early universe processes included electron-positron annihilation, neutrino decoupling, the quantum chromodynamics phase transition, the electroweak phase transition, and baryogenesis, believed to be responsible for the preponderance of matter over antimatter in the universe. See Ref. [14] for a thorough treatment of the above.

The physics of the very early universe takes place at sufficiently high energies that our theories of particle physics may need to be modified. An energy scale of particular

---

<sup>4</sup>I follow the standard convention in cosmology and astronomy of implicitly including leptons when I refer to 'baryonic matter'.

interest is the Planck scale,  $M_{\text{P}}$ , beyond which the quantum effects of gravity are expected to dominate. A full understanding of the physics of the beginning of the universe will require a quantum theory of gravity, the search for which is a major unsolved problem in theoretical physics. See Ref. [15] for a pedagogical review of the search for a quantum theory of gravity and Ref. [16] for a more technical discussion.

## 1.5 Cold dark matter

There is now a great deal of evidence that the majority of matter in the universe is dark, in the sense of not emitting electromagnetic radiation. So far, dark matter has only been observed via its gravitational interactions, its interactions with the more familiar Standard Model matter being either very weak or non-existent. A brief discussion of the search for a dark matter candidate is found in Section 1.7.1; in the present section I do not discuss the fundamental nature of dark matter and focus instead on the role it plays in cosmology.

Some of the earliest strong evidence for the existence of dark matter came from the measurement of the rotation of galaxies, pioneered by Vera Rubin, Kent Ford, and Ken Freeman in the 1960s and 1970s [17, 18]. The radial velocities of galaxies that are oriented edge-on to us can be measured spectroscopically by measuring the Doppler shifting of absorption and emission spectrums of stars and interstellar gas. If the mass of a galaxy were concentrated near its centre, as the luminous matter appears to be, then Kepler's laws predict that the velocity of objects near the outer edge of the galaxy should decrease with the radius as  $v(r) \sim r^{-1/2}$ . Contrary to this prediction, galactic rotation curves of  $v(r)$  consistently show a substantially higher orbital speed for large  $r$ . See Ref. [19] for a review of measurements of galaxy rotation curves. If Newton's laws of gravity are correct, the shape of the rotation curves implies that galaxies are enveloped in halos of dark matter that are much larger and more massive than the galaxies themselves.

Dark matter can also be observed on larger scales by studying galaxy clusters, which are gravitationally bound structures containing hundreds to thousands of galaxies. Efforts in this direction date back to Fritz Zwicky, who in 1933 found that application of the virial theorem to the Coma cluster predicted about 400 times the mass that could be seen as luminous matter [20]. More recently, gravitational

lensing has been employed to measure and map the distribution of the mass of galaxy clusters. As discussed in Section 1.1, general relativity predicts that the presence of matter curves space-time. Light follows geodesics of the curved space-time and so takes a curved path when passing by regions containing a large amount of matter. By analysing the way in which images of galaxies behind a cluster are distorted, researchers are able to calculate the total mass present in the cluster [21–24]. As well as telling us that the total mass in clusters is greater than the luminosity would suggest, gravitational lensing can be used to identify places where the dark matter and the baryonic matter have been separated due to interactions between clusters, as in the case of the ‘Bullet Cluster’ [25], thus providing very strong evidence of the presence of a large amount of non-baryonic matter.

There are many other sources of evidence for dark matter, some of the most convincing coming from analysis of the cosmic microwave background and the large-scale structure of the universe, which are introduced in the next section. Measurements carried out on a wide range of scales and employing many independent techniques, consistently indicate that around 85% of the matter in the universe is non-baryonic in nature.

The model of dark matter strongly favoured by the data is so-called ‘cold dark matter’ (CDM), which was originally published in 1982 by three independent groups [26–28] and further developed in Ref. [29]. Cold dark matter has an equation of state  $w_c = 0$  while so-called ‘warm’ and ‘hot’ dark matter have  $w > 0$ . Hot dark matter was the first to be proposed historically, since it can be very naturally described by neutrinos which were already known to exist and not interact with electromagnetism. However, cosmological N-body simulations demonstrate that hot dark matter does not give rise to sufficient structure formation on small scales to be consistent with observations [30], while cold dark matter does [31, 32]. Warm dark matter has not been ruled out but is becoming increasingly tightly constrained [33, 34].

Because the two largest contributions to the cosmic energy density are believed to be the cosmological constant and cold dark matter, the name  $\Lambda$ CDM is given to the standard cosmological model. Modern cosmology can test this model, and deviations from it, very rigorously, as described in the next section.

## 1.6 Precision cosmology

The assumptions of homogeneity and isotropy made in Section 1.2, can only take one so far in understanding the universe. Even on large scales there are small inhomogeneities and anisotropies that can be measured, and on very small scales these can be very large such that the assumptions of homogeneity and isotropy completely break down. On all but very small scales, however, the deviations from the background average are small compared to the magnitude of the background itself and one can employ perturbation theory as mentioned in Section 1.2. Understanding the growth of these perturbations, and hence the growth of structure in the universe, is one of the most important issues for cosmology to address.

### 1.6.1 Cosmic microwave background

The cosmic microwave background (CMB) (see Ref. [35] for a recent review), discovered in 1965 by Penzias and Wilson [36, 37], is a nearly isotropic blackbody spectrum of electromagnetic radiation with a temperature of 2.725 K and was the first major piece of evidence in support of the hot big bang theory described in Section 1.4. It is believed to consist of radiation emitted during recombination; when the universe was 380,000 years old it cooled sufficiently that protons and electrons ceased to be an opaque plasma and formed atoms through which electromagnetic radiation could pass. This produced a ‘surface of last scattering’ still observable today. The fluctuations in the temperature of the CMB are only  $\mathcal{O}(10^{-5})$  of the background temperature, but they contain a great deal of information about the evolution of the early universe.

The temperature peaks in the CMB power spectrum as shown in Fig. 1.1 result from acoustic oscillations of the tightly coupled baryon–photon fluid prior to photon decoupling. The odd and even peaks correspond to modes which were under either compression or rarefaction respectively when decoupling occurred, while the troughs correspond to the intermediate parts of the oscillation. The presence of dark matter brings about an enhancement of compression but not of rarefaction, resulting in the odd-numbered peaks being increased relative to the even-numbered peaks. The oscillations are damped at small scales due to photon diffusion, giving rise to the decaying tail seen at high  $l$ . There are many smaller contributions to the CMB power spectrum

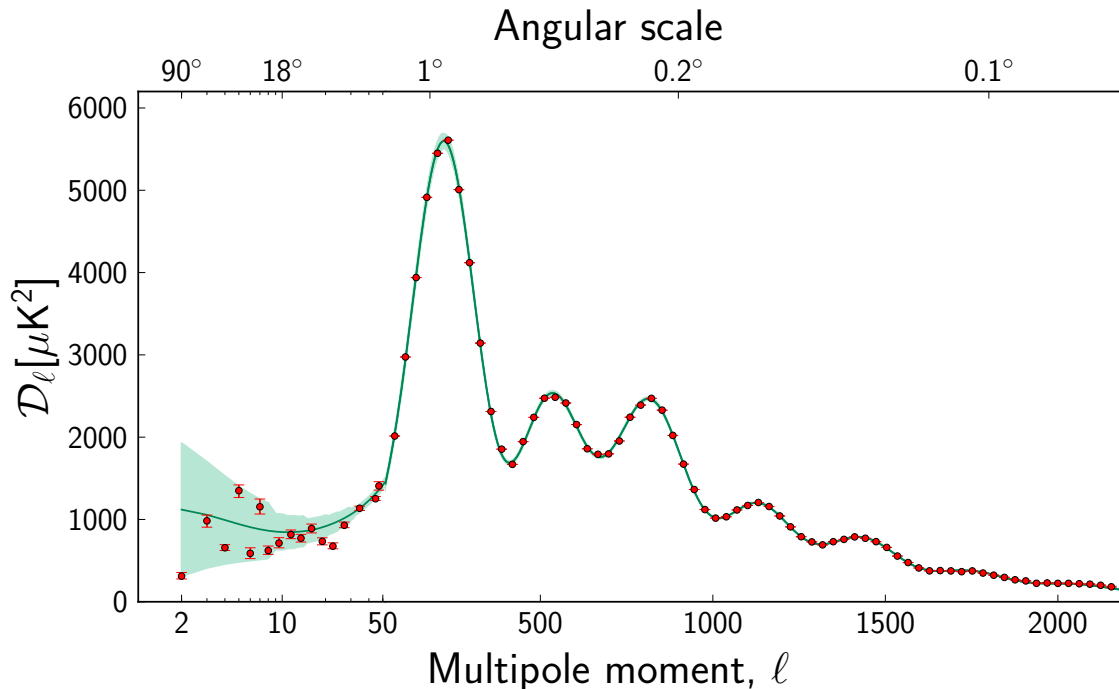


Figure 1.1: Power spectrum of temperature fluctuations of the cosmic microwave background. The green curve corresponds to the best-fit prediction of  $\Lambda$ CDM and the red points represent the results of measurements made by Planck. The broad green region at low multipole moment is due to cosmic variance, while the error bars on the red points include only measurement error and do not take account of cosmic variance. Image reproduced from Ref. [38].

including gravitational lensing of CMB photons as they pass through potential wells between the surface of last scattering and the point of observation, and Doppler shifting due to relative motions of different parts of the pre-recombination baryon–photon fluid. There are also spectral distortions such as the Sunyaev–Zel’dovich (SZ) effect, caused by low-energy CMB photons gaining energy by inverse Compton scattering with high-energy cluster electrons [39]. Making precise measurements of the CMB can thus reveal a great deal of information about cosmological parameters, making it a vitally important area of research.

### 1.6.2 Cosmic inflation

The observed structure of the CMB raises various issues for the hot big bang model. Perhaps the most important of these is the origin of the fluctuations that gave rise to the temperature anisotropies in the CMB. Other issues include the ‘horizon problem’

and the ‘flatness problem’, which concern why parts of the universe that do not seem to have been in causal contact have such similar temperatures, and why the universe is so close to being spatially flat. The inflationary paradigm addresses all of these questions as well as the ‘monopole problem’ of why the universe does not contain an abundance of monopoles, expected to be produced by phase transitions in the early universe. Inflation, first proposed by Alan Guth and Alexei Starobinsky in 1980 [40, 41], posits that there was a period of accelerated expansion very early in the universe’s history. For a review of inflation, see Ref. [42]. Typical inflationary models consist of a single scalar field, termed the ‘inflaton’, slowly rolling in a very flat potential such that it gains a negative pressure. The almost exponential growth of the universe means that the aforementioned apparently disconnected regions of the CMB were in fact in thermal contact at an earlier time, and the temperature fluctuations naturally arise as a result of quantum fluctuations in the inflaton field.

A simple model of inflation has the inflaton  $\phi$  obeying the field equation:

$$\phi_{,tt} + 3H\phi_{,t} + V_{,\phi} = 0, \quad (1.16)$$

where  $V(\phi)$  is the scalar field potential. The inflaton energy density and pressure are given by:

$$\rho_\phi = \frac{1}{2}\phi_{,t}^2 + V(\phi), \quad (1.17)$$

and

$$p_\phi = \frac{1}{2}\phi_{,t}^2 - V(\phi), \quad (1.18)$$

respectively. The Hubble parameter evolves according to the Friedmann equation, Eq. (1.7), which for a scalar field takes the form:

$$H^2 = \frac{1}{3M_{\text{P}}^2} \left[ V(\phi) + \frac{1}{2}\phi_{,t}^2 \right]. \quad (1.19)$$

One can immediately see that if the scalar field energy density is potential dominated, with  $V(\phi) \gg \phi_{,t}^2$ , then the equation of state  $w_\phi \rightarrow -1$  and the universe expands at an approximately exponential rate. This feature, known as ‘slow roll’ proves to be relevant not just for inflation but for scalar field dark energy, which I discuss in Chapter 2. Unlike dark energy, however, an inflation model must provide a mechanism for slow roll to end and allow the hot big bang to take place. The process that occurs at the end of inflation when the inflaton gives way to the Standard Model

particles is known as reheating [43].

Inflation produces scalar and tensor perturbations with an approximately scale-invariant spectrum. Deviations from scale invariance in the primordial fluctuations are constrained by CMB analyses, such as by the Planck Collaboration [44]. The power spectrum, and possibly higher-order correlations of primordial fluctuations generated by inflation, depend on the details of the inflation model and are important for understanding the initial conditions from which the fluctuations in the CMB and the large-scale structure of the present universe develop.

### 1.6.3 Large-scale structure

The CMB is not the only precision test of cosmology. Another crucial source of data is the large-scale structure of the universe, in other words the distribution of matter on large scales. See Ref. [45] for a review. On small scales matter is organised into galaxies, which on larger scales comprise galaxy groups, clusters, and superclusters. On larger scales still there are structures known as sheets, walls, filaments, and vast empty voids between them [46]. Several of these features are visible in Fig. 1.2.

Large-scale structure forms by gravitational collapse of overdensities. Cold dark matter, which does not experience pressure nor other non-gravitational forces, forms stable structures after the transition from radiation domination to matter domination. After recombination, when the baryons and photons decouple, the baryonic matter can fall into the potential wells created by the dark matter. This can cause the baryonic matter to become hot and give rise to astrophysical features such as stars and galaxies.

A convenient way to analyse the matter distribution is through the matter power spectrum, which can be defined as the Fourier transform of the matter density contrast autocorrelation:

$$P(\vec{k}) = \int d\vec{r} \langle \delta_m(\vec{x}) \delta_m(\vec{x} + \vec{r}) \rangle e^{-i\vec{k}\cdot\vec{r}}, \quad (1.20)$$

where  $\vec{r}$  is the separation between two points in space  $\vec{x}$  and  $\vec{x} + \vec{r}$ , and the quantity  $\langle \delta_m(\vec{x}) \delta_m(\vec{x} + \vec{r}) \rangle$  quantifies the correlation between the matter density contrast  $\delta_m(\vec{x})$  at each point. The wavevector is denoted by  $\vec{k}$ . The matter density contrast  $\delta_m(\vec{x})$  can be estimated by measuring the galaxy distribution using large-scale structure

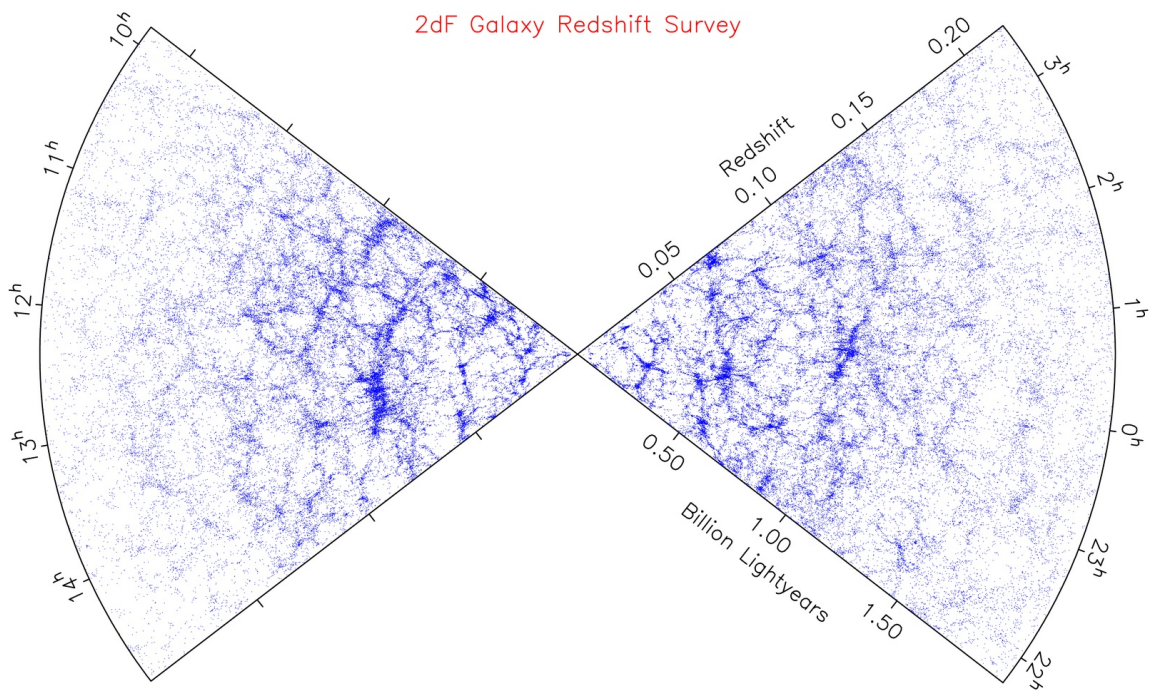


Figure 1.2: Data from the spectroscopic survey 2dF. Each point corresponds to a galaxy detected by the survey. The distance of a galaxy from us is inferred from its redshift. Regions containing many closely spaced points correspond to structures such as clusters, filaments, and walls, while sparsely populated regions are voids. Image reproduced from Ref. [47].

surveys such as 2dF [48], SDSS [49], DES [50], and CFHTLenS [51].

One can take an average over the matter overdensities by defining a length scale  $R$  and filtering  $\delta_m(\vec{x})$  by a spherical top-hat window function:

$$W_R(\vec{x}) = \begin{cases} 1/(4\pi R^3) & |\vec{x}| < R \\ 0 & \text{otherwise.} \end{cases} \quad (1.21)$$

This allows us to define the quantity:

$$\sigma_R^2 = \int \frac{d^3\vec{k}}{(2\pi)^3} W_R^2(k) P(\vec{k}), \quad (1.22)$$

where  $W_R(k)$  is the Fourier transform of the window function  $W_R(\vec{x})$ , given by

$$W_R(k) = \frac{3}{k^3 R^3} [\sin(kR) - kR \cos(kR)]. \quad (1.23)$$

In particular, the scale  $R = 8h^{-1}\text{Mpc}$  is often used, giving rise to the quantity  $\sigma_8$ ,

which quantifies matter clustering on the scale of galaxy clusters and is a useful quantity for the comparison of theory and observations. We will return to these statistical measures in Chapter 4, when we investigate the impact of coupled quintessence models on the formation of structure.

### 1.6.4 Numerical simulations

An important aspect of precision cosmology is the use of numerical methods to compute various predictions for cosmological observables for comparison to observation. Boltzmann codes, discussed in more detail in Chapter 4, allow fast and accurate calculation of the CMB and matter power spectrums. These are often used in combination with Markov chain Monte Carlo (MCMC) methods to extract cosmological parameters from datasets using Bayesian statistics [52, 53]. For the study of non-linear regimes N-body simulations are employed, taking a large number of ‘particles’ which interact gravitationally, letting the system evolve and comparing to observations [31]. Such methods have been instrumental in understanding how dark matter affects the formation of structure in the universe.

## 1.7 Problems with $\Lambda$ CDM

It must be stressed that the standard cosmological paradigm of a universe with very little spatial curvature, obeying the Einstein field equations, and consisting mainly of a cosmological constant and cold dark matter is an extraordinarily successful one. Not only is it a very simple framework with only six free parameters, but it fits the available observational evidence very well, from the expansion history of the universe to the statistical properties of its inhomogeneities and anisotropies. There are, however, some problems with the  $\Lambda$ CDM model and in this section I briefly discuss three theoretical and two observational problems that do not yet have widely accepted solutions.

### 1.7.1 Theoretical problems

Perhaps the most famous problem in cosmology is the cosmological constant problem. This is the problem of understanding the magnitude of the cosmological constant

introduced in Section 1.1.1. Quantum field theory predicts that the vacuum contains a zero-point energy, a fact that has been confirmed experimentally, for example via its manifestation in the Casimir effect [54]. The Casimir effect, and other experiments concerning the vacuum energy density, do not probe the absolute magnitude of the vacuum energy density. General relativity, on the other hand, predicts that space-time curves in response to all energy and momentum, and so the vacuum energy should gravitate. Furthermore, because vacuum energy remains constant as the universe expands, it should be expected to play the role of a cosmological constant. Unfortunately, the simplest quantum field theory calculation of the size of the vacuum energy predicts  $\Lambda \sim M_{\text{P}}^4$ , a factor of  $10^{120}$  larger than the observed value of the cosmological constant. Supersymmetric theories can reduce this unfathomably large discrepancy to a factor of  $10^{60}$ , but of course this still constitutes a very serious problem.

The cosmological constant problem seems at first glance like a fine-tuning problem, albeit a very severe one. One can introduce a ‘bare’ cosmological constant whose value is just right to cancel out the vacuum energy contributions from all the matter fields and leave the observed cosmological constant. However, even this rather unsatisfying approach is not sufficient, since the exact amount of fine-tuning depends on the energy cut-off of the theory and is sensitive to the details of unknown high-energy physics. It has been argued that this radiative instability is the true crux of the cosmological constant problem, rather than simply an extreme fine-tuning problem [55]. For more details on the cosmological constant problem, and proposed solutions, see Refs. [56–60] and references therein.

Another problem related to the size of the cosmological constant is the coincidence problem. This is based on the observation that the dark energy and dark matter densities are very similar at the present epoch despite evolving at different rates as described in Section 1.3. Figure 1.3 illustrates the coincidence; the energy densities of matter and the cosmological constant are different by many orders of magnitude for the majority of the universe’s evolution, but are almost the same size today. The coincidence problem motivates the study of dynamical alternatives to the cosmological constant. If the energy density of dark energy was not constant for most of the universe’s history but instead decreased in the early universe as matter and radiation do (for example as a scaling solution [61]), then the present similar values of  $\rho_{\text{m}}$  and  $\rho_{\text{DE}}$  would not be a coincidence. Such a scenario should also involve

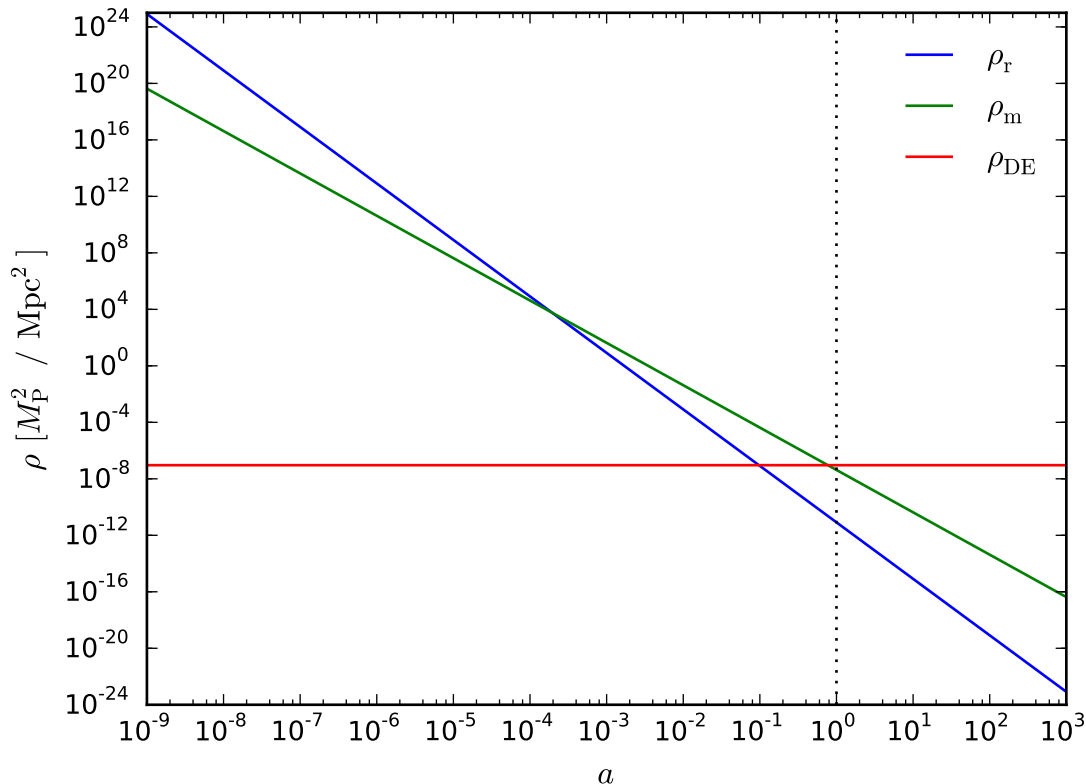


Figure 1.3: The evolution of the energy densities of matter, radiation, and cosmological constant dark energy as a function of the scale factor of the universe. The vertical dotted line denotes the present epoch, at which  $\rho_m \approx \rho_{\text{DE}}$ .

a physical mechanism for the dark energy field to switch to being close to constant in the recent epoch in order to match observations. This scenario is achieved in growing neutrino quintessence models [62, 63], which are the subject of Chapter 3.

The third theoretical problem I wish to mention concerns the cold dark matter content of the universe. Under  $\Lambda$ CDM it is very precisely known how much of the universe dark matter comprises, but we do not at present have a convincing underlying theory of dark matter. Hypothetical answers to this question have included dense objects composed of normal baryonic matter that are too cold to emit detectable radiation (known as massive compact halo objects, or MACHOs) [64, 65], primordial black holes (PBHs) formed by collapsing overdensities in the early universe [66, 67]<sup>5</sup>, hypothetical elementary particles known as axions [68, 69], and so-called weakly

<sup>5</sup>PBHs are often included under the umbrella term of MACHOs in the literature. Here I reserve the term ‘MACHO’ for objects composed of baryonic matter.

interacting massive particles (WIMPs) that would have to be described by some extension to the Standard Model of particle physics, possibly supersymmetry [70].

All of the above dark matter candidates have difficulties, some greater than others. Constraints from the CMB and big bang nucleosynthesis mean that MACHOs (or any other form of dark matter that is baryonic in origin) cannot constitute a significant fraction of dark matter. The baryon fraction  $\Omega_b h^2$  is inferred as  $0.0224 \pm 0.0001$  [6] and  $0.0225 \pm 0.0015$  [71] by CMB measurements and nucleosynthesis respectively, where  $h$  is the Hubble constant in units of  $100 \text{ km s}^{-1} \text{ Mpc}^{-1}$ . This is significantly lower than the total matter density fraction in the universe, which CMB measurements find as  $\Omega_m h^2 = 0.1430 \pm 0.0011$  [6], meaning that there is simply not enough baryonic matter in the universe for baryonic dark matter candidates to constitute a significant fraction of the dark matter.

Due to incomplete understanding of the physical conditions under which they might form, PBHs can in principle exist within a very wide mass window. Different PBH mass ranges are constrained by a wide variety of methods including the gamma ray background [72], disruption of white dwarf stars [73], gravitational lensing [74–78], disruption of pulsars [79], gravitational wave measurements [80, 81], and the CMB [82]. A recent summary of constraints on PBHs can be found in Ref. [83].

Axions and WIMPs are both particles that would require an extension to the Standard Model of particle physics. Both have been searched for extensively and, as yet, unsuccessfully. Axion searches such as ADMX [84] involve the interaction between the axion and electromagnetism. WIMPs, on the other hand, have no coupling to electromagnetism and must be detected via their Weak force interaction. This is done in three distinct ways: direct detection, in which a large detector awaits a collision by a dark matter WIMP as the Earth passes through the dark matter halo of our galaxy [85]; indirect detection, in which one searches for the products of WIMP annihilation in regions of high dark matter density [86]; and collider-based experiments, in which Standard Model particles are collided in the hope of creating WIMPs [87].

The very strong evidence for the existence of dark matter, combined with the lack of discovery of a plausible candidate, remains one of the great unanswered questions in modern cosmology.

## 1.7.2 Observational problems

The two issues I wish to discuss here concern tensions between early- and late-universe measurements. Whether one regards them as problems for  $\Lambda$ CDM or for the experiments involved is something of a matter of taste, but I include them here because whether their resolution comes from a better understanding of experimental systematics or from a modification to the cosmological model, they are certainly issues in our current understanding of cosmology. The two tensions I wish to discuss are the ‘ $H_0$  tension’ and the ‘ $\sigma_8$  tension’. In both cases, there is data from local, late-universe, model-independent observations on one hand and data from the CMB on the other. The latter is highly dependent on the cosmological model, which can motivate the study of modifications to  $\Lambda$ CDM as a means of resolving the tension.

Tension between measurements of the Hubble constant  $H_0$  has received much attention recently [88]. At the time of writing, the most precise early-universe measurements of the Hubble constant<sup>6</sup> are from the Planck Collaboration [6] and the Dark Energy Survey [89]<sup>7</sup>. These measurements give  $H_0 = (67.4 \pm 0.5) \text{ km s}^{-1} \text{ Mpc}^{-1}$  and  $H_0 = (67.4_{-1.2}^{+1.1}) \text{ km s}^{-1} \text{ Mpc}^{-1}$  respectively.

Late-universe measurements, however, give significantly larger expansion rates. One of the most important approaches are ‘distance ladder’ measurements, which employ standard candles introduced in Section 1.4. See Ref. [93] for a review. As well as Type Ia supernovas and Cepheid variables already mentioned, the brightest red-giant-branch stars in a galaxy can also be used as standard candles [91]. This is referred to as the tip of the red-giant branch (TRGB). Other approaches to measuring the Hubble constant are strong lensing of distant galaxies [94], interferometry observations of masers around supermassive black holes [95], and surface brightness fluctuations of galaxies [96, 97]. A summary of recent measurements of the Hubble parameter is presented in Fig. 1.4. It can be seen that early-universe predictions of  $H_0$  are consistently lower than late-universe observations. An intriguing exception is the Carnegie-Chicago Hubble Program (CCHP) measurement, which uses a distance ladder method

---

<sup>6</sup>I use the word ‘measurement’ here somewhat loosely. A more accurate description might be ‘value of  $H_0$  inferred from early-universe observations combined with certain assumptions about the cosmological model’. In the interest of readability I shall sometimes opt for the briefer description, even if it is strictly speaking less accurate.

<sup>7</sup>The Dark Energy Survey data itself is late-universe data of tomographic shear, galaxy–galaxy lensing and galaxy–galaxy clustering. However, the analysis of Ref. [89] also relies on baryon acoustic oscillations and big bang nucleosynthesis experiments and the assumption of the  $\Lambda$ CDM model so it is more appropriate to include it with the Planck result as an early-universe probe of  $H_0$ .

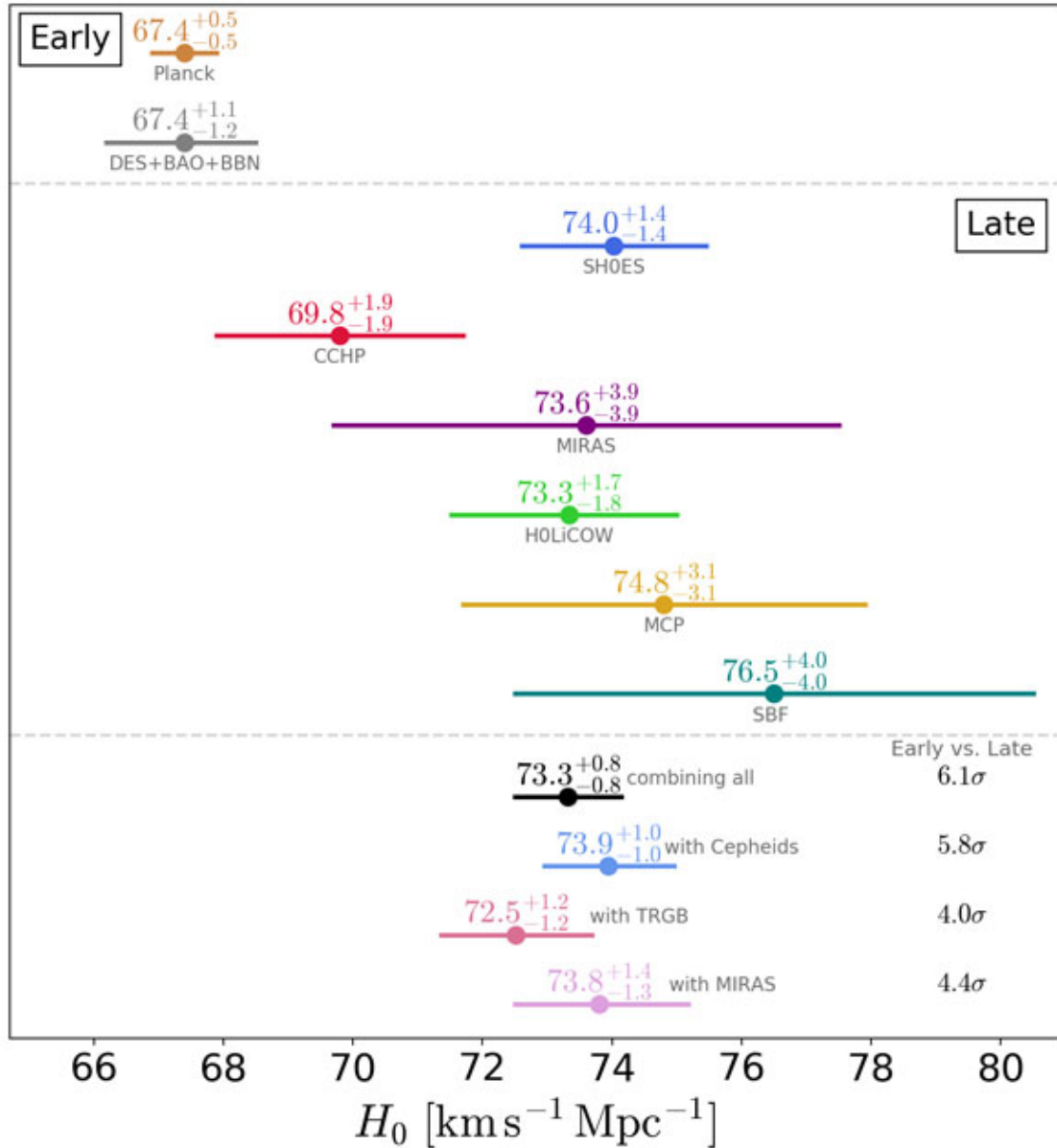


Figure 1.4: A compilation of early- and late-universe measurements of the Hubble constant. The results in this figure come from the following references: Planck: Ref. [6], DES+BAO+BBN: Ref. [89], SH0ES: Ref. [90], CCHP: Ref. [91], HOLiCOW: Ref. [92]. The MIRAS, MCP and SBF results have not yet been published but were reported at a recent workshop [88]. Figure reproduced from Ref. [88] with credit to Vivien Bonvin.

based on TRGB and obtains a value of  $H_0 = (69.8 \pm 1.9) \text{ km s}^{-1} \text{ Mpc}^{-1}$  [91], bridging the gap between the early-universe predictions and the rest of the late-universe observations.

The recent measurement of gravitational waves [98], a breakthrough which earned Rainer Weiss, Kip Thorne, and Barry Barish the 2017 Nobel Prize in physics, has led to the exciting prospect of gravitational-wave multi-messenger astronomy [99]. One application of this is using binary neutron-star mergers as ‘standard sirens’ which can be used to give a measurement of the Hubble constant [100]. At present the precision of this method is not competitive with other approaches, giving a result of  $70.0_{-8.0}^{+12.0} \text{ km s}^{-1} \text{ Mpc}^{-1}$ , with much larger uncertainties than other methods. It is an intriguing prospect, however, and future developments in the young field of gravitational-wave astronomy may allow for much greater precision.

Though it depends on exactly which datasets are included, the tension between early- and late-universe measurements of the Hubble parameter is around the  $5\sigma$  level of significance, and finding a resolution is an important unsolved problem in cosmology. Proposed explanations for the disagreement include systematic errors in the data that have not been fully taken into consideration and replacing  $\Lambda\text{CDM}$  with a different cosmological model. Both approaches have their difficulties, however. If systematic errors are to blame then they would need to be responsible for shifting the results of several measurements by approximately the same amount, while modifying  $\Lambda\text{CDM}$  is difficult to do in a way that does not sacrifice agreement with other cosmological observations.

The other major source of tension between early and late cosmology is in structure formation. This is often quantified by the parameter  $\sigma_8$ , introduced in Section 1.6. Similarly to the measurements of  $H_0$  described above,  $\sigma_8$  can be predicted by numerically simulating the evolution of the universe from initial conditions based on early-universe observations. The latest result from the Planck Collaboration, assuming  $\Lambda\text{CDM}$ , is  $\sigma_8 = 0.811 \pm 0.006$  [101]. Late-universe measurements of  $\sigma_8$  involve inferring cluster counts from the SZ effect and weak lensing and generally give lower values of  $\sigma_8$ , corresponding to less structure formation, than CMB measurements assuming  $\Lambda\text{CDM}$ . However, galaxy clustering is also sensitive to the matter fraction  $\Omega_m$ , so the parameter  $S_8 \equiv \sigma_8(\Omega_m/0.3)^{0.5}$  is often used instead of  $\sigma_8$  directly. A further complication is that the mass of clusters as inferred from X-rays is expected to be biased below the true mass by up to 30% and the inferred value of  $\sigma_8$  is dependent on

this. Taking a mass bias of 20%, SZ cluster counts give  $\sigma_8 = 0.77 \pm 0.02$  [102] while recent weak lensing measurements give  $S_8 = 0.745 \pm 0.039$  [103],  $S_8 = 0.651 \pm 0.058$  [104], and  $S_8 = 0.67 \pm 0.03$  [105]. This tension, around 2–3  $\sigma$ , is much less severe than the Hubble parameter tension discussed above, but finding a solution is still an important pursuit. In Chapter 4 I discuss a class of modifications to  $\Lambda$ CDM that can lessen the tension by means of a momentum coupling between dark energy and dark matter [106].

## 1.8 Beyond $\Lambda$ CDM

$\Lambda$ CDM is an extraordinarily successful cosmological model, agreeing with data from a wide range of scales and epochs to a remarkable level of precision, and involving only six free parameters. However, as discussed above, it has several theoretical and experimental problems that motivate the study of alternative models.

One important class of alternative theories to  $\Lambda$ CDM are so-called modified gravity theories, in which the fundamental theory of gravity on which the cosmological model rests is taken not to be general relativity, but some other theory. Approaches to modified gravity include introducing gravitational fields in addition to the metric tensor, allowing higher-order derivatives in the equations of motion, and embedding the theory of gravity in a higher-dimensional framework. See Ref. [107] for a review of modified gravity and its implications for cosmology.

Another widely studied approach is setting the cosmological constant  $\Lambda = 0$  and introducing a dynamical field to play the role of dark energy. This is the approach I focus on in this thesis.

The rest of this thesis is organised as follows: In Chapter 2 I present a brief review of dynamical dark energy. In particular, I introduce the coupled quintessence models studied in Chapters 3 and 4. In Chapter 3 I present work on growing neutrino quintessence (GNQ) models. I discuss how early dark energy bounds can be used to constrain GNQ models, detail an analytic calculation finding disagreement with previous work, and present the linear perturbation equations for a particular GNQ model. In Chapter 4 I present work on coupled dark energy with a pure momentum coupling to the dark matter. I review previous work which has found such models can relieve some of the observational tensions I have introduced in this chapter, and

present a novel approach to understanding the underlying mechanism by which this can occur. The focus then turns to generalising the models previously considered to investigate how generic the effect is. In Chapter 5 I summarise all the work carried out in this thesis and discuss its broader implications and prospects for future study.

# Chapter 2

## Dynamical dark energy

### 2.1 Introduction

In Chapter 1 I presented an introduction to cosmology, discussing  $\Lambda$ CDM and several modern methods for measuring and analysing the properties of the universe.  $\Lambda$ CDM is a remarkably effective paradigm for matching a wide set of cosmological observations. However, it does suffer from a number of problems. These problems, as well as a few proposed solutions, were discussed in Chapter 1. In the present chapter I introduce a broad class of modifications to  $\Lambda$ CDM in which the cosmological constant  $\Lambda$  is assumed to be equal to zero and dark energy is instead described by a dynamical field.

The most common choice is to introduce a single scalar field to play the role of dark energy. Scalar fields arise in many extensions to the Standard Model of particle physics including string theory, which can make them an attractive dark energy candidate. They have gained particular interest due to the recently proposed ‘String Swampland criteria’ which prohibit a cosmological constant and put constraints on cosmologies involving scalar field dark energy [108, 109].

There are many examples of scalar field dark energy that have been studied in the literature. The most widely studied example is quintessence [110], in which the scalar field  $\phi$  is minimally coupled to gravity and described by the action:

$$S = \int d^4x \sqrt{-g} [-Y - V(\phi)], \quad (2.1)$$

where  $Y = (1/2)\nabla_\mu\phi\nabla^\mu\phi$  is the kinetic term and  $V(\phi)$  is the scalar field potential. If the scalar field rolls slowly down the potential its energy density is potential dominated and it acquires a negative equation of state in a manner analogous to slow-roll inflation. A more general class of models is K-essence [111], also inspired

by an inflation model [112], in which the scalar field is described by the action:

$$S = \int d^4x \sqrt{-g} F(Y, \phi). \quad (2.2)$$

K-essence dark energy models acquire a negative equation of state through the non-canonical kinetic term  $F(Y, \phi)$ . Another type of scalar field dark energy is tachyonic dark energy, in which the scalar field is described by the action:

$$S = - \int d^4x V(\phi) \sqrt{-\det(g_{\mu\nu} + \nabla_\mu \phi \nabla_\nu \phi)}, \quad (2.3)$$

where  $V(\phi)$  is the tachyon potential. Tachyonic models of dark energy have an equation of state which depends on the time derivative of the scalar field, and can vary smoothly between 0 and  $-1$ . The final class of models I wish to mention here is phantom dark energy, with the action:

$$S = \int d^4x \sqrt{-g} [Y - V(\phi)], \quad (2.4)$$

which is similar to the quintessence action but with a ‘wrong sign’ kinetic term. These models give rise to an equation of state  $w_\phi < -1$ . For more detail on these and other dynamical dark energy models, see Ref. [113] and references therein.

In the next section I present a more detailed discussion of quintessence. I then introduce interacting dark energy in Section 2.3, in which one posits a non-gravitational interaction between dark energy and another cosmological species, most commonly dark matter. In particular, I discuss the classification scheme of Ref. [114] based on a Lagrangian formulation of interactions between dark energy and a generic fluid. In Section 2.4 I introduce models in which the dark energy is coupled to the neutrino sector, called growing neutrino quintessence models, which are the subject of Chapter 3. Finally, in Section 2.5 I briefly summarise the topics discussed in this chapter.

## 2.2 Quintessence

Quintessence, described by the action in Eq. (2.1), involves a scalar field minimally coupled to gravity with a particular potential that gives rise to accelerated universal

expansion at late times. As with the simple model of inflation introduced briefly in Chapter 1, if the gradient of the quintessence potential is sufficiently small, one can obtain slow roll giving rise to an equation of state close to  $-1$  and accelerated expansion.

Here I limit the discussion to quintessence scenarios with exponential potentials, though other potentials have also been widely studied, notably those with the form of a power law [110]. Consider a scalar field  $\phi$  which obeys Eq. (1.16) with a potential of the form  $V(\phi) = Ae^{-\lambda\phi/M_{\text{P}}}$ . There are two regimes with particularly interesting dynamics for cosmological applications. These are  $\lambda^2 < 2$  and  $\lambda^2 > 3(w_{\text{d}} + 1)$ , where  $w_{\text{d}}$  is the equation of state of the dominant fluid at a particular epoch. For  $\lambda^2 < 2$ , the potential is sufficiently flat that slow roll occurs and the field gives rise to inflationary solutions in which the universe expands at an accelerating rate. The other case, where  $\lambda^2 > 3(w_{\text{d}} + 1)$ , corresponds to scaling solutions, in which the energy density of the scalar field tracks that of the dominant fluid species [61]. Such solutions are not able to give rise to accelerated expansion, since  $w_{\text{DE}} = w_{\text{d}}$  and the scalar field simply acts effectively as a small increase in the radiation or matter density of the universe.

Combined with a mechanism for ending the scaling regime and producing inflationary behaviour, scaling solutions have an intriguing application in cosmology as a solution to the coincidence problem. As discussed in Chapter 1, a cosmological constant has the problem that there is no apparent reason why its energy density should be comparable to that of matter in the present epoch. Scaling solutions partially solve this problem by ensuring that the dark energy density is a constant fraction of that of the dominant species as the universe evolves. Furthermore, scaling solutions have been shown to be attractor solutions, meaning that they do not require finely tuned initial conditions [61]. The coincidence problem is replaced by the problem of ending the scaling solution at the appropriate time to give rise to dark energy domination in the present epoch. This is sometimes known in the literature as the ‘why now?’ problem<sup>8</sup>.

---

<sup>8</sup>Precise definitions of the coincidence problem and the ‘why now?’ problem in the literature vary, with some authors employing the terms synonymously. In this thesis I follow the terminology of Ref. [115]. In this terminology the coincidence problem is encountered by models in which  $w_{\text{DE}} \approx -1$  for a long time in cosmological terms, such as a cosmological constant, and refers to the coincidence that two species which redshift in such a drastically different way should happen to be of the same order today. On the other hand, the ‘why now?’ problem is an issue for models in which the dark energy tracked dark matter and only recently acquired  $w_{\text{DE}} \approx -1$  and refers to the

One way to bring an end to the scaling regime is to employ a double exponential potential as in Ref. [116]:

$$V(\phi) = A_1 e^{-\lambda_1 \phi/M_{\text{P}}} + A_2 e^{-\lambda_2 \phi/M_{\text{P}}}, \quad (2.5)$$

where we take  $A_1$ ,  $A_2$ ,  $\lambda_1$ , and  $\lambda_2$  to be positive. A potential of the form of Eq. (2.5) can provide both scaling solutions and inflationary solutions for appropriate choices of the parameters  $\lambda_1$  and  $\lambda_2$ . Suppose, for instance, that  $\lambda_1^2 > 3(w_{\text{d}} + 1)$  and  $\lambda_2^2 < 2$ . For appropriate choices of  $A_1$  and  $A_2$ , the first term in Eq. (2.5) will dominate in the early universe when  $\phi$  is small and the second term will come to dominate in the late universe as  $\phi$  grows. Thus, during radiation and matter domination the conditions for a scaling solution are satisfied since the first term dominates and  $\lambda_1^2 > 3(w_{\text{d}} + 1)$ , while after the transition into domination by the second term, the conditions for accelerated expansion are satisfied since  $\lambda_2^2 < 2$ . Whilst this approach solves the coincidence problem, it does not solve the ‘why now?’ problem as the values of  $A_1$  and  $A_2$  must be chosen to ensure that the transition from the scaling regime to the dark energy–dominated regime takes place at the appropriate time. In Section 2.4 I introduce growing neutrino quintessence models, which do solve the ‘why now?’ problem by linking the time at which dark energy comes to dominate to the neutrino mass.

Another issue with scaling solutions is that of early dark energy. If the scalar field energy density tracks that of the dominant species then it must have a constant energy density fraction  $\Omega_\phi$  during radiation and matter domination. Cosmologies with this behaviour were studied phenomenologically by Doran and Robbers [117], who introduced a parametrisation for early dark energy and used it to constrain the early dark energy fraction using CMB, large-scale structure, and supernova data. The most recent CMB constraints using Doran and Robbers’s parametrisation require that the early dark energy fraction is less than 0.0036 at recombination [101]. Due to the model-independent nature of Doran and Robbers’s approach, it is possible to apply early dark energy constraints to a wide range of models. In Chapter 3 I present work that follows this approach, obtaining constraints on growing neutrino quintessence models by finding the predicted fraction of early dark energy and fitting to the Doran and Robbers parametrisation.

---

question of why the dark energy equation of state changed from  $w_{\text{DE}} \approx 0$  to  $w_{\text{DE}} \approx -1$  so recently. See Section 1.1 of Ref. [115] for more details.

## 2.3 Interacting dark energy

In  $\Lambda$ CDM, as well as in the quintessence scenarios I have already discussed, dark energy and dark matter are independent of each other save for gravitational effects. There is no fundamental reason why this should be the case, and the consequences of relaxing this assumption have been widely studied [118–178]. One reason to study such couplings is that they can provide a solution to the coincidence problem. For a recent review of interacting dark energy, see Ref. [179].

Traditionally, couplings between dark energy and dark matter are introduced at the level of the equations of motion, for example:

$$\nabla^\mu T_{\mu\nu}^{(c)} = J_\nu, \quad \nabla^\mu T_{\mu\nu}^{(\text{DE})} = -J_\nu, \quad (2.6)$$

such that the overall energy–momentum tensor  $T_{\mu\nu} = T_{\mu\nu}^{(c)} + T_{\mu\nu}^{(\text{DE})}$  is conserved as usual.  $J_\nu$  is the flow of energy and momentum between dark matter and dark energy. A notable example was pioneered by Wetterich and Amendola [180–182] in which  $J_\nu = \beta T^{(c)} \nabla_\nu \phi$ , where  $\beta$  is a constant and  $\phi$  is the quintessence field. Other couplings that have been proposed in the literature include promoting  $\beta$  to be a function of  $\phi$  [183, 184], introducing a direct dependence on the expansion rate [127, 185], and couplings with non-linear dependence on the energy–momentum tensor or the scalar field gradient [186, 187].

There are several observational tests one can use to put constraints on interacting dark energy models. A given model can be confronted with observational data on the expansion history, the CMB, and large-scale structure [121, 123, 132, 137, 141, 145–147, 152, 154, 155, 157–159, 161, 163, 164, 166, 170, 173]. A recently proposed alternative [188] is to apply the parametrised post-Friedmannian framework developed for testing theories of modified gravity [189–192] to interacting dark energy. This framework involves finding the linear scalar modes of  $J_\mu$  in terms of the metric and fluid perturbations and a series of coefficients. In this way any given interacting dark energy model can be described by these coefficients, and observational tests on the coefficients can in principle constrain multiple models at once, making the parametrised post-Friedmannian framework for interacting dark energy a potentially very efficient method for putting constraints on models.

In Ref. [114], a construction was developed using the pull-back formalism for

fluids to introduce dark energy–dark matter couplings at the level of the action. Defining the coupling at the level of the action is desirable for several reasons. It is often a more intuitive way to see the coupling, and it is easier to connect it to more fundamental physics. Perhaps more importantly, instabilities can often be more easily identified and avoided, saving time and computation when studying new models. In the formalism of Ref. [114], the Lagrangian for a fairly general coupled fluid–scalar system is of the form:

$$L = L(n, Y, Z, \phi), \quad (2.7)$$

where  $n$  is the fluid number density and

$$Z = u^\mu \nabla_\mu \phi \quad (2.8)$$

is a direct coupling between the gradient of the scalar field and the fluid velocity  $u^\mu$ . Uncoupled quintessence and K-essence are both special cases in this formalism, with  $L = Y + V(\phi) + f(n)$  and  $L = F(Y, \phi) + f(n)$  respectively. By varying Eq. (2.7) with respect to  $g_{\mu\nu}$ , the usual Einstein field equations, Eq. (1.1), are obtained, with the total energy–momentum tensor given by

$$T_{\mu\nu} = L_{,Y} \nabla_\mu \phi \nabla_\nu \phi + (nL_{,n} - ZL_{,Z}) u_\mu u_\nu + (nL_{,n} - L) g_{\mu\nu}. \quad (2.9)$$

Varying with respect to  $\phi$  yields the scalar field equation:

$$\nabla_\mu (L_{,Y} \nabla^\mu \phi + L_{,Z} u^\mu) - L_{,\phi} = 0. \quad (2.10)$$

The authors of Ref. [114] stress that the Lagrangian in Eq. (2.7) cannot be interpreted as a coupled system of two distinct species but describes a single entity. This is made clear by Eq. (2.9), which cannot be written as the sum of a contribution from the scalar field and a contribution from the fluid. In order to separate the dark energy field from the dark matter fluid, they decompose Eq. (2.7) in three distinct ways. They name the resulting classes of models Types 1, 2, and 3.

According to this classification scheme, a Type 1 model is defined by a Lagrangian of the form

$$L(n, Y, Z, \phi) = F(Y, \phi) + f(n, \phi). \quad (2.11)$$

As an illustration of a Type 1 model, let us consider  $F(Y, \phi) = Y + V(\phi)$  and

$f(n, \phi) = \xi_1(n)e^{\alpha(\phi)}$  for some functions  $V(\phi)$ ,  $\xi_1(n)$ , and  $\alpha(\phi)$ . In this case one may write the energy–momentum tensor as a sum of a scalar field contribution  $T_{\mu\nu}^{(\phi)}$  and a fluid contribution  $T_{\mu\nu}^{(c)}$ , which we identify with the cold dark matter fluid:

$$T_{\mu\nu} = T_{\mu\nu}^{(\phi)} + T_{\mu\nu}^{(c)}, \quad (2.12)$$

where

$$T_{\mu\nu}^{(\phi)} = \nabla_\mu \phi \nabla_\nu \phi - [Y + V(\phi)]g_{\mu\nu}, \quad (2.13)$$

and

$$T_{\mu\nu}^{(c)} = (\rho + p)u_\mu u_\nu + pg_{\mu\nu}, \quad (2.14)$$

where we have identified  $\rho = \xi_1(n)e^{\alpha(\phi)}$  as the fluid density and  $p = [n\xi_{1,n} - \xi_1(n)]e^{\alpha(\phi)}$  as the pressure. For cold dark matter we can further impose

$$n\xi_{1,n} - \xi_1(n) = 0, \quad (2.15)$$

such that its pressure  $p = 0$ .

Finally we can relate this to the traditional method of defining interacting dark energy sketched in Eq. (2.6) by calculating the coupling current  $J_\nu = -\nabla^\mu T_{\mu\nu}^{(\phi)}$  as

$$J_\nu = -\rho\alpha_{,\phi}\nabla_\nu\phi. \quad (2.16)$$

If we set  $\alpha(\phi) = -\beta\phi$ , for constant  $\beta$ , we recover the model studied by Wetterich and Amendola [180–182]. For a more general treatment of Type 1 models, see Refs. [114, 188].

Type 1 models do not depend on the momentum coupling  $Z$ , such that the coupling between the scalar field and the fluid is only through the density (and pressure) of the fluid and not through the fluid velocity  $u^\mu$ . In contrast, Type 2 and Type 3 models do depend on  $Z$ , but differ in how the dependence is manifest. Type 2 models are classified by

$$L(n, Y, Z, \phi) = F(Y, \phi) + f(n, Z). \quad (2.17)$$

For the sake of illustration, let us again consider a simple model with  $F(Y, \phi) = Y + V(\phi)$  and  $f(n, Z) = n\xi_2(Z)$ , where this latter choice depends on the assumption

that  $p = 0$ . As in the case of Type 1, the energy–momentum tensor can be divided into Eqs. (2.13) and (2.14), with the difference being in how  $\rho$  (and  $p$  had it not been set equal to zero) depends on the scalar field. In the Type 2 case,  $\rho = n\xi_2(Z)$ . The coupling current  $J_\nu$  can then be calculated as

$$J_\nu = \nabla_\mu [\rho \tilde{\xi}_2(Z) u^\nu] \nabla_\nu \phi, \quad (2.18)$$

where  $\tilde{\xi}_2(Z)$  has been defined by

$$\xi_2(Z) = \exp \left[ \int dZ \frac{\tilde{\xi}_2(Z)}{1 + Z \tilde{\xi}_2(Z)} \right]. \quad (2.19)$$

Once again I refer the reader to Ref. [114] for details of the above procedure.

The third and final class of models identified in Ref. [114] is classified by

$$L(n, Y, Z, \phi) = F(Y, Z, \phi) + f(n). \quad (2.20)$$

Type 3 models have the interesting property that the scalar field and the fluid are not coupled at the level of the energy density but via a pure momentum coupling. This gives them interesting cosmological behaviour as I discuss in detail in Chapter 4. A model with pure momentum transfer between dark matter and dark energy has previously been studied, known as a ‘dark scattering’ model [193]. However, in the dark scattering case the coupling was introduced at the level of the equations and it has been shown that it is in fact distinct from Type 3 interacting dark energy [188].

The energy–momentum tensor for the scalar field in Type 3 models is

$$T_{\mu\nu}^{(\phi)} = F_{,Y} \nabla_\mu \phi \nabla_\nu \phi - F g_{\mu\nu} - Z F_{,Z} u_\mu u_\nu, \quad (2.21)$$

while that of the fluid is given by Eq. (2.14). The coupling current  $J_\nu$  takes a more complex form than for Types 1 and 2:

$$J_\nu = \nabla_\mu (F_{,Z} u^\mu) D_\nu \phi + F_{,Z} D_\nu Z + Z F_{,Z} u^\mu \nabla_\mu u_\nu, \quad (2.22)$$

where  $D_\mu = (u_\mu u^\nu + \delta_\mu^\nu) \nabla_\nu$ . Unlike the coupling currents for Types 1 and 2, Eq. (2.22) does not depend on the fluid density  $\rho$ , meaning that Type 3 models do not allow energy exchange between dark matter and dark energy.

As discussed above, Type 1 models were studied extensively in the literature prior to the classification scheme of Ref. [114] being developed. Types 2 and 3, on the other hand, only gained attention following their classification. Type 3 models seem to be the more interesting of these two new avenues because their lack of coupling via the energy density makes them more easily able to produce the correct background evolution for a wide range of couplings. Furthermore, Type 3 couplings have been shown to alleviate the tension between early- and late-universe probes of structure growth [106], making them a particularly exciting subject for further study. I review the recent research on Type 3 models in more detail, as well as presenting new results, in Chapter 4.

## 2.4 Growing neutrino quintessence

Instead of coupling dark energy to dark matter, one can also introduce a coupling to the neutrinos. Growing neutrino quintessence (GNQ) is an example of such an approach. The basic mechanism by which GNQ works is that a coupling between the dark energy scalar field and the neutrinos brings about a halt in the scalar field evolution once the neutrinos become non-relativistic in the recent past. Rather generic potentials can give rise to GNQ; unlike uncoupled quintessence, the scalar field is not required to roll slowly down the potential because it will be halted by the neutrino coupling. The main attraction of GNQ models is that they can provide a solution to the coincidence and ‘why now?’ problems by linking the onset of dark energy to the neutrino mass. However, GNQ models have the side effect of introducing an attractive fifth force between the neutrinos that is much stronger than gravity. This force gives rise to dense neutrino ‘lumps’ that under some circumstances can have undesired effects on the cosmological evolution. In the remainder of this section I discuss in more detail the GNQ mechanism, including how it provides a solution to the coincidence problem, and the implications of the presence of neutrino lumps. In Chapter 3 I present my work on GNQ models.

The proposal to couple dark energy to the neutrino sector was first made by Fardon, Nelson, and Weiner in 2004 [115]. They proposed a model of mass-varying neutrinos, an approach that was pursued by several other authors [194–200] in the following few years. The model was motivated by the observed similarity between the neutrino mass and the energy scale of dark energy. Assuming  $\Lambda$ CDM, recent

measurements indicate that the energy scale of dark energy is [6]

$$(\rho_{\text{DE}})^{\frac{1}{4}} = 2.25 \times 10^{-3} \text{eV}. \quad (2.23)$$

Neutrino masses cannot yet be precisely measured. However, neutrino oscillation measurements measure mass-squared differences between the different neutrino mass eigenstates. The most recent measurement of the larger difference is  $|\Delta m_\nu^2| = (2.32_{-0.08}^{+0.12}) \times 10^{-3} \text{eV}^2$  [201], from which it can be inferred that at least one neutrino has a mass of at least 0.05 eV. Cosmological measurements, meanwhile, put an upper bound on the sum of the neutrino masses. The most recent such bound, using CMB data and assuming  $\Lambda$ CDM, is  $\sum m_\nu < 0.12 \text{eV}$  [6]. Since the present discussion concerns modifications to  $\Lambda$ CDM, these numbers cannot be taken at face value. They do, however, provide an approximate indication of the energy scales under consideration and hence a motivation for mass-varying neutrino models.

In Fardon *et al.*'s original paper [115], they consider mass-varying neutrinos in a model-independent way, allowing the neutrino mass  $m_\nu$  to be a dynamical field with some potential  $V_0(m_\nu)$  which is minimised for a large value of  $m_\nu$ . By combining the energy contribution of the neutrino energy density with that of the potential  $V_0(m_\nu)$ , and taking the non-relativistic limit, they find an effective potential

$$V(m_\nu) = m_\nu n_\nu + V_0(m_\nu), \quad (2.24)$$

where  $n_\nu$  is the number density of the neutrinos. They then derive, in a model-independent way, the equation of state for the neutrino sector as

$$1 + w = -\frac{m_\nu dV_0/dm_\nu}{V(m_\nu)}, \quad (2.25)$$

which gives  $w$  close to the desired  $-1$  for relatively flat potentials. They note that the constraints on the flatness of the potential are not as strict as in uncoupled quintessence scenarios, which I discussed in Section 2.2.

GNQ models were proposed a few years after mass-varying neutrino models by Amendola, Baldi and Wetterich [62, 63]. These models have a scalar field  $\phi$  playing the role of dark energy coupled to the neutrinos in such a way that they provide a ‘trigger’ that causes the scalar field to leave a scaling regime and enter an inflationary regime. GNQ has also generated considerable interest, mostly involving the study of

the neutrino ‘lumps’ that are produced by the coupling to the scalar field [202–213].

The GNQ mechanism works by introducing a coupling between the quintessence field and the neutrinos. The energy density conservation equations are

$$\rho_{\nu,t} + 3H(\rho_{\nu} + p_{\nu}) = -\frac{\beta}{M_{\text{P}}}(\rho_{\nu} - 3p_{\nu})\phi_{,t}, \quad (2.26)$$

$$\rho_{\phi,t} + 3H(\rho_{\phi} + p_{\phi}) = \frac{\beta}{M_{\text{P}}}(\rho_{\nu} - 3p_{\nu})\phi_{,t}, \quad (2.27)$$

where the coupling parameter  $\beta$  can in general be some function of  $\phi$ . Even before exploring the dynamics of GNQ models one can see from Eqs. (2.26) and (2.27) that the coupling only plays a role when the neutrinos are non-relativistic, since relativistic neutrinos have  $p_{\nu} \approx \rho_{\nu}/3$  and so the right-hand sides of Eqs. (2.26) and (2.27) are both negligible such that the standard, uncoupled conservation equations are recovered. This is the situation at early times, when the neutrino momentum is much greater than their mass. As the universe cools, the average momentum of the neutrinos falls, until at late times (typically after a redshift of around five or six [62, 63]) their momentum is much smaller than their mass and they are non-relativistic, with  $w_{\nu} \rightarrow 0$ . When this occurs the coupling term in Eqs. (2.26) and (2.27) can no longer be neglected.

Before the neutrinos become non-relativistic, the scalar field evolves as an ordinary quintessence field, rolling down its potential  $V(\phi)$ . As the scalar field evolves, the neutrino mass grows (for negative  $\beta(\phi)$ ) as

$$m_{\nu}(\phi) = \bar{m}_{\nu} \exp\left(-\int \frac{\beta(\phi)}{M_{\text{P}}} d\phi\right), \quad (2.28)$$

hence the name ‘growing neutrino quintessence’.

As discussed in Section 2.2, a scalar field rolling down a sufficiently steep exponential potential can exhibit a scaling solution whereby its energy density tracks the energy density of the dominant matter fluid. GNQ provides an elegant mechanism for ending the scaling regime and producing accelerated expansion. The scalar field equation can be written as

$$\phi_{,tt} + 3H\phi_{,t} + V_{,\phi} - \frac{\beta}{M_{\text{P}}}(\rho_{\nu} - 3p_{\nu}) = 0. \quad (2.29)$$

For an exponential potential  $V(\phi) = Ae^{-\lambda\phi/M_{\text{P}}}$  with  $\lambda > 2$ , the scalar field  $\phi$  will undergo a scaling solution during radiation and matter domination as demonstrated in Ref. [61]. During most of this time the neutrinos are relativistic and the last term in Eq. (2.29) does not contribute. Once the neutrinos become non-relativistic (at a time which depends on the present-day neutrino mass) the last term in Eq. (2.29) stops the further evolution of the scalar field, resulting in it redshifting like a cosmological constant and giving rise to accelerated expansion.

To illustrate the mechanism, let us take  $\beta = \text{const}$  and consider the effective potential consisting of both the original potential  $V(\phi)$  and the neutrino term:

$$V_{\text{eff},\phi} = V_{,\phi} - \frac{\beta}{M_{\text{P}}}\rho_{\nu}, \quad (2.30)$$

where we have neglected the neutrino pressure because we are working in the non-relativistic limit. Because the neutrino mass depends on  $\phi$  according to Eq. (2.28), the energy density  $\rho_{\nu}$  evolves as

$$\rho_{\nu} = \rho_{\nu 0} \exp\left(-\frac{\beta(\phi - \phi_0)}{M_{\text{P}}}\right) a^{-3}, \quad (2.31)$$

where  $\rho_{\nu 0}$  is the present-day neutrino energy density and  $\phi_0$  is the present-day value of the scalar field. By substitution of Eq. (2.31) into Eq. (2.30) we obtain

$$V_{\text{eff},\phi} = V_{,\phi} - \frac{\beta}{M_{\text{P}}}\rho_{\nu 0} \exp\left(-\frac{\beta(\phi - \phi_0)}{M_{\text{P}}}\right) a^{-3}. \quad (2.32)$$

If we assume an exponential potential  $V(\phi)$  and integrate Eq. (2.32) with respect to  $\phi$  we obtain

$$V_{\text{eff}}(\phi) = A \exp\left(-\frac{\lambda\phi}{M_{\text{P}}}\right) + \rho_{\nu 0} \exp\left(-\frac{\beta(\phi - \phi_0)}{M_{\text{P}}}\right) a^{-3} + \text{const}. \quad (2.33)$$

For sufficiently large values of  $\lambda$  and  $-\beta$ , this effective potential has a global minimum around which the scalar field oscillates at late times. In the numerical tests of Amendola *et al.*, these parameters were chosen as  $\lambda = 10$  and  $\beta = -52$  [63].

It is also possible to calculate from the background equations of motion a simple analytic expression for the relationship between the energy densities of the scalar field and the neutrinos. In the case of constant  $\beta$ , and making the approximation that  $\beta \gg \lambda$ , the present-day density parameter of the scalar field is related to the

present-day neutrino density parameter  $\Omega_{\nu 0}$  by [63]

$$\Omega_{\phi 0} = -\frac{\beta}{\lambda}\Omega_{\nu 0}. \quad (2.34)$$

Equation (2.34) can be used to find a relation between the energy density of dark energy and the neutrino mass as follows. The neutrino density parameter is related to the sum of the neutrino masses by [214]

$$\Omega_{\nu 0} = \frac{\sum m_{\nu 0}}{93.14 h^2 \text{ eV}}, \quad (2.35)$$

where  $h$  is the present-day Hubble parameter in units of  $100 \text{ km s}^{-1} \text{ Mpc}^{-1}$ . Substituting Eq. (2.35) into Eq. (2.34) and using  $\Omega_i \equiv \rho_i / \rho_{\text{crit}}$  gives the present-day energy density of the scalar field as

$$\rho_{\phi 0}^{\frac{1}{4}} = 0.81 \left( -\frac{\beta \sum m_{\nu 0}}{\lambda \text{ eV}} \right)^{\frac{1}{4}} 10^{-3} \text{ eV}, \quad (2.36)$$

where we have set  $h = 0.72$ . GNQ is thus able to provide a justification for the small energy scale of dark energy by relating it to the size of the neutrino masses.

Providing a mechanism to trigger the onset of dark energy and relating the energy scale of dark energy to a particle physics energy scale are both attractive features of GNQ. A less attractive feature is the formation of neutrino ‘lumps’. The coupling between the neutrinos and the scalar induces a fifth force acting only on the neutrinos. This force takes the form [203]:

$$\vec{F}_5 = \beta \vec{\nabla} \delta \phi, \quad (2.37)$$

which for large  $\beta$  is much stronger than the gravitational force:

$$\vec{F}_g = \vec{\nabla} \Phi_{\nu}, \quad (2.38)$$

where  $\Phi_{\nu}$  is the gravitational potential of the neutrinos. This fifth force gives rise to non-linear neutrino structures on scales of order 10 Mpc or larger, depending on the specific model [202]. In some circumstances the lumps can produce strong backreaction effects [209] whereby the behaviour of the perturbations can influence the background evolution. This is in stark contrast to the  $\Lambda$ CDM case, in which it has

been shown that the effects of the perturbations on the background are small [215]. The effect of the backreaction in GNQ models has been studied by a number of authors [204–213]. In particular, in Ref. [213], two distinct regimes were identified. When the neutrino masses were taken to be small the neutrino lumps were found to form and dissolve periodically, and the backreaction effect was small. This behaviour comes about because as the neutrinos fall into the potential wells created by the lumps, they are accelerated to relativistic speeds and the fifth force switches off again. This causes the lumps to dissipate until the neutrinos become non-relativistic once more, at which point the fifth force switches back on and the neutrino lumps re-form, once again accelerating them to relativistic speeds. Because the backreaction effects are small, such a scenario is able to produce a realistic cosmology with a present-day equation of state close to  $-1$ . The authors of Ref. [213] find a threshold present-day neutrino mass of  $0.5\text{ eV}$ ; for smaller masses the above process occurs, and the lumps do not affect observations. For larger neutrino masses, however, the lumps are stable and realistic cosmologies are difficult to obtain.

## 2.5 Summary

In this chapter I have discussed a number of models of scalar field dark energy, with a focus on quintessence and various models in which the dark energy is allowed to interact non-gravitationally with other species. Uncoupled quintessence can give rise to two particularly interesting types of behaviour: scaling solutions and inflationary solutions. Both of these have important applications in cosmology, discussed in Section 2.2. I then discussed interacting dark energy, in which a coupling is introduced between dark energy and another species. The coupling is normally introduced at the level of the equations of motion, but a construction has recently been developed for defining the coupling at the level of the action [114]. I described this construction and the three ‘Types’ of interacting dark energy it gives rise to in Section 2.3. An interesting example of interacting dark energy is growing neutrino quintessence (GNQ), which can provide a solution to the coincidence problem. In Section 2.4 I described the mechanism by which GNQ works and discussed the neutrino ‘lumps’ it gives rise to as a by-product.

Having introduced the necessary background on standard cosmology (Chapter 1) and dynamical dark energy (this chapter), I now proceed to present the research I

have carried out, on GNQ models in Chapter 3 and Type 3 interacting dark energy in Chapter 4.

# Chapter 3

## Growing neutrino quintessence

### 3.1 Introduction

While neutrinos play an important role in early-universe cosmology, their impact on the late universe is relatively minor in  $\Lambda$ CDM. There are some cosmological models, however, in which neutrinos are given a central role in the late universe by means of a coupling to the dark energy. One of the major motivations for this is to address the coincidence problem, discussed in Chapter 1, since an appropriate coupling can result in the neutrinos acting as a ‘trigger’ that causes the dark energy to become dominant. There are two main types of models that employ such a coupling: mass-varying neutrino models [115, 194–200] and growing neutrino quintessence (GNQ) models [62, 63]. Both classes of models were introduced in Chapter 2; in the present chapter we focus on GNQ.

As discussed in Chapter 2, GNQ models introduce a coupling between the dark energy scalar field  $\phi$  and the neutrinos such that, during the regime in which the neutrinos are non-relativistic, the neutrino masses increase while  $\phi$  obeys a scaling solution. Once the neutrinos become non-relativistic, the neutrino–scalar coupling results in the end of the scaling solution and the onset of dark energy domination. As a by-product of the neutrino–scalar coupling, there is an attractive fifth force acting on the neutrinos which gives rise to non-linear ‘neutrino lumps’ on large scales. These features have been extensively studied using linear approximation [202, 205], N-body simulations [208–213], spherical collapse [204], and other methods [203, 206, 207]. The effect the neutrino lumps have on the cosmological history depends on the masses of neutrinos. As found in Ref. [213], for large neutrino masses the neutrino lumps can be stable and can lead to significant backreaction effects. For smaller neutrino masses, however, the neutrino lumps are unstable; they form and dissociate periodically such that backreaction effects are small.

In 2015, Christof Wetterich proposed a novel cosmological model that combines several ingredients including GNQ [216]. The model is an example of ‘quintessential inflation’, unifying inflation and quintessence by using the same scalar field  $\chi$  to describe both. The work is motivated by the approximate scale symmetry exhibited by both inflation and quintessence, using this to posit the existence of two fixed points of running dimensionless couplings. One of these is an ultraviolet fixed point corresponding to the distant past, during inflation, and the other is an infrared fixed point corresponding to dark energy domination in the distant future. The model is presented in a frame in which the strength of gravity depends on the scalar field that plays the role of the inflaton and quintessence field, which results in the universe not having a beginning, but instead inflation can be extended into the infinite past. This frame is termed the ‘freeze frame’.

In the Wetterich model all particle masses are generated by breaking of the scale symmetry. There is an explicit symmetry breaking which results in the primordial power spectrum not being scale invariant, and also brings about the end of inflation. There is also spontaneous symmetry breaking which gives rise to the spectrum of massive particles present today. The model posits a two-stage crossover between the fixed points. The first stage corresponds to the end of inflation and sees all particles apart from the neutrinos acquiring their present mass ratios. In the intermediate region before the second stage of the crossover, the scalar field  $\chi$  exhibits a scaling solution, giving rise to early dark energy during the radiation- and matter-dominated epochs. The neutrino masses increase rapidly in the second stage of the crossover, becoming non-relativistic at a redshift  $z \approx 5$  and acting as the trigger event to end the scaling solution and bring about a transition to dark energy domination. After this point the neutrino masses also become constant relative to the other particle masses. In the freeze frame in which the model is presented, none of the particle masses are constant but increase with the scalar field  $\chi$ . In fact, in the crossover region, the particle masses (with the exception of neutrinos) are proportional to  $\chi$  and so is the effective Planck mass. Thus it can be more convenient to work in the Einstein frame, in which the Planck mass and the particle masses take their usual constant values, with only the neutrino masses increasing. This casts the model in the usual form for growing neutrino quintessence.

This chapter is organised as follows: I present the action and equations of motion of the GNQ models we investigate in Section 3.2 and also discuss the meaning of

conformal frame transformations, making it clear how the Einstein frame and the freeze frame of the Wetterich model are defined. In Sections 3.3 and 3.4 the focus is on the scaling solution of radiation and matter domination and the transition brought about by the neutrinos to dark energy domination. We work in the Einstein frame, where the Planck mass and particle masses are constant. This work is applicable to the second stage of the crossover in the Wetterich model but is also generalised to other GNQ models. Working at the level of the background equations we use constraints on early dark energy from Planck [101] to constrain model parameters. In Section 3.5 we work in the freeze frame of the Wetterich model and perturb the equations of motion to linear order with the intention of carrying out a numerical analysis of the model using the Code for Anisotropies in the Microwave Background (CAMB). Finally, in Section 3.6 I summarise our conclusions and discuss the future outlook of GNQ models.

## 3.2 Equations of motion

Growing neutrino quintessence models can be described by the following action:

$$S = \int d^4x \sqrt{-g} \left[ \frac{1}{2} M_{\text{P}}^2 R - \frac{1}{2} k^2(\phi) \nabla_\mu \phi \nabla^\mu \phi - V(\phi) \right] \\ + S_{\text{b}}[\Psi_{\text{b}}, g_{\mu\nu}] + S_{\text{c}}[\Psi_{\text{c}}, g_{\mu\nu}] + S_{\gamma}[\Psi_{\gamma}, g_{\mu\nu}] + S_{\nu}[\Psi_{\nu}, C(\phi)^2 g_{\mu\nu}], \quad (3.1)$$

where  $k^2(\phi)$ ,  $V(\phi)$ , and  $C(\phi)$  are respectively the kinetic, potential, and neutrino-scalar coupling functions and must be specified in order to choose a particular model.  $\Psi_{\text{b}}$ ,  $\Psi_{\text{c}}$ ,  $\Psi_{\gamma}$ , and  $\Psi_{\nu}$  correspond to the baryonic, cold dark matter, radiation, and neutrino fields respectively. The key feature of growing neutrino quintessence models is the function  $C(\phi)$ , which couples neutrinos to the scalar field and effectively gives the neutrinos a time-dependent mass given by:

$$m_{\nu}(\phi) = \bar{m}_{\nu} C(\phi), \quad (3.2)$$

where  $\bar{m}_{\nu}$  is a mass scale. For simplicity we take all neutrino masses to be equal. It is often convenient to work in terms of the dimensionless function:

$$\beta(\phi) \equiv -M_{\text{P}} \frac{d \log C(\phi)}{d\phi}. \quad (3.3)$$

By varying the action, Eq. (3.1), with respect to the metric  $g_{\mu\nu}$ , one obtains the gravitational field equations:

$$R_{\mu\nu} + \frac{1}{2}Rg_{\mu\nu} = \frac{1}{M_{\text{P}}^2}T_{\mu\nu} + \frac{1}{M_{\text{P}}^2} \left[ k^2(\phi)\nabla_\mu\phi\nabla_\nu\phi - \frac{1}{2}k^2(\phi)\nabla_\rho\phi\nabla^\rho\phi g_{\mu\nu} - V(\phi)g_{\mu\nu} \right], \quad (3.4)$$

and varying with respect to the scalar field  $\phi$  yields the scalar field equation of motion:

$$-k^2\nabla_\mu\nabla^\mu\phi - \frac{1}{2}(k^2)_{,\phi}\nabla_\mu\phi\nabla^\mu\phi + V_{,\phi} + \beta\frac{T_{\mu}^{(\nu)\mu}}{M_{\text{P}}} = 0. \quad (3.5)$$

Here  $T_{\mu\nu}$  is the total energy–momentum tensor of all species apart from the scalar field (including neutrinos) and  $T_{\mu\nu}^{(\nu)}$  is the energy–momentum tensor of the neutrinos. As usual, subscript comma notation denotes differentiation.

If we assume a spatially flat Friedmann–Lemaître–Robertson–Walker metric of the form

$$ds^2 = -dt^2 + a(t)^2\delta_{ij}dx^i dx^j, \quad (3.6)$$

and take the scalar field to be homogeneous, then Eqs. (3.4) and (3.5) become:

$$H^2 = \frac{\rho}{3M_{\text{P}}^2}, \quad (3.7)$$

$$H_{,t} = -\frac{\rho + p}{2M_{\text{P}}^2}, \quad (3.8)$$

and

$$\phi_{,tt} + 3H\phi_{,t} + \frac{1}{2k^2}(k^2)_{,\phi}\phi_{,t}^2 + \frac{1}{k^2}V_{,\phi} - \frac{\beta}{M_{\text{P}}}(\rho_\nu - 3p_\nu) = 0, \quad (3.9)$$

where  $\rho = \rho_{\text{m}} + \rho_\nu + \rho_\gamma + \rho_\phi$  and  $p = p_{\text{m}} + p_\nu + p_\gamma + p_\phi$  are the energy density and pressure of all species. The energy density and pressure of the homogeneous scalar field are defined as:

$$\rho_\phi = \frac{k^2}{2}\phi_{,t}^2 + V, \quad (3.10)$$

$$p_\phi = \frac{k^2}{2}\phi_{,t}^2 - V. \quad (3.11)$$

Matter and radiation obey the usual conservation equations:  $\rho_{\text{m},t} + 3H\rho_{\text{m}} = 0$  and  $\rho_{\gamma,t} + 4H\rho_\gamma = 0$ . However, the neutrinos obey a modified conservation equation due to their interaction with the scalar field given by Eq. (2.26).

As discussed in Chapter 2, for most of the Universe’s history, the neutrinos are highly relativistic and  $\rho_\nu - 3p_\nu \approx 0$  such that the scalar field and the neutrinos are effectively uncoupled and the scalar field energy density tracks that of the dominant species. After the neutrinos become non-relativistic the coupling becomes important and, for large enough  $|\beta|$ , effectively stops the evolution of the scalar field by providing a force to counter that caused by the gradient of the potential in Eq. (3.9). As a result, the scalar field’s energy density and pressure are dominated by the potential and the equation of state  $w_\phi \equiv p_\phi/\rho_\phi$  approaches  $-1$ , which is consistent with observations [6].

### 3.2.1 Conformal frames

A conformal transformation, also known as a Weyl transformation, is a local rescaling of the metric tensor that has the effect of changing length scales but not angles. A conformal transformation may be written as

$$\tilde{g}_{\mu\nu} = \Omega^2(x)g_{\mu\nu}, \quad (3.12)$$

where  $g_{\mu\nu}$  is the metric tensor and  $\Omega(x)$  is a function of space-time, not to be confused with the energy density parameters. Conformal transformations are useful when studying modified theories of gravity because one can often use them to cast a particular theory in a frame in which its equations take a simpler form, making it easier to study. As an example, let us consider a simple scalar–tensor theory with the following action:

$$S = \frac{1}{2}M_{\text{P}}^2 \int d^4x \sqrt{-g} \left[ \phi R - \frac{\omega(\phi)}{\phi} \nabla_\mu \phi \nabla^\mu \phi - 2\Lambda(\phi) \right] + S_{\text{m}}(\Psi, g_{\mu\nu}). \quad (3.13)$$

For a review of modified gravity, including the use of conformal transformations and the interpretation of different conformal frames, see Ref. [107]. The present discussion is based on Section 3.1 of that review. Equation (3.13) is written in a frame known as the Jordan frame. The matter part of the action,  $S_{\text{m}}(\Psi, g_{\mu\nu})$ , is not coupled to the scalar field  $\phi$ , which means that test particles follow geodesics of the metric  $g_{\mu\nu}$  and particle masses are constant. In this frame, the modification to gravity comes about due to the factor of  $\phi$  multiplying the Ricci scalar in the gravitational part of the action. This gives rise to modified gravitational field equations that depend

on  $\phi$  and are more complex to deal with than the standard Einstein equations. The presence of  $\phi$  in front of the Ricci scalar is sometimes referred to as a varying Planck mass. Via a conformal transformation

$$\tilde{g}_{\mu\nu} = \phi g_{\mu\nu}, \quad (3.14)$$

Eq. (3.13) can be recast in the following form:

$$S = \frac{1}{2}M_{\text{P}}^2 \int d^4x \sqrt{-\tilde{g}} \tilde{R} - \int d^4x \sqrt{-\tilde{g}} \left[ \frac{1}{2} \tilde{\nabla}_\mu \psi \tilde{\nabla}^\mu \psi + V(\psi) \right] + S_{\text{m}}(\Psi, \phi^{-1} \tilde{g}_{\mu\nu}), \quad (3.15)$$

where all quantities denoted by a tilde are in terms of the metric  $\tilde{g}_{\mu\nu}$ ,  $\psi$  is a scalar field related to  $\phi$  by a field redefinition:

$$\frac{d\phi}{d\psi} = -4\phi \sqrt{\frac{\pi}{3 + 2\omega(\phi)}}, \quad (3.16)$$

and the potential  $V(\psi)$  is related to  $\Lambda(\phi)$  by

$$V(\psi) = \phi^{-2} \Lambda(\phi). \quad (3.17)$$

Equation (3.15) is written in the so-called Einstein frame. This frame is notable because the gravitational field equations take the same form as the Einstein equations of general relativity. As demonstrated explicitly in Eq. (3.15), the action for the scalar field  $\psi$  may be separated from the gravitational part of the action leaving an Einstein–Hilbert term. In this frame the modification to gravity comes about by the presence of the scalar field in the matter part of the action. This results in particles not following geodesics of the metric  $\tilde{g}_{\mu\nu}$ . This is sometimes described as the particle masses not being constant and depending on the scalar field. In the Einstein frame, the energy–momentum tensor is not conserved as it is in general relativity and in the Jordan frame of a scalar–tensor theory. Instead one has

$$\tilde{\nabla}_\mu \tilde{T}^\mu_\nu = -\tilde{T}^\mu_\nu \frac{\tilde{\nabla}_\nu \Omega}{\Omega}. \quad (3.18)$$

We now apply this understanding of conformal transformations to the Wetterich model in Ref. [216]. The action for the Wetterich model in the freeze frame is given

by

$$S = \int d^4x \sqrt{-g} \left( \frac{1}{2} \chi^2 R - \mu^2 \chi^2 - \frac{1}{2} \left[ B \left( \frac{\chi}{\mu} \right) - 6 \right] \nabla^\rho \chi \nabla_\rho \chi \right) + S_m, \quad (3.19)$$

where  $B(\chi/\mu)$  is the ‘kinetial’ and it obeys the flow equation:

$$\mu \frac{\partial B}{\partial \mu} = \frac{\kappa \sigma B^2}{\sigma + \kappa B}. \quad (3.20)$$

In Ref. [216], the dimensionless function  $B$  is described as running from  $B^{-1} \rightarrow 0$  at the ultraviolet fixed point to  $B \rightarrow 0$  at the infrared fixed point. Meanwhile, the dimensionless ratio  $\chi/\mu$  runs from 0 at the ultraviolet fixed point to  $\infty$  at the infrared fixed point. Here we will not concern ourselves with the details of the discussion on running couplings and instead refer the reader to Section II of Ref. [216]. For our present purposes it suffices to consider the implicit solution to Eq. (3.20) [216]:

$$B^{-1} - \frac{\kappa}{\sigma} \log B = \kappa \log \left( \frac{\chi}{m} \right), \quad (3.21)$$

where the constant of integration  $c_t$  has been absorbed in the parameter  $m = \mu e^{c_t}$ . Here we treat  $\sigma$ ,  $\kappa$ ,  $\mu$ , and  $m$  as parameters that must be chosen to specify a particular model. Hereafter we will consider  $\mu$  to be a constant and the function  $B(\chi/\mu)$  will be treated as a function of  $\chi$  only. The parameter  $m$  is important for determining the scale at which the model makes the transition from inflation to post-inflationary cosmology. During inflation,  $\chi \ll m$ ,  $B^{-1} \rightarrow 0$  such that the first term of Eq. (3.21) can be neglected, and the kinetic function takes the form  $B(\chi) = (m/\chi)^\sigma$ . After the end of inflation,  $\chi \gg m$ ,  $B \rightarrow 0$  such that the second term of Eq. (3.21) can be neglected, and the kinetic function takes the form

$$B(\chi) = \frac{1}{\kappa \log(\chi/m)}. \quad (3.22)$$

Our analysis concerns only post-inflationary cosmology, so hereafter we shall take Eq. (3.22) as the form of the kinetic function.

It is taken as an assumption in Ref. [216] that, in the freeze frame, all particle masses apart from neutrinos are proportional to  $\chi$ , while the neutrino masses increase proportional to  $\chi^{2\tilde{\gamma}+1}$ , where  $\tilde{\gamma} = \tilde{\gamma}(\chi)$  can be a function of  $\chi$  in general. This allows

us to infer the form of the matter action in Eq. (3.19) as:

$$S_m = S_b[\Psi_b, \chi^2 g_{\mu\nu}] + S_c[\Psi_c, \chi^2 g_{\mu\nu}] + S_\gamma[\Psi_\gamma, g_{\mu\nu}] + S_\nu[\Psi_\nu, \chi^{4\tilde{\gamma}+2} g_{\mu\nu}]. \quad (3.23)$$

Thus we can see that the freeze frame is neither Einstein nor Jordan frame, since  $\chi$  is coupled non-minimally both to the gravitational action and the matter action. In fact there is no Jordan frame for this model, since different parts of the matter action are coupled to the scalar field in different ways.

By applying the conformal transformation  $\tilde{g}_{\mu\nu} = (\chi/M_P)^2 g_{\mu\nu}$ , Eq. (3.19) can be brought into the Einstein frame, Eq. (3.1). Following Ref. [216], we carry out the field redefinition:

$$\phi = \frac{2M_P}{\lambda} \log\left(\frac{\chi}{\mu}\right), \quad (3.24)$$

and define the kinetic, potential, and neutrino–scalar coupling function as follows:

$$k^2(\phi) = \frac{M_P \lambda}{2\kappa(\phi - \bar{\phi})}, \quad (3.25)$$

$$V(\phi) = M_P^4 \exp\left(-\frac{\lambda\phi}{M_P}\right), \quad (3.26)$$

$$C(\phi) = \exp\left(-\int \frac{\beta(\phi)}{M_P} d\phi\right), \quad (3.27)$$

where

$$\bar{\phi} = \frac{2M_P}{\lambda} \log\left(\frac{m}{\mu}\right), \quad (3.28)$$

and

$$\beta(\phi) = -\lambda\tilde{\gamma}(\phi). \quad (3.29)$$

The parameter  $\bar{\phi}$  can be interpreted as the value of the scalar field at the end of inflation; in other words when  $\chi = m$ ,  $\phi = \bar{\phi}$ . The dimensionless parameter  $\kappa$ , first introduced in Eq. (3.20), can be interpreted as setting the size of the kinetic. The parameter  $\lambda$  does not play a physical role and effectively acts as a dimensionless scaling for  $\phi$ . It can be set equal to unity and ignored or used to normalise the present-day value of the kinetic  $k^2(\phi_0) = 1$  according to convenience.

For our purposes the Einstein frame is a very convenient choice of frame because the gravitational equations are those of general relativity and, with the exception of

the neutrinos, all matter particles follow geodesics of the Einstein frame metric, have constant mass in that frame, and obey the usual energy–momentum conservation equations as written above. In this frame the neutrinos obey the modified conservation equation Eq. (2.26), by which they can exchange energy and momentum with the scalar field  $\phi$ . As discussed above, this coupling is what gives rise to the GNQ mechanism by which dark energy becomes dominant in the present epoch. Note that since photons are massless particles, they follow null geodesics of the metric. Null geodesics of one metric are null geodesics in any conformally related metric, so there is no coupling between the scalar field and the photons in any conformal frame. Another way to see this is to notice that, as massless particles, the trace of the photon energy–momentum tensor is equal to zero so the right-hand side of Eq. (3.18) will receive no contribution from the photons irrespective of the choice of  $\Omega(x)$ .

We work in the Einstein frame, basing our analysis on Eq. (3.1), in Sections 3.3 and 3.4, in which we present our analytic and numerical solutions for the background evolution of the Wetterich model and other GNQ models. We return to the freeze frame and Eq. (3.19) in Section 3.5, in which we present the linear perturbation equations in the Wetterich model and discuss our attempt to solve these using the Boltzmann code CAMB.

### 3.3 Approximate analytic solutions

Under certain simplifying assumptions, it is possible to solve the scalar field equation, Eq. (3.9), analytically. In this section we consider the behaviour of  $\phi$  before the neutrinos become non-relativistic, both for an exponential and an inverse power-law potential. For the exponential case the scalar field evolves linearly with  $N \equiv \log(a)$  and there is an approximately constant fraction of early dark energy present. In the inverse power-law case we find instead that  $\log(\phi)$  evolves linearly with  $N$ .

#### 3.3.1 Exponential potential

An approximate analytic solution for the background evolution of the Wetterich model in the Einstein frame was presented in Section IV of Ref. [216] (based on

an earlier calculation by the same author in Ref. [180]). We followed closely the procedure in Ref. [216] and found an important disagreement with their results. In this section, our version of the calculation is presented, making clear where we differ from Ref. [216].

Working in the Einstein frame, Eq. (3.1), we first consider a constant kinetic function  $k^2(\phi) = k_c^2 = \text{const}$  and an exponential potential  $V(\phi) = M_{\text{P}}^4 \exp(-\lambda\phi/M_{\text{P}})$ , where  $\lambda$  is a dimensionless parameter that determines the slope of the potential. At present we consider only the regime in which the neutrinos are highly relativistic, so it is not necessary to specify a coupling function  $C(\phi)$ . Before the neutrinos have become non-relativistic, the model exhibits a scaling solution whereby the energy density of the scalar field tracks that of the dominant species (radiation or matter, depending on the epoch) with the result that the energy density fraction of the scalar field is constant. It is convenient to introduce the energy density of the dominant species as  $\rho_{\text{d}}$ , which is equal to  $\rho_{\gamma} + \rho_{\nu}$  in the radiation-dominated epoch and  $\rho_{\text{m}}$  in the matter-dominated epoch. Since we are considering the epoch in which neutrinos are highly relativistic, they can be treated simply as radiation along with the photons.

Sufficiently far from matter–radiation equality one can neglect whichever of matter and radiation is subdominant and write:

$$\rho_{\text{tot}} = \rho_{\text{d}} + \rho_{\phi}, \quad (3.30)$$

where the energy density of the dominant species evolves as

$$\rho_{\text{d}} \propto \exp(-nN), \quad (3.31)$$

where  $N \equiv \log a$  such that  $N = 0$  at the present time,  $n = 4$  for radiation domination and  $n = 3$  for matter domination. In the scaling solution,

$$\rho_{\phi} \propto \exp(-nN), \quad (3.32)$$

and the (constant) energy density fraction of the scalar field is given by

$$\Omega_{\phi} = \frac{nk_c^2}{\lambda^2}. \quad (3.33)$$

(Note that this  $\Omega$  refers to an energy density fraction and not the conformal factor

used in Eq. (3.12).) We will also employ the fraction  $f$  defined as:

$$\rho_\phi \equiv f \rho_d. \quad (3.34)$$

The scalar field itself obeys the following particular solution of Eq. (3.9)

$$\phi = M_{\text{P}} \frac{nN}{\lambda} + \hat{\phi}, \quad (3.35)$$

where  $\hat{\phi}$  is the value  $\phi$  would take at  $N = 0$  (though note that this bears no relation to realistic present-day values of  $\phi$  since at some point before  $N = 0$  the neutrinos become important and the scaling solution becomes invalid).

For a slowly varying kinetic function  $k^2(\phi)$  one can expect behaviour that approximates this scaling solution. To find the deviation from scaling that results, we allow  $f$  to vary as a function of  $\phi$ :

$$\rho_\phi = f(\phi) \rho_d, \quad (3.36)$$

and allow a small deviation  $\delta(N)$  from the scaling solution result for  $\phi$  (Eq. (3.35)):

$$\phi = M_{\text{P}} \frac{nN}{\lambda} + \hat{\phi} + M_{\text{P}} \delta(N). \quad (3.37)$$

Differentiating Eq. (3.36), one obtains

$$(\log f)' = (\log \rho_\phi)' - (\log \rho_d)', \quad (3.38)$$

where primes denote differentiation with respect to  $N$ . It will be necessary to employ the  $\rho_\phi$  conservation equation, Eq. (2.27) (with  $p_\nu = \rho_\nu/3$ ), as well as the definitions of  $\rho_\phi$  and  $p_\phi$ , Eqs. (3.10) and (3.11). Using  $N$  as the time variable, these are given by:

$$\rho'_\phi = -3(\rho_\phi + p_\phi), \quad (3.39)$$

$$\rho_\phi = \frac{k^2 H^2}{2} \phi'^2 + V, \quad (3.40)$$

and

$$p_\phi = \frac{k^2 H^2}{2} \phi'^2 - V. \quad (3.41)$$

It proves convenient to introduce the constant of proportionality in Eq. (3.31) as follows:

$$\rho_d = \rho^* M_{\text{P}}^4 \exp(-nN - \lambda\hat{\phi}/M_{\text{P}}), \quad (3.42)$$

where  $\rho^*$  is a dimensionless constant. Substituting Eqs. (3.39) to (3.42) into Eq. (3.38) yields

$$(\log f)' = -6 \left(1 - \frac{V}{\rho_\phi}\right) + n. \quad (3.43)$$

Now, using Eqs. (3.36), (3.37), and (3.42)

$$\frac{V}{\rho_\phi} = \frac{M_{\text{P}}^4 \exp(-\lambda\phi/M_{\text{P}})}{f\rho^* M_{\text{P}}^4 \exp(-nN - \lambda\hat{\phi}/M_{\text{P}})} = \frac{1}{f\rho^*} \exp(-\lambda\delta). \quad (3.44)$$

Hence Eq. (3.43) becomes:

$$(\log f)' = n - 6 + \frac{6}{f\rho^*} \exp(-\lambda\delta). \quad (3.45)$$

Differentiating Eq. (3.37) gives

$$\delta' = \frac{\phi'}{M_{\text{P}}} - \frac{n}{\lambda}. \quad (3.46)$$

Rearranging Eq. (3.40), we write  $\phi'$  in terms of  $\rho_\phi$  and  $V$ :

$$\phi' = \left[ \frac{2\rho_\phi}{k^2 H^2} \left(1 - \frac{V}{\rho_\phi}\right) \right]^{\frac{1}{2}}, \quad (3.47)$$

and hence

$$\phi' = M_{\text{P}} \left[ \frac{6\Omega_\phi}{k^2} \left(1 - \frac{1}{f\rho^*} \exp(-\lambda\delta)\right) \right]^{\frac{1}{2}}, \quad (3.48)$$

where we have used Eq. (3.44) again. Substituting into Eq. (3.46) yields

$$\delta' = -\frac{n}{\lambda} + \left[ \frac{6\Omega_\phi}{k^2} \left(1 - \frac{1}{f\rho^*} \exp(-\lambda\delta)\right) \right]^{\frac{1}{2}}. \quad (3.49)$$

In the case of the scaling solution, in which  $k^2 = \text{const}$ ,  $f = \text{const}$ , and  $\delta = 0$ , Eq. (3.45) gives

$$\frac{1}{f} = \left(1 - \frac{n}{6}\right) \rho^*. \quad (3.50)$$

If, however,  $k^2$  varies smoothly one may expect only a small deviation from this

solution. We introduce a function  $\zeta(N)$  to quantify the deviation of  $f$  from the scaling solution value given by Eq. (3.50):

$$\frac{1}{f} = \left(1 - \frac{n}{6}\right) \rho^* \exp(-\lambda\zeta). \quad (3.51)$$

Differentiating Eq. (3.51) gives

$$\zeta' = \frac{1}{\lambda} (\log f)', \quad (3.52)$$

which, using Eq. (3.45), gives

$$\zeta' = \frac{1}{\lambda} \left[ n - 6 + \frac{6}{f\rho^*} \exp(-\lambda\delta) \right]. \quad (3.53)$$

Equations (3.49) and (3.53), both contain the term  $1/(f\rho^*) \exp(-\lambda\delta)$ , which using Eq. (3.51) can be written as

$$\frac{1}{f\rho^*} \exp(-\lambda\delta) = \left(1 - \frac{n}{6}\right) \exp(-\lambda(\delta + \zeta)). \quad (3.54)$$

Equations (3.49) and (3.53) can now be written as

$$\delta' = -\frac{n}{\lambda} + \left[ \frac{n\Omega_\phi}{k^2} \right]^{\frac{1}{2}} \left[ 1 + \left( \frac{6}{n} - 1 \right) (1 - \exp[-\lambda(\delta + \zeta)]) \right]^{\frac{1}{2}}, \quad (3.55)$$

and

$$\zeta' = \frac{n-6}{\lambda} [1 - \exp(-\lambda(\delta + \zeta))], \quad (3.56)$$

respectively.

Now we recall Eq. (3.33), but introduce a small deviation  $u(N)$ , by

$$\Omega_\phi = \frac{nk^2}{\lambda^2} (1 - u), \quad (3.57)$$

and group the small functions  $\delta$  and  $\zeta$  through the small function  $\Delta$ , defined by

$$\Delta = \left( \frac{6}{n} - 1 \right) (1 - \exp[-\lambda(\delta + \zeta)]). \quad (3.58)$$

Differentiating Eq. (3.58), we find

$$\Delta' = \lambda \left( \frac{6}{n} - 1 \right) \exp[-\lambda(\delta + \zeta)](\delta' + \zeta'). \quad (3.59)$$

We can make use of Eqs. (3.57) and (3.58) to simplify our equations for  $\delta'$  and  $\zeta'$ , Eqs. (3.55) and (3.56) as follows:

$$\delta' = \frac{n}{\lambda} \left( \sqrt{(1-u)(1+\Delta)} - 1 \right), \quad (3.60)$$

$$\zeta' = -\frac{n}{\lambda} \Delta. \quad (3.61)$$

Substituting Eqs. (3.58), (3.60), and (3.61) into Eq. (3.59) gives

$$\Delta' = [6 - n(1 + \Delta)](\sqrt{(1-u)(1+\Delta)} - 1 - \Delta). \quad (3.62)$$

The differential equation for  $u$  follows from differentiating Eq. (3.57) and rearranging as

$$u' = (1-u) \left[ \frac{d \log k^2}{d\phi} \phi' - (\log \Omega_\phi)' \right], \quad (3.63)$$

which in turn yields

$$u' = (1-u) \left[ M_{\text{P}} \frac{d \log k^2}{d\phi} \left( \frac{n}{\lambda} + \delta' \right) - \frac{\lambda}{1+f} \zeta' \right], \quad (3.64)$$

where we have made use of Eqs. (3.46) and (3.56) and the fact that  $\Omega_\phi = f/(1+f)$ . Equations (3.62) and (3.64) can be compared to Eq. (108) in Ref. [216]. We find two instances of the factor  $(1-u)$  instead of  $(1+u)$ , and the second term in Eq. (3.64) differs by a factor of  $\Omega_\phi$ . This latter difference follows through to give an extra factor of  $\Omega_\phi$  in Eq. (3.73) compared to Ref. [216] which, as discussed below, has a crucial impact on the range of possible values for the parameter  $\kappa$ .

We continue following the procedure of Ref. [216] but with our versions of the  $\Delta$  and  $u$  equations in order to find an approximate form for  $u$ . Using Eqs. (3.60) and (3.61), Eq. (3.64) can be rewritten as

$$u' = (1-u) \left[ \frac{M_{\text{P}} n}{\lambda} \frac{d \log k^2}{d\phi} \sqrt{(1-u)(1+\Delta)} + \frac{n}{1+f} \Delta \right]. \quad (3.65)$$

Close to the scaling solution  $\Delta$ ,  $u$ , and  $M_{\text{P}} d \log k^2 / d\phi$  are all small. Expanding Eqs. (3.62) and (3.65) to linear order in small quantities gives

$$\begin{aligned}\Delta' &= \frac{n-6}{2}(\Delta + u) \\ u' &= \frac{nM_{\text{P}}}{\lambda} \frac{d \log k^2}{d\phi} + n(1 - \Omega_{\phi})\Delta.\end{aligned}\tag{3.66}$$

Setting  $\Delta' = u' = 0$ , we see that this system of equations admits a constant solution:

$$\bar{u} = -\bar{\Delta} = \frac{M_{\text{P}}}{\lambda(1 - \Omega_{\phi})} \frac{d \log k^2}{d\phi}.\tag{3.67}$$

One can then split  $u = \bar{u} + \hat{u}$  and  $\Delta = \bar{\Delta} + \hat{\Delta}$  into their  $N$ -independent and  $N$ -dependent components. The equations of motion for only the  $N$ -dependent parts are as follows:

$$\hat{\Delta}' = \frac{n-6}{2}(\hat{\Delta} + \hat{u})\tag{3.68}$$

$$\hat{u}' = n(1 - \Omega_{\phi})\hat{\Delta},\tag{3.69}$$

which can be written in the following form:

$$\begin{pmatrix} \hat{\Delta} \\ \hat{u} \end{pmatrix}' = A \begin{pmatrix} \hat{\Delta} \\ \hat{u} \end{pmatrix},\tag{3.70}$$

where

$$A = \frac{n-6}{2} \begin{pmatrix} 1 & 1 \\ \frac{2n(1-\Omega_{\phi})}{n-6} & 0 \end{pmatrix}.\tag{3.71}$$

The real parts of the eigenvalues of the matrix  $A$  are both negative, which implies that the  $N$ -dependent parts of  $\Delta$  and  $u$  decay with  $N$ . Thus the solution with  $u = \bar{u}$  and  $\Delta = \bar{\Delta}$  is approached and it is appropriate to use  $\bar{u}$  in Eq. (3.57):

$$\Omega_{\phi} = \frac{nk^2}{\lambda^2} (1 - \bar{u}).\tag{3.72}$$

Our result for  $\bar{u}$ , Eq. (3.67), differs from the corresponding result in Ref. [216] by a factor of  $\Omega_{\phi}$ . As an example, we consider the particular kinetic function used in Ref. [216], given by Eq. (3.25) in this thesis. Substituting Eq. (3.25) into Eq. (3.67),

one obtains

$$\bar{u} = -\frac{2\kappa\Omega_\phi}{n(1-\Omega_\phi)}. \quad (3.73)$$

The corresponding result in Ref. [216] is given by

$$\bar{u} = -\frac{2\kappa}{n(1-\Omega_\phi)}, \quad (3.74)$$

from which it follows that  $\kappa$  must be small compared to 1, in order to give a small  $\bar{u}$  and hence produce behaviour close to the scaling solution. However, since  $\Omega_\phi$  is small, we find no such constraint on  $\kappa$ ;  $\bar{u}$  is small automatically in Eq. (3.73).

This has implications for the prospects of constraining the model. A larger value of  $\kappa$  gives smaller values of the function  $k^2(\phi)$  and hence smaller values of  $\Omega_\phi$  [216]. There is a tight upper bound from the Planck experiment on the value of  $\Omega_\phi$  at early times. This can translate into a lower bound on  $\kappa$ , discussed in more detail in Section 3.4. Based on Eq. (3.74) one would conclude that there are both upper and lower bounds on  $\kappa$ , which could potentially put a very tight constraint on the model. However, based on our result for  $\bar{u}$ , which is small irrespective of the magnitude of  $\kappa$ , one finds no upper bound on  $\kappa$ . As will be shown in Section 3.4, we can consider values of  $\kappa$  much larger than the upper bound found in Ref. [216]. Our numerical results in that section match closely our prediction and there is no evidence of any approximation breaking down for large  $\kappa$  (see, for example Figs. 3.3 and 3.4).

### 3.3.2 Inverse power-law potential

An approximate analytic solution can also be found for models with inverse power-law potentials of the form

$$V(\phi) = M_{\text{P}}^4 \tilde{V} (M_{\text{P}}/\phi)^\alpha, \quad (3.75)$$

where  $\tilde{V}$  and  $\alpha$  are dimensionless constants.

While the neutrinos are relativistic, Eq. (3.9) becomes

$$\phi_{,tt} + 3H\phi_{,t} + \frac{1}{2k^2}(k^2)_{,\phi}\phi_{,t}^2 + \frac{1}{k^2}V_{,\phi} = 0. \quad (3.76)$$

Using the same kinetic function as for the exponential potential case, Eq. (3.25), but with  $\lambda = 1$  and  $\bar{\phi} = 0$  since these parameters relate to the specific model presented

in Ref. [216], we have

$$k^2(\phi) = \frac{M_{\text{P}}}{2\kappa\phi}. \quad (3.77)$$

For our choice of  $k^2(\phi)$  and  $V(\phi)$ , Eq. (3.76) becomes:

$$\phi_{,tt} + 3H\phi_{,t} - \frac{\phi_{,t}^2}{2\phi} - 2\alpha\kappa M_{\text{P}}^{3+\alpha}\tilde{V}\phi^{-\alpha} = 0. \quad (3.78)$$

Using  $N$  as the time variable, we have:

$$H^2\phi'' + HH'\phi' + 3H^2\phi' - \frac{H^2\phi'^2}{2\phi} - 2\alpha\kappa M_{\text{P}}^{3+\alpha}\tilde{V}\phi^{-\alpha} = 0. \quad (3.79)$$

Finally introducing  $\mathcal{F}$  via

$$\phi = M_{\text{P}} \exp(\mathcal{F}/M_{\text{P}}), \quad (3.80)$$

Eq. (3.79) becomes:

$$\mathcal{F}'' + \frac{\mathcal{F}'^2}{2M_{\text{P}}} + \left(\frac{H'}{H} + 3\right)\mathcal{F}' - 2\alpha\kappa \frac{M_{\text{P}}^3\tilde{V}}{H^2} \exp(-(\alpha+1)\mathcal{F}/M_{\text{P}}) = 0. \quad (3.81)$$

The Hubble parameter evolves according to  $H^2 = \tilde{H}^2 \exp(-nN)$ , where  $n = 4$  for a radiation-dominated universe,  $n = 3$  for a matter-dominated universe, and  $\tilde{H}$  is a normalising factor. Equation (3.81) then becomes:

$$\mathcal{F}'' + \frac{\mathcal{F}'^2}{2M_{\text{P}}} + \left(3 - \frac{n}{2}\right)\mathcal{F}' - 2\alpha\kappa \frac{M_{\text{P}}^3\tilde{V}}{\tilde{H}^2} \exp(nN - (\alpha+1)\mathcal{F}/M_{\text{P}}) = 0. \quad (3.82)$$

Motivated by results from numerical simulation (see Section 3.4), which show linear solutions for  $\mathcal{F}$ , we make the following ansatz:

$$\mathcal{F} = qM_{\text{P}}N + \hat{\mathcal{F}}, \quad (3.83)$$

where  $q$  is a dimensionless constant and  $\hat{\mathcal{F}}$  is the value  $\mathcal{F}$  would take if this solution were extrapolated to  $N = 0$ .

Under this ansatz Eq. (3.82) becomes:

$$\frac{1}{2}q^2M_{\text{P}} + \left(3 - \frac{n}{2}\right)qM_{\text{P}} - 2\alpha\kappa \frac{M_{\text{P}}^3\tilde{V}}{\tilde{H}^2} \exp(nN - (\alpha+1)qN - (\alpha+1)\hat{\mathcal{F}}/M_{\text{P}}) = 0. \quad (3.84)$$

Treating the  $N$ -dependent and  $N$ -independent parts of the equation separately, we obtain

$$q = \frac{n}{\alpha + 1}, \quad (3.85)$$

which, substituting into Eq. (3.84), gives

$$\frac{1}{2} \left( \frac{n}{\alpha + 1} \right)^2 + \left( 3 - \frac{n}{2} \right) \frac{n}{\alpha + 1} - 2\alpha\kappa \frac{M_{\text{P}}^2 \tilde{V}}{\tilde{H}^2} \exp(-(\alpha + 1)\hat{\mathcal{F}}/M_{\text{P}}) = 0. \quad (3.86)$$

Rearranging, we find  $\hat{\mathcal{F}}$  as

$$\hat{\mathcal{F}} = -\frac{M_{\text{P}}}{\alpha + 1} \log \left\{ \frac{\tilde{H}^2}{2\alpha\kappa M_{\text{P}}^2 \tilde{V}} \left[ \frac{1}{2} \left( \frac{n}{\alpha + 1} \right)^2 + \left( 3 - \frac{n}{2} \right) \frac{n}{\alpha + 1} \right] \right\}. \quad (3.87)$$

Thus, in contrast to the previous section, we find that inverse power-law potentials admit solutions in which  $\log(\phi)$  evolves linearly with  $N$  as opposed to  $\phi$  evolving linearly as in the exponential potential case.

It is also instructive to find an expression for the dark energy density fraction. Substituting our solution for  $\phi$  (Eqs. (3.80) and (3.83)) into Eq. (3.10) gives the energy fraction:

$$\Omega_{\phi} = \frac{q^2}{12\kappa} \exp(qN + \hat{\mathcal{F}}/M_{\text{P}}) + \frac{M_{\text{P}}^2 \tilde{V}}{3\tilde{H}^2} \exp(nN - \alpha qN - \alpha \hat{\mathcal{F}}/M_{\text{P}}). \quad (3.88)$$

Recalling Eq. (3.85), one can write

$$\Omega_{\phi} = \left[ \frac{q^2}{12\kappa} \exp(\hat{\mathcal{F}}/M_{\text{P}}) + \frac{M_{\text{P}}^2 \tilde{V}}{3\tilde{H}^2} \exp(-\alpha \hat{\mathcal{F}}/M_{\text{P}}) \right] \exp(qN). \quad (3.89)$$

Thus it turns out that  $\Omega_{\phi}$  is proportional to  $\phi$ :

$$\Omega_{\phi} = \left[ \frac{q^2}{12\kappa} \exp(2\hat{\mathcal{F}}/M_{\text{P}}) + \frac{M_{\text{P}}^2 \tilde{V}}{3\tilde{H}^2} \exp((- \alpha + 1)\hat{\mathcal{F}}/M_{\text{P}}) \right] \frac{\phi}{M_{\text{P}}}, \quad (3.90)$$

where  $q$  and  $\hat{\mathcal{F}}$  are given by Eqs. (3.85) and (3.87). In contrast to the exponential case, where there is an approximately constant fraction of early dark energy, here the fact the dark energy fraction has an exponential dependence on  $N$  implies that at early times (i.e. large negative values of  $N$ ), it automatically makes a negligible

contribution to the energy density. These results are confirmed in Section 3.4, with Figs. 3.6 and 3.7 showing  $\log(\phi)$  and  $\log(\Omega_\phi)$  evolving linearly with  $N$  with a gradient given by  $q$ .

### 3.4 Numerical background evolution

In addition to the analytic approach laid out in Section 3.3, we numerically solved the equations of motion. This allows us to confirm the results of Section 3.3 and to probe the late-universe cosmology that our analytic approach did not capture.

To generate our results we modified the code used by Barreira *et al.* in Ref. [217], which the authors kindly shared with us, in turn a modified version of the Boltzmann code CAMB [218]<sup>9</sup>. We modified the background part of the code such that it solved the background equations of motion laid out in Section 3.2.

We consider the following choices for the kinetic, coupling, and potential functions:

Kinetic function:

- $k_c^2(\phi) = \text{const}$ ,
- $k_1^2(\phi) = \frac{M_{\text{P}}\lambda}{2\kappa(\phi-\phi_c)}$ .

Coupling function:

- $\beta_c(\phi) = \text{const}$ ,
- $\beta_1(\phi) = -\frac{M_{\text{P}}}{\phi_c-\phi}$ ,
- $\beta_2(\phi) = -\left(\frac{M_{\text{P}}}{\phi_c-\phi}\right)^2$ ,
- $\beta_3(\phi) = -\frac{\gamma M_{\text{P}}}{\phi}$ .

Potential function:

- $V_{\text{exp}}(\phi) = M_{\text{P}}^4 \exp(-\lambda\phi/M_{\text{P}})$ ,
- $V_{\text{IPL}}(\phi) = \tilde{V} M_{\text{P}}^4 (M_{\text{P}}/\phi)^\alpha$ .

---

<sup>9</sup>available at <https://camb.info>

The motivation for choosing these functions is as follows. In Ref. [216], the functions  $k_1^2(\phi)$  and  $V_{\text{exp}}(\phi)$  are used, with  $\beta(\phi)$  unspecified. We use this as a starting point, and we specify  $\beta(\phi) = \beta_1(\phi)$  as employed in Ref. [213]. We then widen the scope by choosing other functions that could be expected to give rise to growing neutrino quintessence behaviour. Inverse power-law potentials have a qualitatively similar ‘decaying’ form to exponential potentials. The couplings  $\beta_c$ ,  $\beta_1$ ,  $\beta_2$ , and  $\beta_3$  each correspond to a function  $C(\phi)$  via Eq. (3.3), or equivalently:

$$C(\phi) = \exp\left(-\frac{1}{M_{\text{P}}}\int\beta(\phi)d\phi\right). \quad (3.91)$$

The four functions  $\beta(\phi)$  considered here all correspond to a rapidly rising  $C(\phi)$ . Thus  $V(\phi)$  and  $C(\phi)$  give rise to an effective potential for the scalar field that has a minimum, which is a necessary condition for growing neutrino quintessence.

Section 3.4.1 focuses on  $k_1^2(\phi)$ ,  $\beta_1(\phi)$ , and  $V_{\text{exp}}(\phi)$ . The scaling solution discussed in Section 3.3 is verified and a constraint is found on the parameter  $\kappa$  in  $k_1^2(\phi)$  due to its effect on the amount of early dark energy. In Section 3.4.2 we consider  $k_1^2(\phi)$ ,  $\beta_1(\phi)$ , and  $V_{\text{IPL}}(\phi)$ , which give rise to qualitatively similar behaviour for the scalar field  $\phi$  but do not produce early dark energy. I discuss the various options for  $\beta(\phi)$  in Section 3.4.3.

### 3.4.1 Exponential potential

In this section I present the results of numerical calculations using  $V_{\text{exp}}(\phi)$ ,  $k_1^2(\phi)$ , and  $\beta_1(\phi)$ . During radiation and matter domination  $\phi$  evolves linearly with  $N$  according to the scaling solution Eq. (3.35). After the neutrinos become non-relativistic,  $\phi$  starts to oscillate around the minimum of the effective potential formed by  $V(\phi)$  and  $\beta(\phi)$  and comes to a halt to behave as an effective cosmological constant. This behaviour is illustrated in Fig. 3.1.

Figure 3.2 shows the evolution of the equation of state of the scalar field. It can be seen that it mimics radiation with a value of  $w_\phi = 1/3$  when the Universe is radiation dominated, then approaches  $w_\phi = 0$ , mimicking matter when the Universe is matter dominated, and finally tends towards  $w_\phi = -1$  after the neutrinos halt the evolution of the scalar field and it mimics a cosmological constant. The first two regimes illustrate the scaling solution, where the energy density of the scalar field

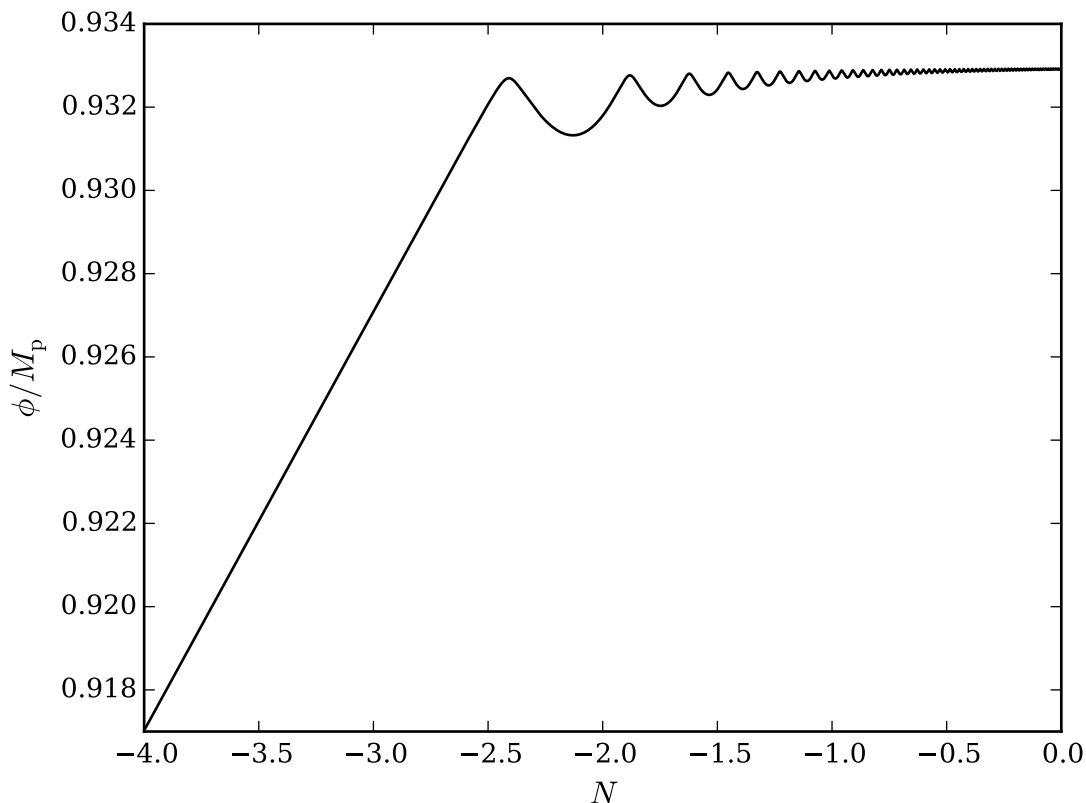


Figure 3.1: The late-time evolution of the scalar field for an exponential potential  $V_{\text{exp}}(\phi) = M_{\text{P}}^4 \exp(-\lambda\phi/M_{\text{P}})$ , kinetic function  $k_1^2(\phi) = M_{\text{P}}\lambda/(2\kappa(\phi-\bar{\phi}))$ , and coupling function  $\beta_1(\phi) = -M_{\text{P}}/(\phi_c - \phi)$ , with  $\lambda = 300$ ,  $\kappa = 1.8$ ,  $\bar{\phi} = 0.0933$ , and  $\phi_c = 0.933$ .  $\bar{\phi}$  is set using Eq. (3.28) with  $\log(m/\mu) = 14$  as in Ref. [216];  $\phi_c$  is tuned by the code to produce the correct dark energy density at the present epoch;  $\kappa$  is set to the lower limit inferred from early dark energy constraints (see Section 3.4.1); and  $\lambda$ , which does not affect the physics but merely scales  $\phi$ , has been chosen such that  $\phi$  does not exceed the Planck scale.

tracks that of the dominant species as discussed in Section 3.3. This is also illustrated in Fig. 3.3, in which we have plotted the predictions of the energy density fraction of the scalar field assuming the scaling solution is exactly satisfied both for radiation and matter domination. It can be seen that in the early Universe the numerical result closely follows  $\Omega_\phi = 4k^2(\phi)/\lambda^2$  and at later times it follows  $\Omega_\phi = 3k^2(\phi)/\lambda^2$ , with a transition in between, as expected.

Figure 3.4 shows the effect of varying the model parameter  $\kappa$  in  $k_1^2(\phi)$  on the energy density fraction of the scalar field. Note that the larger the value of  $\kappa$  the smaller the amount of early dark energy. This agrees with the scaling solution result,

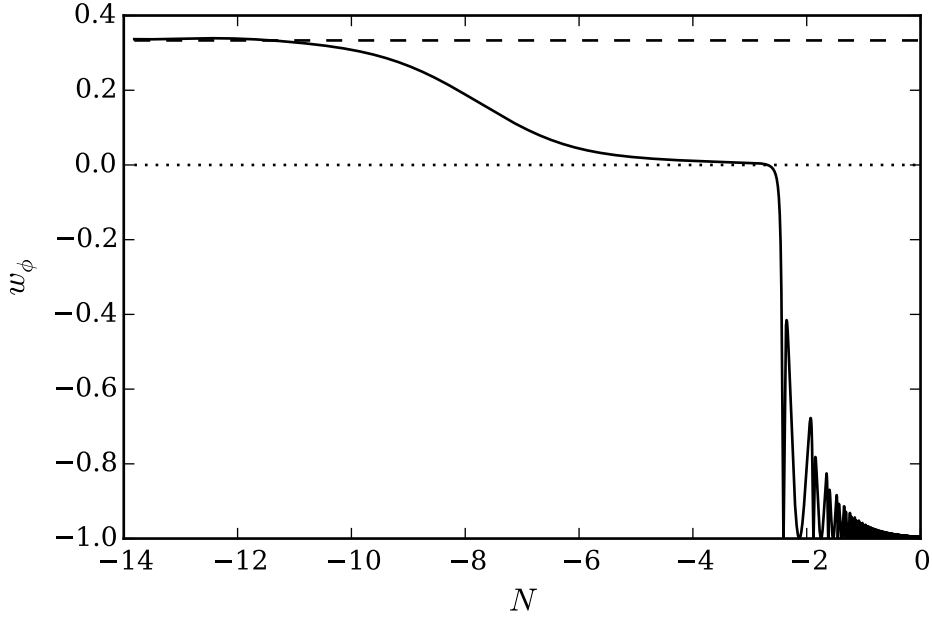


Figure 3.2: The evolution of the equation of state of the scalar field,  $w_\phi$ , for the same functions and parameters as in Fig. 3.1. The dashed and dotted lines show the equation of state during radiation and matter domination respectively.

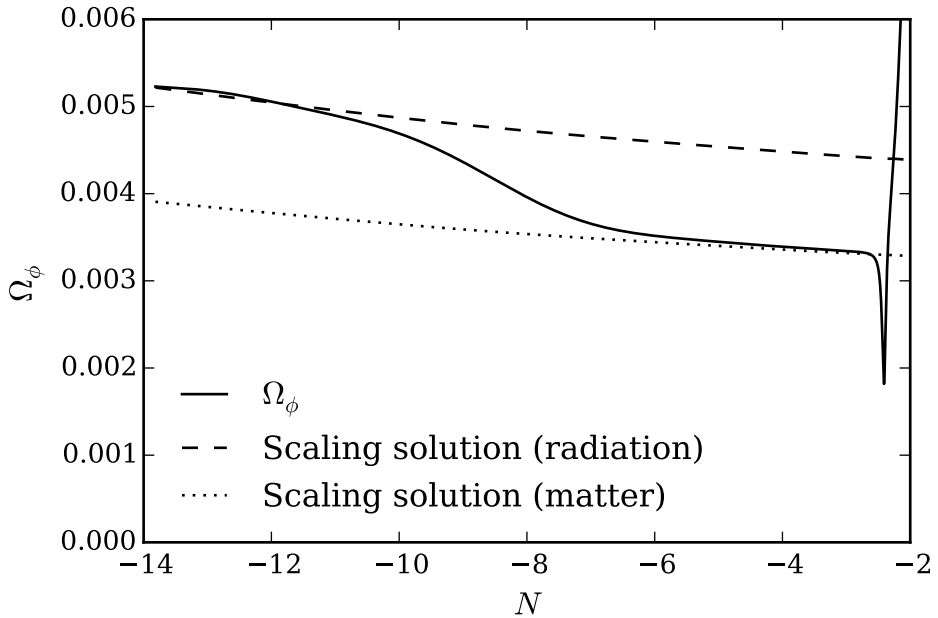


Figure 3.3: The evolution of the energy density fraction of the scalar field,  $\Omega_\phi$ , during radiation and matter domination (solid line) for the same functions and parameters as in Fig. 3.1. The dashed and dotted lines respectively show the predicted evolution of  $\Omega_\phi$ , Eq. (3.72), under the assumption of a radiation-dominated and matter-dominated universe where the scalar field obeys the scaling solution discussed in Section 3.3.

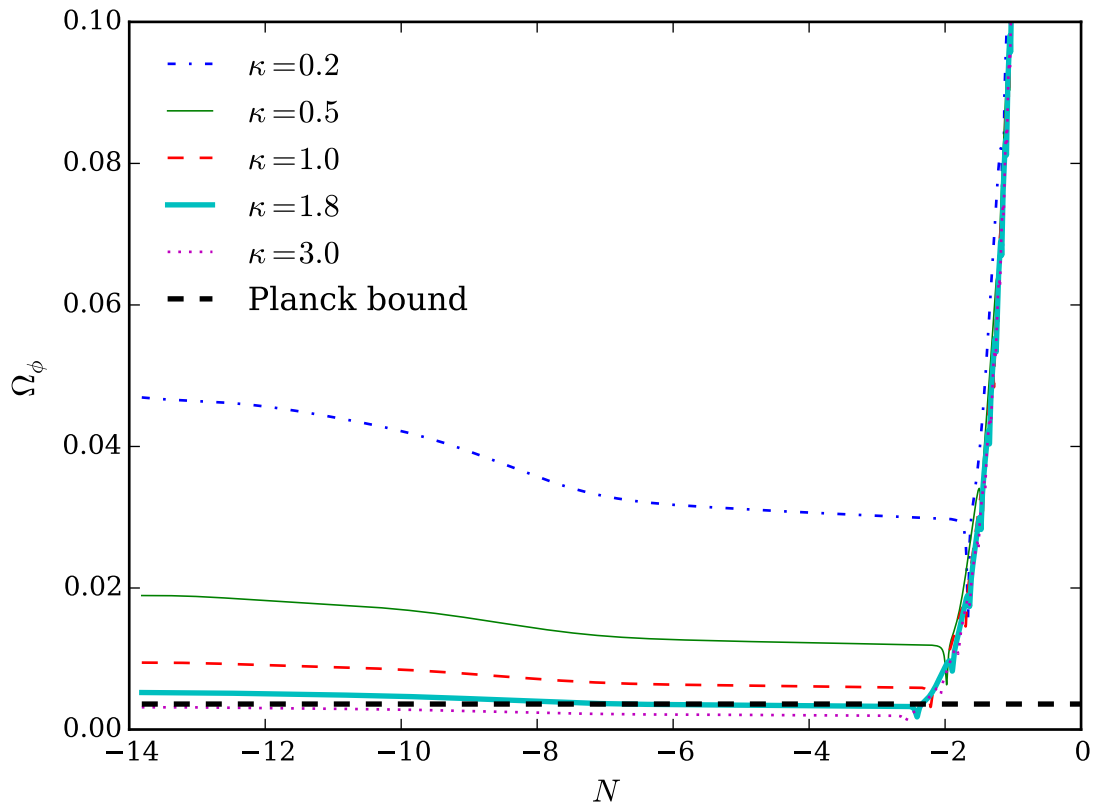


Figure 3.4: The evolution of the energy density fraction of the scalar field for a range of values of  $\kappa$  and otherwise the same functions and parameters as in Fig. 3.1. Also shown is the Planck upper bound on  $\Omega_e < 0.0036$ .

Eq. (3.33) in Section 3.3, since  $\kappa$  is effectively a constant that controls the size of the kinetic function  $k_1^2(\phi)$  as can be seen in Eq. (3.25).

We find that our numerical results for the evolution of dark energy are well approximated by the early dark energy parametrisation of Doran and Robbers [117], in which the dark energy density fraction is parametrised as follows:

$$\Omega_{\text{DE}}(a) = \frac{\Omega_{\text{DE}}^0 - \Omega_e(1 - a^{-3w_0})}{\Omega_{\text{DE}}^0 + \Omega_{\text{m}}^0 a^{3w_0}} + \Omega_e(1 - a^{-3w_0}), \quad (3.92)$$

where  $\Omega_e$  (the fraction of early dark energy) and  $w_0$  (the present-day equation of state) are parameters to be fitted, and  $\Omega_{\text{DE}}^0$  and  $\Omega_{\text{m}}^0$  are the present-day dark energy and matter fractions. For a given value of  $\kappa$  we carry out a least-squares fitting of our numerical results to the Doran and Robbers parametrisation to find  $w_0$  and  $\Omega_e$ . The Planck Collaboration [101] finds an upper bound on the parameter  $\Omega_e$  of 0.0036.

Our results (Fig. 3.4) show that the value of  $\kappa$  required to give rise to this value of  $\Omega_e$  is  $\kappa = 1.8$ , with larger values of  $\kappa$  resulting in smaller values of  $\Omega_e$  and vice versa. We therefore find a lower bound on  $\kappa$  of 1.8.

As discussed in Section 3.3, Ref. [216] finds a requirement that  $\kappa \ll 1$  in order to ensure that  $u$ , the deviation of  $\Omega_\phi$  from the scaling solution at early times, is small. If this requirement were valid then the model of Ref. [216] would have been ruled out by the constraints on early dark energy. However, due to our finding in Section 3.3 that  $u$  is given by Eq. (3.73) and not Eq. (3.74), we find that there is no requirement for  $\kappa$  to be small and hence our constraint that  $\kappa > 1.8$  does not rule out the model.

Varying the parameter  $\lambda$  in the potential merely results in a rescaling of  $\phi$  and does not have any effect on the physics. We also studied the case of a constant kinetic function  $k_c^2$  and found that it made little difference to the results, as demonstrated by Fig. 3.5.

### 3.4.2 Inverse power-law potential

In this section I present the results for models with  $V_{\text{IPL}}(\phi)$ ,  $k_1^2(\phi)$ , and  $\beta_1(\phi)$ , with  $\kappa = 1.8$ ,  $\lambda = 1$ , and  $\bar{\phi} = 0$ . We considered several different values of the power  $\alpha$  as shown in Figs. 3.6 and 3.7. For each value of  $\alpha$ , an appropriate value of  $\tilde{V}$  was chosen to produce the correct dark energy density fraction at the present day. For ease of comparison, the same present-day value of  $\phi$  was chosen for each value of  $\alpha$ , with  $\phi_c$  being tuned in each case to achieve this.

The choice of  $\kappa = 1.8$  was made for ease of comparison with the exponential potential, but has no special significance in the inverse power-law case. Larger values of  $\kappa$  result in an upward shift in  $\phi$  and a corresponding downward shift in  $\Omega_\phi$ .

Compared to the models with exponential potentials already discussed, the behaviour of models with inverse power-law potentials is not drastically different. During radiation and matter domination we find that  $\phi$  evolves exponentially with  $N$  as opposed to linearly as it does for models with  $V_{\text{exp}}(\phi)$ . However, the qualitative behaviour, of the field increasing as long as neutrinos are relativistic and then effectively stopping once they become non-relativistic, is still present. Figure 3.6 shows the evolution of the logarithm of the scalar field against  $N$  for different inverse power-law potentials. Before the neutrinos become non-relativistic,  $\log(\phi)$  evolves

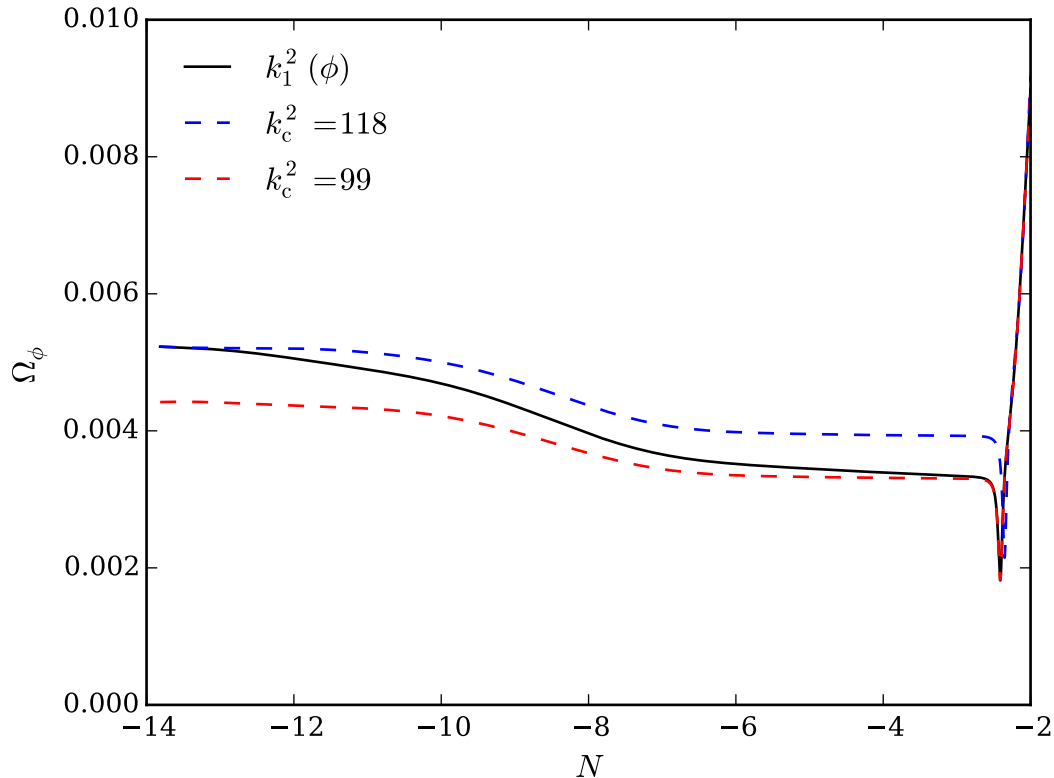


Figure 3.5: The evolution of the energy density fraction of the scalar field for three choices of the kinetic function. The black solid line corresponds to the varying kinetic  $k_1^2(\phi)$  for the same choices of functions and parameter values as in Fig. 3.1. The blue and red dashed lines correspond to constant kinetic, with the value of  $k_c^2$  chosen to match the value of  $k_1^2(\phi)$  in the early and late universe respectively. The varying kinetic results in a slightly larger drop in  $\Omega_\phi$  from the early universe to the late universe than for the constant kinetic case.

approximately linearly with a gradient of  $n/(\alpha+1)$  and an intercept of  $\hat{\mathcal{F}}$  as predicted in Eqs. (3.85) and (3.87).

The evolution of the energy density of the scalar field is shown in Fig. 3.7. From this it is clear that these models do not give rise to early dark energy; looking back in time, the energy density of the scalar field continues to drop off rapidly. The constraint on  $\kappa$  that we found for exponential potentials therefore does not apply to models with inverse power-law potentials.

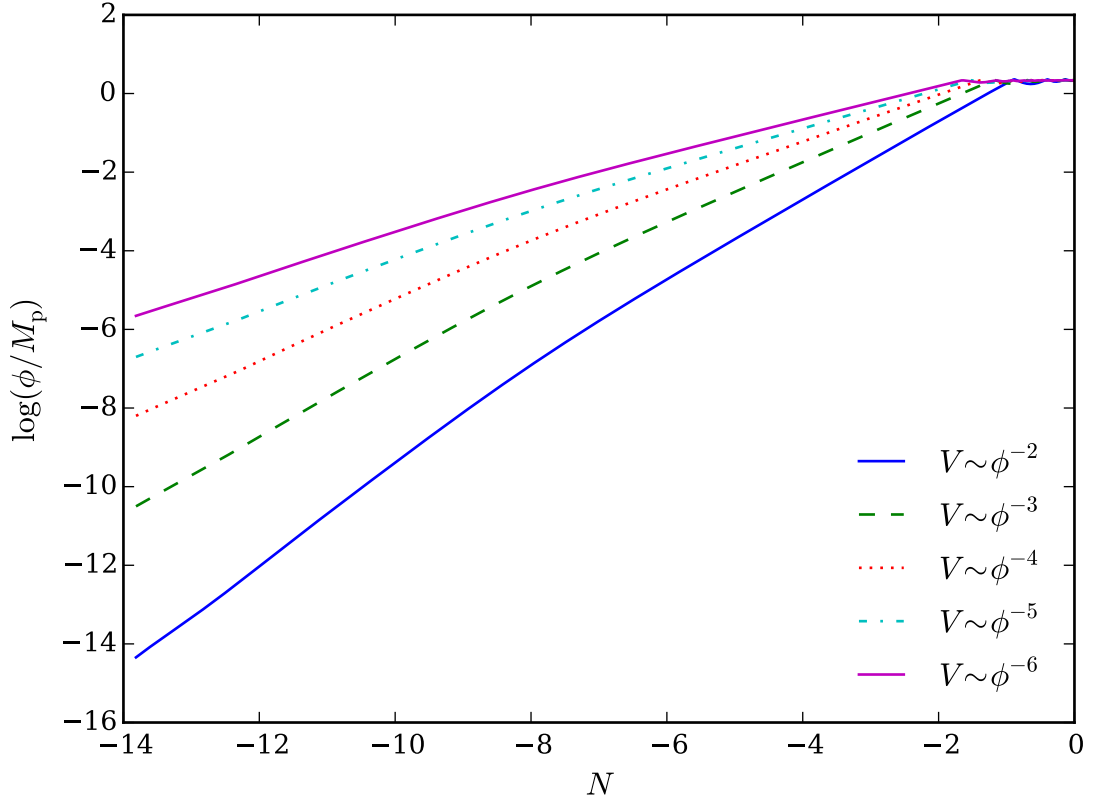


Figure 3.6: The evolution of the logarithm of the scalar field for inverse power-law potentials of the form  $V_{\text{IPL}}(\phi) = \tilde{V} M_{\text{P}}^4 (M_{\text{P}}/\phi)^\alpha$  with kinetic function  $k_1^2(\phi) = M_{\text{P}}/(2\kappa\phi)$  and coupling function  $\beta_1(\phi) = -M_{\text{P}}/(\phi_c - \phi)$ . We fix  $\kappa = 1.8$  and the parameters  $\tilde{V}$  and  $\phi_c$  take different values for different values of  $\alpha$  (see text for details).

### 3.4.3 Coupling function

In addition to the coupling  $\beta_1(\phi)$  already considered, we investigated  $\beta_c$ ,  $\beta_2(\phi)$ , and  $\beta_3(\phi)$ . None of these choices led to behaviour significantly different to the  $\beta_1(\phi)$  case, provided  $|\beta|$  is sufficiently large at the time at which neutrinos become non-relativistic. This requirement is automatically satisfied for  $\beta_1(\phi)$  and  $\beta_2(\phi)$ , since as  $\phi$  approaches  $\phi_c$ ,  $|\beta(\phi)|$  tends to infinity. The scalar field is never allowed to reach  $\phi_c$ , however, because the neutrino coupling term in the scalar field equation, Eq. (3.9), always acts to decrease the value of  $\phi$ . It can be seen that the value of  $\phi_c$  in  $\beta_1(\phi)$  and  $\beta_2(\phi)$  determines the present-day value of  $\phi$ , since the latter will approach ever closer to it but can never exceed it. This is demonstrated in Fig. 3.1.

For  $\beta_c$  and  $\beta_3(\phi)$  one does not automatically obtain large  $|\beta|$  but it must be set

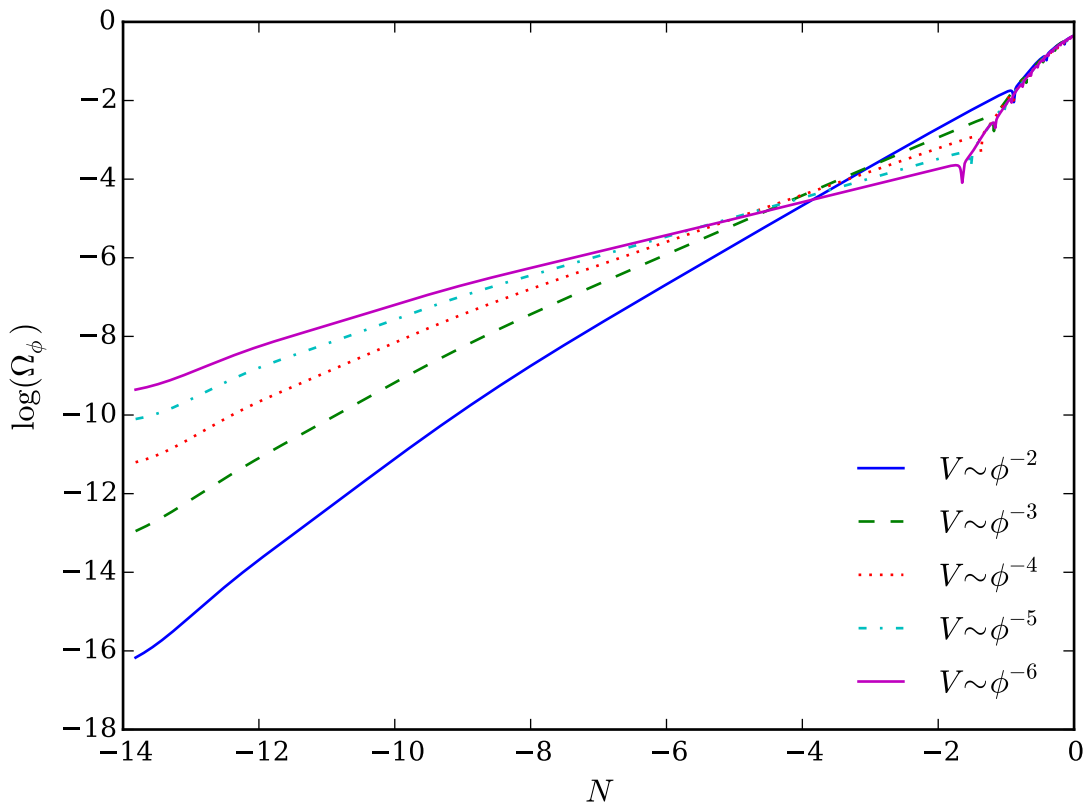


Figure 3.7: The evolution of the logarithm of the energy fraction of the scalar field for the same functions and parameters as in Fig. 3.6.

by an appropriate choice of parameters. In the latter case this means choosing a large value of  $\gamma$ . The requirement on the size of  $|\beta|$  is illustrated by Eq. (2.34).  $|\beta|$  determines the ratio of the energy density of the scalar field to that of the neutrinos. If  $|\beta|$  is too small, the coupling term in Eq. (3.9) will not be large enough to counteract the potential term and the value of  $\phi$  will continue to increase. This will result in both a larger  $\Omega_\nu$  and a smaller  $\Omega_\phi$ . The relationship given by Eq. (2.34) is demonstrated by Fig. 3.8.

### 3.5 Perturbative analysis

Sections 3.3 and 3.4 presented a background analysis of GNQ models by making the assumptions of homogeneity and isotropy. However, as discussed in Chapter 1, one can learn a great deal more about a cosmological model by including perturbations from homogeneity and isotropy. To this end, in this section I present an analysis

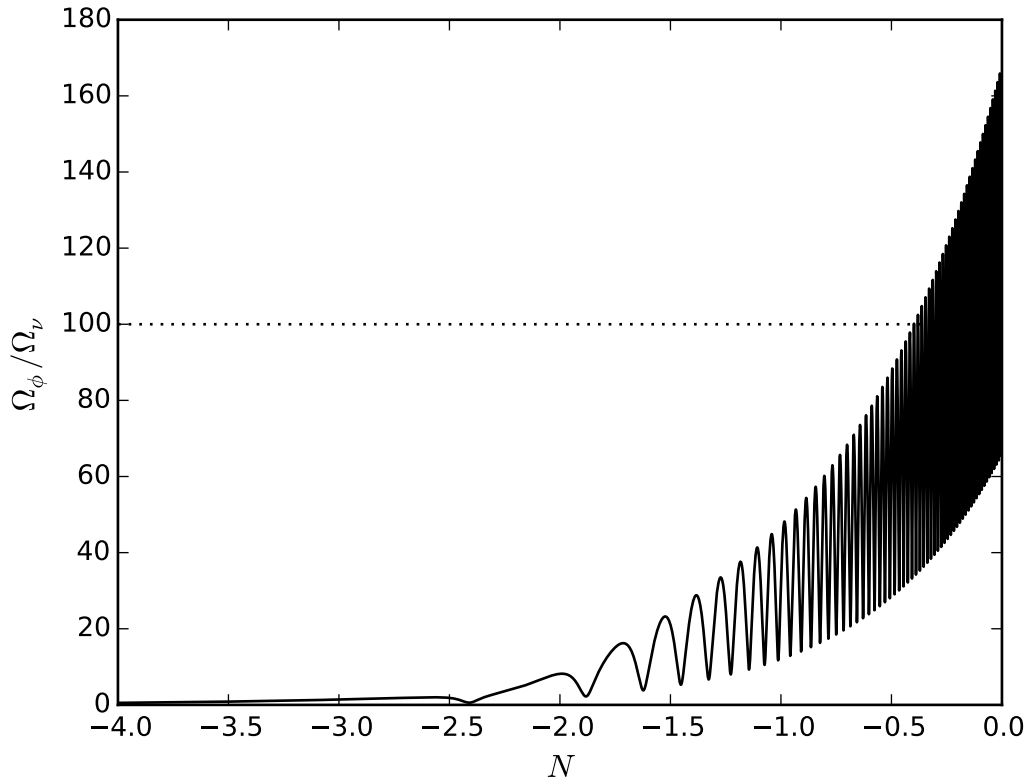


Figure 3.8: The ratio of the energy densities of the scalar field and the neutrinos for a constant coupling  $\beta = -100\lambda$ . In the late universe the ratio oscillates around  $|\beta|/\lambda$  as illustrated by the horizontal dotted line.

that goes beyond the background equations studied in Sections 3.3 and 3.4.

In this section I work in the freeze frame of Ref. [216], as introduced in Section 3.2.1. In some sense this is a difficult frame in which to work, since it involves non-minimal couplings to both gravity and matter. However, it has the advantage of making some of the broader features of the Wetterich model more clear, such as the presence and properties of the fixed points [216].

By varying the action in Eq. (3.19) with respect to  $g^{\mu\nu}$  and  $\chi$  respectively one can derive the gravitational field equations:

$$\begin{aligned} \chi^2 \left( R_{\mu\nu} - \frac{1}{2} R g_{\mu\nu} \right) + \nabla_\rho \nabla^\rho \chi^2 g_{\mu\nu} - \nabla_\mu \nabla_\nu \chi^2 \\ + (B - 6) \left( \frac{1}{2} \nabla^\rho \chi \nabla_\rho \chi g_{\mu\nu} - \nabla_\mu \chi \nabla_\nu \chi \right) + \mu^2 \chi^2 g_{\mu\nu} = T_{\mu\nu}, \quad (3.93) \end{aligned}$$

and the scalar field equation:

$$(B - 6)\nabla_\rho\nabla^\rho\chi + \frac{1}{2}B_{,x}\nabla^\rho\chi\nabla_\rho\chi - 2\mu^2\chi + \chi R + q_\chi = 0. \quad (3.94)$$

Substituting the trace of Eq. (3.93) in Eq. (3.94) yields:

$$\nabla_\rho\nabla^\rho\chi + \frac{B_{,x}}{2B}\nabla^\rho\chi\nabla_\rho\chi + \frac{1}{\chi}\nabla^\rho\chi\nabla_\rho\chi + \frac{2}{B}\mu^2\chi = \frac{T_\rho^\rho}{B\chi} - \frac{q_\chi}{B}, \quad (3.95)$$

where  $q_\chi$  is the variation of the matter action with respect to  $\chi$ . In the freeze frame of the Wetterich model,  $q_\chi \neq 0$  and particle masses can be interpreted as varying with time and possibly space.

In order to derive the linearised equations of motion we write  $\chi$  as the sum of a homogeneous background part and a small inhomogeneous perturbation:

$$\chi \rightarrow \bar{\chi} + \delta\chi. \quad (3.96)$$

We write the metric tensor in the conformal Newtonian gauge, allowing perturbations  $\Psi$  and  $\Phi$ :

$$ds^2 = a^2(\tau)[-(1 + 2\Psi)d\tau^2 + (1 - 2\Phi)\delta_{ij}dx^i dx^j], \quad (3.97)$$

(where  $\Psi$  as defined here is not to be confused with the symbol used to denote particle wavefunctions in Section 3.2). The energy–momentum tensor can be written as follows:

$$[T_\nu^\mu] = \begin{bmatrix} -\bar{\rho} - \delta\rho & (\bar{\rho} + \bar{p})v^i \\ -(\bar{\rho} + \bar{p})v_i & (\bar{p} + \delta p)\delta_j^i + \Sigma_j^i \end{bmatrix}, \quad (3.98)$$

where  $\Sigma_j^i$  is the shear stress and  $v_i$  is the fluid velocity.

Substituting Eqs. (3.96) to (3.98) into Eq. (3.93), and separating into time and spatial components of  $\mu$  and  $\nu$ , yields the linearised gravitational field equations. In the equations that follow,  $\bar{B} \equiv B(\bar{\chi})$ ,  $\bar{B}_{,x} \equiv B_{,x}|_{\chi=\bar{\chi}}$ , and dots denote differentiation with respect to conformal time.

We find the 00 component as:

$$\begin{aligned}
 & 3(\mathcal{H}\bar{\chi} + \dot{\bar{\chi}})^2 - \frac{1}{2}\bar{B}\dot{\bar{\chi}}^2 - \mu^2 a^2 \bar{\chi}^2 \\
 & \quad + 6\mathcal{H}^2\bar{\chi}\delta\chi + 6\mathcal{H}\dot{\bar{\chi}}\delta\chi + 6\mathcal{H}\bar{\chi}\dot{\delta\chi} - 6\mathcal{H}\bar{\chi}^2\dot{\Phi} - 6\bar{\chi}\dot{\bar{\chi}}\dot{\Phi} + 2\bar{\chi}^2\Delta\Phi + 6\dot{\bar{\chi}}\dot{\delta\chi} \\
 & - 2\bar{\chi}\Delta\delta\chi - \bar{B}\dot{\bar{\chi}}\dot{\delta\chi} - \frac{1}{2}\bar{B}_{,x}\dot{\bar{\chi}}^2\delta\chi - 2\mu^2 a^2 \Psi\bar{\chi}^2 - 2\mu^2 a^2 \bar{\chi}\delta\chi = \bar{\rho}a^2 + 2\bar{\rho}a^2\Psi + \delta\rho a^2;
 \end{aligned} \tag{3.99}$$

0*i* components:

$$2\bar{\chi}^2(\dot{\Phi}_{,i} + \mathcal{H}\Psi_{,i}) + 2\bar{\chi}\dot{\bar{\chi}}\Psi_{,i} - 2\bar{\chi}\dot{\delta\chi}_{,i} + 2\mathcal{H}\bar{\chi}\delta\chi_{,i} - (\bar{B} - 4)\dot{\bar{\chi}}\delta\chi_{,i} = (\bar{\rho} + \bar{p})v_i; \tag{3.100}$$

*ij* components, trace, background only:

$$-\bar{\chi}^2(2\dot{\mathcal{H}} + \mathcal{H}^2) - 2\bar{\chi}\ddot{\bar{\chi}} - 2\mathcal{H}\bar{\chi}\dot{\bar{\chi}} - \frac{1}{2}(\bar{B} - 2)\dot{\bar{\chi}}^2 + \mu^2 a^2 \bar{\chi}^2 = \bar{p}a^2; \tag{3.101}$$

*ij* components, trace, first order in perturbations:

$$\begin{aligned}
 & - (2\dot{\mathcal{H}} + \mathcal{H}^2)\bar{\chi}\delta\chi - \ddot{\bar{\chi}}\delta\chi - \bar{\chi}\ddot{\delta\chi} - \mathcal{H}\dot{\bar{\chi}}\delta\chi - \mathcal{H}\bar{\chi}\dot{\delta\chi} - \frac{1}{2}(\bar{B} - 2)\dot{\bar{\chi}}\dot{\delta\chi} - \frac{1}{4}\bar{B}_{,x}\dot{\bar{\chi}}^2\delta\chi + \bar{\chi}^2\ddot{\Phi} \\
 & \quad + \bar{\chi}^2(\mathcal{H} + \frac{\dot{\bar{\chi}}}{\bar{\chi}})(\dot{\Psi} + 2\dot{\Phi}) + \frac{1}{3}\bar{\chi}^2\Delta(\Psi - \Phi) + \frac{2}{3}\bar{\chi}\Delta\delta\chi + \mu^2 a^2 \bar{\chi}\delta\chi + \mu^2 a^2 \bar{\chi}^2\Psi \\
 & \quad = \frac{1}{2}\delta p a^2 + \bar{p}a^2\Psi;
 \end{aligned} \tag{3.102}$$

and finally, *ij* components, traceless:

$$\bar{\chi}^2\Phi_{,ij} - \bar{\chi}^2\Psi_{,ij} - 2\bar{\chi}\delta\chi_{,ij} = a^2\Sigma_{ij}; \tag{3.103}$$

The explicit dependence of the matter part of the action on the scalar field is denoted by  $q_\chi$ :

$$q_\chi = -\frac{\rho_m}{\chi} - (2\tilde{\gamma} + 1)\frac{(\rho_\nu - 3p_\nu)}{\chi}, \tag{3.104}$$

which can be expanded to linear order and substituted along with Eqs. (3.96) to (3.98)

into Eq. (3.95) to yield the linearised scalar field equation:

$$\begin{aligned}
 \ddot{\bar{\chi}} + \delta\ddot{\chi} = & -2\tilde{\gamma} \frac{(\bar{\rho}_\nu - 3\bar{p}_\nu)a^2}{\bar{B}\bar{\chi}} - \frac{\dot{\bar{\chi}}^2}{\bar{\chi}} - 2\mathcal{H}\dot{\bar{\chi}} - \frac{\bar{B}_{,x}\dot{\bar{\chi}}^2}{2\bar{B}} + \frac{2\mu^2 a^2 \bar{\chi}}{\bar{B}} \\
 & - 2\tilde{\gamma} \frac{(\delta\rho_\nu - 3\delta p_\nu)a^2}{\bar{B}\bar{\chi}} + \dot{\bar{\chi}}(\dot{\Psi} + 3\dot{\Phi}) + \left[ -4\tilde{\gamma} \frac{(\bar{\rho}_\nu - 3\bar{p}_\nu)a^2}{\bar{B}\bar{\chi}} + \frac{4\mu^2 a^2 \bar{\chi}}{\bar{B}} \right] \Psi \\
 & - \left( 2\mathcal{H} + \frac{2\dot{\bar{\chi}}}{\bar{\chi}} + \frac{\bar{B}_{,x}\dot{\bar{\chi}}}{\bar{B}} \right) \delta\dot{\chi} + \left[ \frac{1}{2} \left( \frac{\bar{B}_{,x}^2}{\bar{B}^2} - \frac{\bar{B}_{,xx}}{\bar{B}} + \frac{2}{\bar{\chi}^2} \right) \dot{\bar{\chi}}^2 \right. \\
 & \left. + 2\tilde{\gamma} \left( \frac{\bar{B}_{,x}}{\bar{B}} + \frac{1}{\bar{\chi}} \right) \frac{(\bar{\rho}_\nu - 3\bar{p}_\nu)a^2}{\bar{B}\bar{\chi}} + \left( -\frac{\bar{B}_{,x}}{\bar{B}} + \frac{1}{\bar{\chi}} \right) 2\frac{\mu^2 a^2 \bar{\chi}}{\bar{B}} + \Delta \right] \delta\chi. \quad (3.105)
 \end{aligned}$$

The explicit dependence of the matter part of the action on the scalar field  $\chi$  results in a modified energy–momentum conservation equation:

$$\nabla_\mu T_\nu^\mu = q_\chi \nabla_\nu \chi. \quad (3.106)$$

Because baryons and dark matter do not interact with the neutrinos, this equation can be separated, allowing us to consider the neutrino fluid equations in isolation:

$$\nabla_\mu T_\nu^{(\nu)\mu} = -(2\tilde{\gamma} + 1) \frac{(\rho_\nu - 3p_\nu)}{\chi} \nabla_\nu \chi, \quad (3.107)$$

which at the background level is simply:

$$\dot{\bar{\rho}}_\nu + 3\mathcal{H}(\bar{\rho}_\nu + \bar{p}_\nu) - (2\tilde{\gamma} + 1)(\bar{\rho}_\nu - 3\bar{p}_\nu) \frac{\dot{\bar{\chi}}}{\bar{\chi}} = 0, \quad (3.108)$$

and at linear order produces:

$$\begin{aligned}
 \delta\dot{\nu} + 3 \left( \mathcal{H} + \frac{(2\tilde{\gamma} + 1)\dot{\bar{\chi}}}{\bar{\chi}} \right) \left( \frac{\delta p_\nu}{\bar{\rho}_\nu} - \frac{\bar{p}_\nu}{\bar{\rho}_\nu} \delta_\nu \right) - 3 \left( 1 + \frac{\bar{p}_\nu}{\bar{\rho}_\nu} \right) \dot{\Phi} \\
 + \left( 1 + \frac{\bar{p}_\nu}{\bar{\rho}_\nu} \right) v_{,i}^i - \frac{(2\tilde{\gamma} + 1)}{\bar{\chi}} \left( 1 - 3\frac{\bar{p}_\nu}{\bar{\rho}_\nu} \right) \delta\dot{\chi} + \frac{(2\tilde{\gamma} + 1)}{\bar{\chi}^2} \left( 1 - 3\frac{\bar{p}_\nu}{\bar{\rho}_\nu} \right) \dot{\bar{\chi}} \delta\chi = 0, \quad (3.109)
 \end{aligned}$$

$$\begin{aligned}
 \left[ \left( 1 + \frac{\bar{p}_\nu}{\bar{\rho}_\nu} \right) v_i \right] \cdot + \mathcal{H} \left( 1 - 3\frac{\bar{p}_\nu}{\bar{\rho}_\nu} \right) \left( 1 + \frac{\bar{p}_\nu}{\bar{\rho}_\nu} \right) v_i + \frac{\delta p_{\nu,i}}{\bar{\rho}_\nu} + \Sigma_{(\nu)i,j}^j \\
 + \left( 1 + \frac{\bar{p}_\nu}{\bar{\rho}_\nu} \right) \Psi_{,i} + \frac{(2\tilde{\gamma} + 1)}{\bar{\chi}} \left( 1 - 3\frac{\bar{p}_\nu}{\bar{\rho}_\nu} \right) \left( \dot{\bar{\chi}} \left( 1 + \frac{\bar{p}_\nu}{\bar{\rho}_\nu} \right) v_i + \delta\chi_{,i} \right) = 0, \quad (3.110)
 \end{aligned}$$

where  $\delta_\nu \equiv \delta\rho_\nu/\bar{\rho}_\nu$  is the neutrino density contrast.

If one neglects the interaction between baryons and photons (which is a reasonable approximation at late times when the photon density is negligible), one can write the matter (baryons and CDM) fluid equations as:

$$\nabla_\mu T_\nu^{(m)\mu} = -(2\tilde{\gamma} + 1)\frac{\rho_m}{\chi}\nabla_\nu\chi, \quad (3.111)$$

giving

$$\dot{\bar{\rho}}_m + 3\mathcal{H}\bar{\rho}_m - (2\tilde{\gamma} + 1)\bar{\rho}_m\frac{\dot{\bar{\chi}}}{\bar{\chi}} = 0, \quad (3.112)$$

at the background level and

$$\dot{\delta}_m - 3\dot{\Phi} + v_{,i}^i - \frac{\dot{\delta}\chi}{\bar{\chi}} + \frac{\dot{\bar{\chi}}\delta\chi}{\bar{\chi}^2} = 0, \quad (3.113)$$

$$\dot{v}_i + \mathcal{H}v_i + \Psi_{,i} + \frac{\dot{\bar{\chi}}v_i + \delta\chi_{,i}}{\bar{\chi}} = 0, \quad (3.114)$$

to linear order in perturbations. The photons do not couple to the scalar field and their fluid equations are not modified.

Equations (3.99), (3.100), (3.102), (3.103), and (3.105) have been confirmed against a set of gauge-invariant equations [219]. We then translated the gauge-invariant equations into the synchronous gauge and replaced the corresponding equations in `CAMB` with our modified ones. Unfortunately we were unable to produce a fully functional modified version of the code, possibly due to divergences caused by nonlinearities in the neutrino perturbations. Upon a more detailed study of the literature, especially Ref. [213], we concluded that the presence of non-linear neutrino lumps in growing neutrino quintessence models would render our linear approach unable to provide useful insight. This motivated us to pursue the Einstein-frame background analysis presented in Sections 3.3 and 3.4.

## 3.6 Discussion

Growing neutrino quintessence models offer an elegant solution to the coincidence problem by allowing dark energy domination to be triggered by the neutrinos becoming non-relativistic. Soon after the mechanism was proposed, however, it was found

that it led to an attractive fifth force acting on the neutrinos. This force, mediated by the quintessence field, is much stronger than gravity and gives rise to non-linear neutrino lumps on large scales. Most of the research that has gone into GNQ models has focused on the behaviour of these lumps [202–213]. In this work, however, the focus has been on the early dark energy fraction implied by GNQ models.

The model presented in Ref. [216] combines the GNQ mechanism with several other features including inflation. The author carries out an approximate analytic calculation to find the amount of early dark energy predicted by the model and compares it to constraints on early dark energy from the Planck Collaboration. They find a lower bound on the model parameter  $\kappa$ , which controls the scale of the kinetic term, from the early dark energy constraints and an upper bound on the same parameter from their calculation. Intriguingly, these bounds are very close together, meaning that improved measurements of the dark energy fraction present in the early universe could in principle rule out the model (or alternatively find that early dark energy is present, which would be even more exciting). Indeed, in Section 3.4.1 I present an updated lower bound on  $\kappa$  from more recent early dark energy constraints which exceeds the upper bound found in Ref. [216], which on the face of it rules out the model. However, in Section 3.3.1 we have also repeated the approximate analytic procedure of Ref. [216] and found disagreement with their results such that the upper bound on  $\kappa$  is no longer present. We conclude that the model of Ref. [216] is not ruled out by early dark energy constraints.

In addition to carrying out a detailed background analysis, both analytically and numerically on the model in Ref. [216], we have also studied a range of similar GNQ models by varying the kinetic, potential, and neutrino–scalar coupling functions. An analytic solution for the dark energy fraction during radiation and matter domination in the case of an inverse power-law potential is presented in Eq. (3.89), and was confirmed by the numerical analysis presented in Section 3.4.2. However, we found that those models do not give rise to early dark energy, so the constraint we found for the exponential potentials does not apply. Section 3.4.3 discussed the implications of changing the neutrino–scalar coupling function.

We used our background analysis to demonstrate that the following conditions must be met to give rise to growing neutrino quintessence:

- $V(\phi)$  must have a negative gradient in order to cause the value of the scalar

field to increase with time. This gradient must be sufficiently steep that  $\phi$  reaches large enough values in the late Universe to act as dark energy. Note that growing neutrino quintessence models such as the ones considered here do not require that  $V(\phi)$  be flat in the late Universe, as other quintessence models often require. The slow evolution of  $\phi$  necessary for it to mimic a cosmological constant is achieved by the presence of the neutrino coupling term, not by slow roll.

- $|\beta(\phi)|$  must be sufficiently large when the neutrinos become non-relativistic that  $\beta(\rho_\nu - 3p_\nu)$  is able to act as a strong enough restoring force to stop the evolution of  $\phi$  in Eq. (3.9).

Finally, in Section 3.5 I presented the cosmological equations of motion perturbed to linear order for the Wetterich model in the freeze frame. Following this was a discussion of our attempt to implement the equations in a modified version of `CAMB`.

In this chapter I have explored a range of GNQ models using a number of methods, with a particular focus on the model proposed by Wetterich in Ref. [216]. GNQ models have a rich phenomenology and important consequences for the evolution of the universe.

# Chapter 4

## Type 3 interacting dark energy

### 4.1 Introduction

There is still a great deal that is not known about the dark sector of the universe: whether dark energy is dynamical or constant, what kind of particle (if any) is responsible for dark matter and what interactions may occur. As discussed in Chapter 2, the question of whether and how dark energy and dark matter interact with each other has been the subject of extensive study. The most common approach is to introduce an interaction term phenomenologically at the level of the equations of motion, but recently a formalism has been developed for defining the interaction at the level of the action [114]. This formalism results in classification of interacting dark energy into three distinct classes, or ‘Types’. Many previously studied interacting dark energy models were shown to be sub-cases of Type 1, in which the energy density of the dark matter fluid is coupled to functions of the dark energy scalar field  $\phi$ . The other two Types allow couplings between the fluid momentum and the scalar field gradient. In the Type 3 case such couplings are the only interactions allowed, with no energy exchange possible between dark matter and dark energy. The analysis of Ref. [114] found Type 3 models to be less tightly constrained than the other two Types, making them a particularly interesting case to study. Furthermore, Type 3 models have been shown to be able to reconcile tension between early- and late-universe probes of the amount of structure growth in the universe discussed in Chapter 1.

As discussed in Chapter 1, the parameter  $\sigma_8$  is often used to quantify structure formation.  $\sigma_8$  is the amplitude of fluctuations in the matter density on scales that correspond to the size of galaxy clusters. As discussed previously, there are many astrophysical and cosmological probes of  $\sigma_8$ , each with its own challenges and potential sources of error. Very broadly, however, different methods of measuring  $\sigma_8$  can be divided into early- and late-universe probes. Early-universe methods involve constraining cosmological parameters with CMB data and using those to predict

the amount of structure formation in the late universe. This approach requires the use of sophisticated numerical techniques such as Boltzmann codes (described in Section 4.2) to calculate how the universe evolves from the very early universe to the present epoch. Such an approach is highly sensitive to the model one assumes to describe the cosmological evolution. Late-universe probes of  $\sigma_8$ , on the other hand, tend to be less model dependent. These involve counting the galaxy clusters that can be observed, by a variety of techniques from present-day Earth-based observations.

These early- and late-universe probes of  $\sigma_8$  do not agree perfectly, as discussed in Chapter 1. Early-universe predictions of  $\sigma_8$  are larger than the values inferred from cluster counts. Specifically, CMB observations, under the assumption that the cosmological evolution is correctly described by  $\Lambda$ CDM, give  $\sigma_8 = 0.811 \pm 0.006$  [6], while cluster counts from the SZ effect give  $\sigma_8 = 0.77 \pm 0.02$  [102] and weak lensing gives values of  $\sigma_8$  ranging from 0.65 to 0.75 [103–105].

In Ref. [106], it was found that Type 3 coupled quintessence models can alleviate the structure formation tension. The authors noted that this is a particularly exciting result because it is much more common for the introduction of a coupling between dark energy and dark matter to exacerbate the tension. The authors considered a model with the Lagrangian

$$L = \frac{1}{2} \nabla_\mu \phi \nabla^\mu \phi + Ae^{-\lambda\phi/M_{\text{P}}} + \beta_0 Z^2, \quad (4.1)$$

where

$$Z = u^\mu \nabla_\mu \phi \quad (4.2)$$

is the coupling between the CDM momentum and the scalar field gradient and  $\beta_0$  is a dimensionless parameter that determines the strength of the coupling. This is a very simple example of a Type 3 model. As discussed in Chapter 2, it is possible in principle for the Lagrangian to be an arbitrary function of  $\phi$ ,  $Z$  and  $\nabla_\mu \phi \nabla^\mu \phi$ . Even sticking to the canonical form for the kinetic term, there are many possible potential and coupling functions  $V(\phi)$  and  $\gamma(Z)$  one could choose to consider in place of  $Ae^{-\lambda\phi/M_{\text{P}}}$  and  $\beta_0 Z^2$  respectively. Later in this chapter I discuss the implications of introducing a double exponential potential and a more general power-law coupling  $\beta_{n-2} Z^n$ , where  $\beta_{n-2}$  is no longer dimensionless for  $n > 2$ .

The authors of Ref. [106] used a modified version of the Cosmic Linear Aniso-

tropy Solving System (**CLASS**) to numerically solve the system of linear perturbation equations obeyed by a universe in which dark energy is described by the Lagrangian Eq. (4.1). They demonstrated that the effect of the Type 3 coupling on the CMB is not important, modifying  $C_l^{TT}$  at low  $l$  by a few percent depending on the value of  $\beta_0$ , well within the uncertainty due to cosmic variance (left-hand panel of Fig. 2 in Ref. [106]). The matter power spectrum, on the other hand, was found to display a modest suppression with respect to uncoupled quintessence for a wide range of  $\beta_0$  (right-hand panel of Fig. 2 in Ref. [106]). To demonstrate the result more rigorously, the authors carried out a Markov chain Monte Carlo (MCMC) analysis, extracting cosmological parameters for their model from likelihoods provided by Planck TT data [220, 221], baryon acoustic oscillation data from BOSS [222], type 1a supernovas [223], and Planck SZ cluster counts [102, 224]. When Planck SZ cluster data was included, they found the Type 3 model was strongly preferred to  $\Lambda$ CDM, improving the best-fit  $\chi^2$ -value by more than 16.

The work described in this chapter attempts to build on previous work on Type 3 models in three ways:

1. To provide a more detailed physical explanation for why the structure growth suppression discovered by the authors of Ref. [106] is present, with regard to the underlying equations of motion,
2. To carry out an investigation into how sensitive such suppression is to the precise coupling function, by generalising to  $\gamma(Z) = \beta_{n-2}Z^n$  for  $n > 2$ ,
3. To study in detail the dependence of the structure growth suppression on the form of the potential  $V(\phi)$ , including considering double exponential potentials.

Some work has already been done on the second of these. In Ref. [225], the authors considered a coupling of the form  $\gamma(Z) = \beta_1 Z^3$ . The focus of that work was the variable sound speed of dark energy that results from such a coupling. In this work, we are more interested in whether and how such a coupling affects the structure growth suppression studied in detail for the  $n = 2$  case in Ref. [106].

The structure of this chapter is as follows. In Section 4.2, I give a brief overview of the Boltzmann code **CLASS** used in this work, including the underlying perturbation equations and the modifications made by the authors of Ref. [106]. The relevant cosmological evolution equations for the dark energy scalar field and the CDM fluid

in the presence of a Type 3 coupling are laid out in Section 4.2.4. In Section 4.3, I present a physical explanation, by reference to the underlying equations, of the mechanism by which the Type 3 model studied in Ref. [106] brings about suppression of structure growth. In Sections 4.4 and 4.5, I explore how universal the growth suppression is, by generalisation to coupling functions and potentials other than the quadratic coupling and the single exponential potential studied in Ref. [106]. Section 4.6 contains a summary of our main findings, discussion of the limitations of our approach, and an appraisal of possible avenues for future research in this area.

## 4.2 Cosmic Linear Anisotropy Solving System

As discussed in Chapter 1, the evolution of the universe can be approximated as being homogeneous and isotropic by the Friedmann–Lemaître–Robertson–Walker metric. However, since the universe is not perfectly homogeneous and isotropic, one can learn more by allowing for perturbations from this approximation. The simplest extension to the homogeneous background is to allow for linear perturbations. For a complex system such as the universe, in which a large number of particles interact both gravitationally via the Einstein field equations and thermodynamically, even the simple linear approximation is sufficiently involved as to require sophisticated numerical methods.

In the two and a half decades since the pioneering code `COSMICS` was developed for this purpose [226] there have been several publicly available codes released which have tried to solve the linear cosmological equations of motion as efficiently and precisely as possible. Some notable examples are `CMBFAST` [227], `CAMB` [218] and `CMBEASY` [228], collectively referred to as Boltzmann codes. In the work that concerns this chapter, we used the more recent Cosmic Linear Anisotropy Solving System (`CLASS`) [229–232]<sup>10</sup>. In this section I give a brief overview of the equations solved by `CLASS` (and other codes) and how the equations are solved by the code. In what follows I follow Ma and Bertschinger’s seminal work on cosmological perturbation theory [4].

---

<sup>10</sup>available at <http://class-code.net>

### 4.2.1 Equations of motion

The core job of Boltzmann codes is to solve the Einstein equations and the fluid equations. However, before the appropriate equations can even be written down it is necessary to choose a gauge in which to work. The two most common choices are the conformal Newtonian gauge and the synchronous gauge. There are advantages to both gauges, which Ref. [4] elucidates, and CLASS is capable of using either. However, since the present section is not intended as a thorough review of perturbation theory but simply as theoretical background underpinning the work discussed in this chapter, I shall limit my discussion to the synchronous gauge.

The perturbed synchronous gauge metric can be written as follows:

$$ds^2 = a^2(\tau)[-d\tau^2 + (\delta_{ij} + h_{ij})dx^i dx^j], \quad (4.3)$$

where we have assumed zero spatial curvature as discussed in Chapter 1. It is convenient to decompose the metric perturbation  $h_{ij}$  into scalar, vector and tensor parts, since at linear order these three types of perturbation are independent and may be treated separately (at higher orders in perturbation theory there are cross-terms and the scalar, vector and tensor perturbations all affect one another). The way in which this decomposition is typically done is as follows:

$$h_{ij} = h\delta_{ij} + h_{ij}^{\parallel} + h_{ij}^{\perp} + h_{ij}^{\text{T}}, \quad (4.4)$$

where  $h$  is the trace of  $h_{ij}$ , and constitutes one of the two scalar modes,  $h_{ij}^{\parallel}$  represents the other scalar mode, while the vector and tensor modes are  $h_{ij}^{\perp}$  and  $h_{ij}^{\text{T}}$  respectively.  $h_{ij}^{\text{T}}$  is transverse, while the divergences of  $h_{ij}^{\parallel}$  and  $h_{ij}^{\perp}$  are longitudinal and transverse vectors respectively. To make more explicit that  $h_{ij}^{\parallel}$  and  $h_{ij}^{\perp}$  represent scalar and vector modes, they are often written as

$$h_{ij}^{\parallel} = \left( \partial_i \partial_j - \frac{1}{3} \delta_{ij} \nabla^2 \right) \mu, \quad (4.5)$$

$$h_{ij}^{\perp} = \partial_i A_j + \partial_j A_i, \quad \partial_i A^i = 0, \quad (4.6)$$

where  $\mu$  is a scalar and  $A_i$  is a divergenceless vector. All calculations in CLASS are carried out in Fourier space.  $h(\vec{k}, \tau)$  and  $\eta(\vec{k}, \tau)$  are the Fourier transforms of  $h(x_\mu)$  and  $\mu(x_\mu)$  respectively.

Once a gauge is chosen, the Einstein field equations as presented in Chapter 1 can be linearised and written as follows:

$$k^2\eta - \frac{1}{2}\frac{\dot{a}}{a}\dot{h} = 4\pi Ga^2\delta T_0^0, \quad (4.7)$$

$$k^2\dot{\eta} = 4\pi Ga^2(\bar{\rho} + \bar{p})\vartheta, \quad (4.8)$$

$$\ddot{h} + 2\frac{\dot{a}}{a}\dot{h} - 2k^2\eta = -8\pi Ga^2\delta T_i^i, \quad (4.9)$$

$$\ddot{h} + 6\ddot{\eta} + 2\frac{\dot{a}}{a}(\dot{h} + 6\dot{\eta}) - 2k^2\eta = -24\pi Ga^2(\bar{\rho} + \bar{p})\sigma, \quad (4.10)$$

where the energy–momentum tensor  $T_{\mu\nu}$  has been decomposed to linear order as follows:

$$T_0^0 = -(\bar{\rho} + \delta\rho), \quad (4.11)$$

$$T_i^0 = (\bar{\rho} + \bar{p})v_i = -T_0^i, \quad (4.12)$$

$$T_j^i = (\bar{p} + \delta p)\delta_j^i + \Sigma_j^i, \quad (4.13)$$

and the variables  $\vartheta$  and  $\sigma$  are defined as

$$\vartheta \equiv ik^j v_j, \quad (4.14)$$

and

$$(\bar{\rho} + \bar{p})\sigma \equiv -\left(\hat{k}_i\hat{k}_j - \frac{1}{3}\delta_{ij}\right)\Sigma^{ij}, \quad (4.15)$$

where  $\hat{k}$  is the unit vector in the direction of  $\vec{k}$ . As usual, all bars correspond to homogeneous background quantities and dots denote differentiation with respect to conformal time.  $\Sigma_j^i$  is the anisotropic shear stress of the fluid.

The conservation of energy–momentum is implied by the Einstein equations and so is not needed to close the system. However, it is more convenient numerically to employ the fluid equations (derived by linearising energy–momentum conservation) and the first-order Einstein equations, Eqs. (4.7) and (4.8), foregoing the second-order Einstein equations, Eqs. (4.9) and (4.10). The fluid equations are:

$$\dot{\delta} = -(1+w)\left(\vartheta + \frac{\dot{h}}{2}\right) - 3\frac{\dot{a}}{a}\left(\frac{\delta p}{\delta\rho} - w\right)\delta, \quad (4.16)$$

$$\dot{\vartheta} = -\frac{\dot{a}}{a}(1-3w)\vartheta - \frac{\dot{w}}{1+w}\vartheta + \frac{\delta p/\delta\rho}{1+w}k^2\delta - k^2\sigma, \quad (4.17)$$

where  $w \equiv p/\rho$  is the equation of state of the fluid and  $\delta \equiv \delta\rho/\rho$  is the density contrast. Equation (4.16) is often called the ‘continuity equation’ and Eq. (4.17) is the relativistic Euler equation. The above equations are valid for a fluid that has no non-gravitational interactions to other fluids, or for the average of all fluids, but not for individual fluid species that interact non-gravitationally with one another. The most common example is in the early universe when the baryons and photons are tightly coupled. In coupled dark energy models there are also extra terms present in the dark energy and CDM components in Eqs. (4.16) and (4.17). In Type 3 models, the most important extra terms are those introduced to the CDM  $\dot{\vartheta}$  equation.

Considering Eq. (4.17) reveals an important point about the synchronous gauge, which is that for uncoupled cold dark matter, which has zero pressure and anisotropic stress, the velocity of the fluid is equal to zero<sup>11</sup>. In this gauge, the co-ordinates are comoving with the CDM fluid. This ceases to be true if one considers warm or hot dark matter, or if there is a coupling to other species, as in Type 3 models.

## 4.2.2 Boltzmann equation

For some species, especially when interactions are present, it is necessary to go beyond Eqs. (4.16) and (4.17) and consider the Boltzmann equation, which governs the phase-space evolution of the energy–momentum tensor. The energy–momentum tensor can be written as

$$T_{\mu\nu} = \int dP_1 dP_2 dP_3 \frac{1}{\sqrt{-g}} \frac{P_\mu P_\nu}{P^0} f(x^i, P_j, \tau), \quad (4.18)$$

where  $P_\mu$  is the 4-momentum of the particles whose energy–momentum tensor we are interested in and  $f(x^i, P_j, \tau)$  is the distribution of those particles in phase space.  $P_\mu$  has the property that its spatial part is also the conjugate momenta of the phase space. The distribution  $f(x^i, P_j, \tau)$  can be divided into a background part and a perturbed part:

$$f(x^i, P_j, \tau) = f_0(q)[1 + \Psi(x^i, q, n_j, \tau)], \quad (4.19)$$

---

<sup>11</sup>Strictly speaking, Eq. (4.17) implies that  $\vartheta$  for cold dark matter decays exponentially with conformal time. There is, however, a residual gauge freedom in the synchronous gauge, which is normally removed by setting  $\vartheta = 0$  initially, thus giving  $\vartheta = 0$  at all times from Eq. (4.17).

where  $q$  and  $n_j$  are related to  $P_j$  by  $qn_j = ap_j$  and  $P_i = a(\delta_{ij} + h_{ij}/2)p^j$ . The perturbation  $\Psi(x_i, q, n_j, \tau)$  evolves in  $k$ -space according to the Boltzmann equation:

$$\frac{\partial \Psi}{\partial \tau} + i \frac{q}{\epsilon} (\vec{k} \cdot \hat{n}) \Psi + \frac{d \log f_0}{d \log q} \left[ \dot{\eta} - \frac{\dot{h} + 6\dot{\eta}}{2} (\hat{k} \cdot \hat{n})^2 \right] = \frac{1}{f_0} \left( \frac{\partial f}{\partial \tau} \right)_C, \quad (4.20)$$

where  $(\partial f / \partial \tau)_C$  is an interaction term that takes account of collisions experienced by the particles described by  $f$ . The distribution can be related back to the components of the energy–momentum tensor by

$$T_0^0 = -a^{-4} \int q^2 dq d\Omega \sqrt{q^2 + m^2 a^2} f_0(q) (1 + \Psi), \quad (4.21)$$

$$T_i^0 = a^{-4} \int q^2 dq d\Omega q n_i f_0(q) \Psi, \quad (4.22)$$

$$T_j^i = a^{-4} \int q^2 dq d\Omega \frac{q^2 n_i n_j}{\sqrt{q^2 + m^2 a^2}} f_0(q) (1 + \Psi). \quad (4.23)$$

A Boltzmann code such as **CLASS** must solve either the fluid equations, Eqs. (4.16) and (4.17), or the Boltzmann equation, Eq. (4.20), for each individual matter species. A simple species such as cold dark matter requires the solution only of the fluid equations (indeed, only one fluid equation in standard cosmology since  $\vartheta_c = 0$ ) whereas relativistic species such as neutrinos, where higher-order moments such as shear become important, require the solution of the full Boltzmann equation. Baryonic matter has a coupling to photons which results in a Thomson scattering term  $(4\bar{\rho}_\gamma/4\bar{\rho}_b)an_e\sigma_T(\vartheta_\gamma - \vartheta_b)$  being added to the Euler equation. Prior to recombination this term can be very large, resulting in the equations being numerically difficult to solve. In this regime a tight-coupling approximation is adopted, in which the collision time  $\tau_c \equiv (an_e\sigma_T)^{-1}$  is assumed to be very small compared to both  $k^{-1}$  and  $\mathcal{H}^{-1}$ , and a perturbative expansion is carried out in  $\tau_c$ . The photons themselves have perhaps the most involved behaviour of all the species, experiencing collisions with the baryons that depend on the polarisation of the photons. Further, as a relativistic species, the photons exhibit shear and higher-order moments that must be calculated up to a suitable truncation point. I shall not reproduce the full Boltzmann hierarchy for individual species here, instead referring to Ref. [4], where the Boltzmann equations for individual species are laid out in detail both in the synchronous and conformal Newtonian gauges.

### 4.2.3 Implementation in CLASS

In general, Boltzmann codes consist of two stages: first they calculate the time evolution of physical quantities such as the density contrasts of fluid species, and then they use this information to generate manageable and useful data such as power spectrums. In practice, each of these parts typically requires several steps.

**CLASS** is structured in a modular way, consisting of eleven modules that are called in order, with each depending only on earlier modules. I briefly describe the role of each module below; a more detailed overview of the **CLASS** code can be found in Ref. [229].

1. `input.c` interprets the input to **CLASS**, in the form of exactly one `.ini` file and at most one `.pre` file which are specified when running the code. These input files contain information such as cosmological parameters and the desired output spectrums.
2. `background.c` calculates all background quantities by solving the background equations of motion and stores them in an interpolation table for other modules to access.
3. `thermodynamics.c` computes the evolution of thermodynamical quantities, taking account of recombination and reionisation and stores these in an interpolation table. Recombination is solved using code based on **RECFAST** [233] and reionisation is solved using code based on **CAMB** [218].
4. `perturbations.c` solves the fluid equations and Boltzmann equations introduced in Sections 4.2.1 and 4.2.2 to compute the ‘source functions’  $S(k, \tau)$  which are stored in a data structure for use by other modules.
5. `bessel.c` is an entirely geometrical module, calculating spherical Bessel functions.
6. `transfer.c` uses the source functions computed by `perturbations.c` and the Bessel functions computed by `bessel.c` to calculate the ‘transfer functions’  $\Delta_l(k)$ .
7. `primordial.c` computes the primordial power spectrums using simple analytical formulas.

8. `spectra.c` uses the primordial power spectrums, source functions and transfer functions to compute observational power spectrums such as the CMB power spectrum and the matter power spectrum.
9. `nonlinear.c` takes the spectrums computed by `spectra.c` and estimates the non-linear versions of them.
10. `lensing.c` takes the unlensed temperature and polarisation CMB spectrums and uses the CMB lensing potential spectrum to compute lensed CMB spectrums.
11. `output.c` writes the output that has been asked for in `input.c` in data files.

The main improvements that CLASS claims on its predecessors are improved flexibility and user-friendliness due to the modular structure of the code, making it as easy as possible to introduce new species or couplings, and three new approximation schemes which result in improved speed and precision. These are: a baryon–photon tight-coupling approximation, an ultra-relativistic fluid approximation and a radiation streaming approximation [230].

#### 4.2.4 Type 3 modification

A Type 3 coupling between dark matter and dark energy requires CLASS to be modified to solve the coupled equations governing the evolution of dark matter and dark energy as opposed to the default uncoupled ones. The following equations, along with their derivation, can be found in Ref. [114]. The background evolution of the CDM energy density remains unmodified as:

$$\dot{\bar{\rho}}_c + 3\mathcal{H}\bar{\rho}_c = 0, \quad (4.24)$$

as does the continuity equation:

$$\dot{\delta}_c = -k^2\theta_c - \frac{1}{2}\dot{h}, \quad (4.25)$$

where the latter equation is obtained by setting  $p = 0$  in Eq. (4.16). We have also replaced  $\vartheta_c$ , which was defined using the conventions of Ref. [4], with  $\theta_c$ , defined

using the conventions of Ref. [114], according to  $\vartheta_c = k^2\theta_c$ . The latter convention will be followed for the remainder of this chapter.

The Euler equation, which was simply  $\theta_c = 0$  without the Type 3 coupling, becomes

$$\dot{\theta}_c + \mathcal{H}\theta_c = \frac{(3\mathcal{H}\gamma_{,Z} + \gamma_{,ZZ}\dot{\bar{Z}})\delta\phi + \gamma_{,Z}\dot{\delta}\phi}{a(\bar{\rho}_c - \bar{Z}\gamma_{,Z})}, \quad (4.26)$$

where subscript comma notation denotes differentiation. The background part of  $Z$  is given by  $\bar{Z} = -\dot{\bar{\phi}}/a$ . The background and perturbed scalar field equations are modified as:

$$(1 - \gamma_{,ZZ})(\ddot{\bar{\phi}} - \mathcal{H}\dot{\bar{\phi}}) + 3a\mathcal{H}(\gamma_{,Z} - \bar{Z}) + a^2V_{,\phi} = 0, \quad (4.27)$$

and

$$(1 - \gamma_{,ZZ})(\delta\ddot{\phi} + 2\mathcal{H}\dot{\delta}\phi) - \gamma_{,ZZZ}\dot{\bar{Z}}\dot{\delta}\phi + (k^2 + a^2V_{,\phi\phi})\delta\phi + \frac{1}{2}(\dot{\bar{\phi}} + a\gamma_{,Z})\dot{h} + ak^2\gamma_{,Z}\theta_c = 0, \quad (4.28)$$

respectively. The equations governing the evolution of the metric perturbations are given by Eqs. (4.7) and (4.8) and are not modified by the introduction of a Type 3 coupling.

The authors of Ref. [106] replaced the default equations in **CLASS** with the above equations. This required defining  $\bar{Z}$ ,  $\dot{\bar{Z}}$  and  $\gamma(Z)$  and its derivatives since these variables do not appear in default **CLASS**. We further modified the code, which the authors of Ref. [106] kindly made available to us, by implementing several more coupling functions,  $\gamma(Z)$ , on top of the quadratic one used in Ref. [106] We also created a simple means by which to add further functions and choose between the ones already implemented. We have used this modified version of **CLASS** to compute the numerical results in this chapter.

### 4.3 Semi-analytic explanation of structure growth suppression

In Ref. [106], it was demonstrated using numerical computation of linear perturbations that a Type 3 coupling of the form  $\gamma(Z) = \beta_0 Z^2$ , with a single exponential potential  $V(\phi) = Ae^{-\lambda\phi/M_{\text{P}}}$  could help to reduce the  $\sigma_8$  tension between the CMB and large-scale structure. In this section I present an analytic explanation for this behaviour.

In broad terms, the Type 3 coupling affects the scalar field evolution, through a term  $(1 - \gamma_{,ZZ})$  multiplying the kinetic term (Eq. (4.27)), and the cold dark matter velocity divergence  $\theta_c$  (Eq. (4.26)). Each of these effects has a small impact on the cold dark matter density contrast  $\delta_c$  (Eq. (4.25)), whose statistical properties are described by the matter power spectrum  $P(k)$  and  $\sigma_8$ .

In order to reduce the  $\sigma_8$  tension between the CMB and large-scale structure, one needs a model which predicts a smaller amplitude of matter fluctuations than  $\Lambda$ CDM does. As will be demonstrated later, the contribution of  $\theta_c$  to  $\delta_c$  in Eq. (4.25) always has the opposite sign to the dominant contribution from the metric perturbation  $h$ . Thus, increasing  $\theta_c$  reduces the absolute value of  $\delta_c$  and so lowers  $\sigma_8$  slightly, providing the basis for the amelioration of the tension.

In this section we fix the potential parameter  $\lambda = 1.22$  and set the scalar field initial conditions as  $\bar{\phi}_{\text{ini}} = 10^{-4}$  and  $\dot{\bar{\phi}}_{\text{ini}} = 0$  following Ref. [106]. CLASS tunes the other potential parameter  $A$  to fix either the present-day Hubble parameter  $H_0$  or the sound horizon at recombination  $\theta_s$  to a desired value. In this section we fix  $H_0 = 67.3 \text{ km s}^{-1} \text{ Mpc}^{-1}$ , which is consistent with recent Planck data [6]. In later sections we fix  $\theta_s = 0.0104$ , since this is more directly and precisely measured by Planck [6], but fixing  $H_0$  allows the structure growth suppression to be more easily understood.

The overall effect of the Type 3 coupling on  $\sigma_8$  is illustrated in Fig. 4.1. The limit as  $\beta_0 \rightarrow 0$  corresponds to uncoupled quintessence. One can see that moderately large values of  $|\beta_0|$  give rise to a reduction in  $\sigma_8$  and hence a suppression of structure growth, while very large  $|\beta_0|$  results in an enhancement of structure growth. Note that we only consider negative values of  $\beta_0$ . This is to avoid a ‘wrong sign’ kinetic term in the scalar field equation as discussed below.

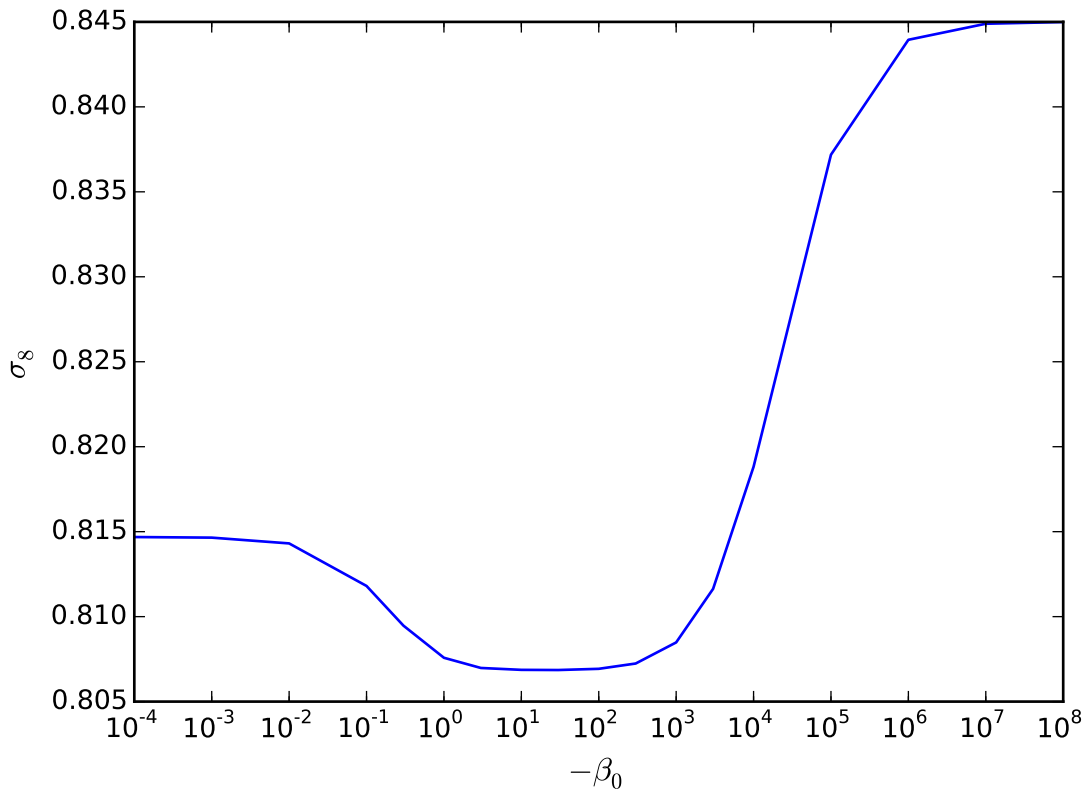


Figure 4.1: The dependence of  $\sigma_8$  on  $\beta_0$ . For moderate values of  $\beta_0$  there is a slight reduction in  $\sigma_8$  relative to uncoupled quintessence (given by the limit of small  $|\beta_0|$ ). For large values of  $|\beta_0|$  we see enhancement of  $\sigma_8$  relative to uncoupled quintessence. The slope of the potential is held fixed at  $\lambda = 1.22$  and the present-day value of the Hubble parameter is held fixed at  $H_0 = 67.3 \text{ km s}^{-1} \text{ Mpc}^{-1}$ .

### 4.3.1 Effect of the coupling on the background evolution of the scalar field

Introducing a coupling between the scalar field and the cold dark matter has an effect on the evolution of both. In the case of Type 3 couplings, the more interesting effect is on the dark matter, but in order to understand this it is first necessary to consider the effect that the coupling has on the scalar field  $\phi$ . Substituting the quadratic coupling  $\gamma(Z) = \beta_0 Z^2$  into the scalar field equation, Eq. (4.27), gives:

$$(1 - 2\beta_0)(\ddot{\phi} + 2\mathcal{H}\dot{\phi}) + a^2 V_{,\phi} = 0. \quad (4.29)$$

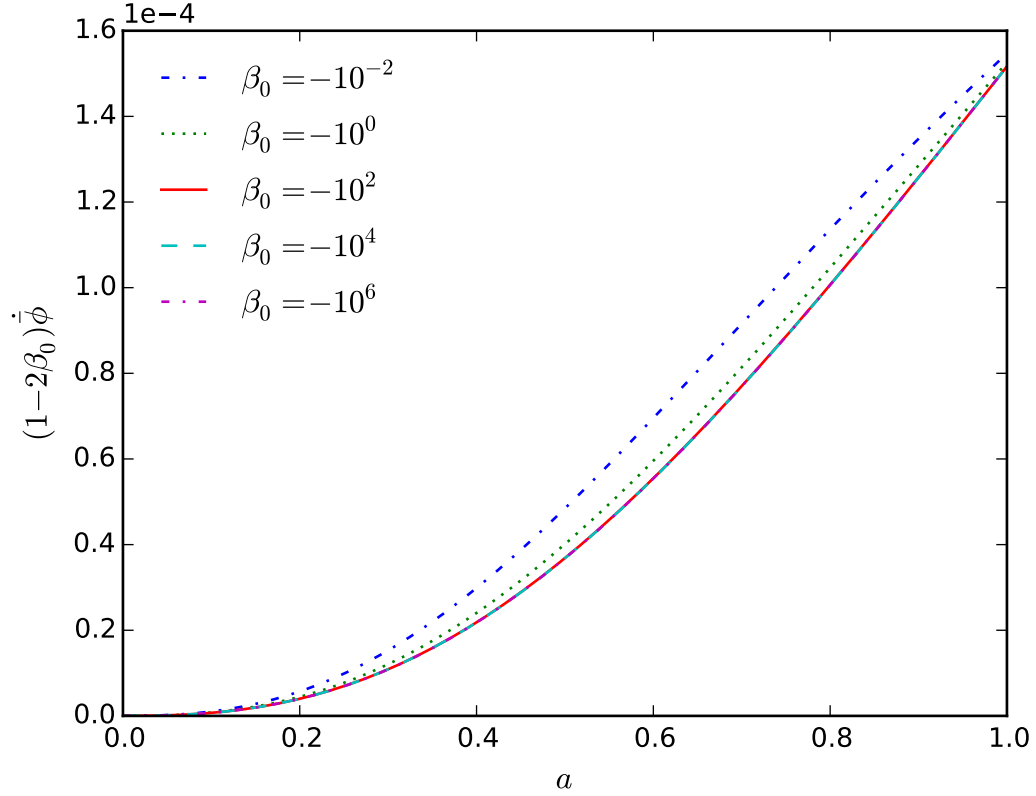


Figure 4.2: The evolution of the time derivative of the background scalar field  $\dot{\bar{\phi}}$  with the scale factor  $a$ , for a range of values of the coupling parameter  $\beta_0$ , with increasing  $|\beta_0|$  from top to bottom. All values of  $\dot{\bar{\phi}}$  have been multiplied by  $(1 - 2\beta_0)$  in order to illustrate the scaling. Without this, the lines would be separated by many orders of magnitude. The fact that the lines do not lie exactly on top of one another is due to the effect of the background expansion rate on the metric perturbation  $h$ , described in Section 4.3.3.2, but this effect is negligible in comparison to the  $(1 - 2\beta_0)$  scaling.  $H_0$  and  $\lambda$  are held fixed as in Fig. 4.1.

One can see immediately that if the coupling parameter gets too large and positive,  $\beta_0 \geq 0.5$ , then the model will have problems. In fact there is a strong coupling problem as  $\beta_0 \rightarrow 0.5$  and a ghost instability for  $\beta_0 > 0.5$  [114]. To be sure of avoiding these problems, we consider only negative values of  $\beta_0$ . As  $\beta_0 \rightarrow 0$  one recovers the case of uncoupled quintessence, and as  $|\beta_0|$  grows, any given point in the potential  $V(\phi)$  will produce a slower evolution of  $\bar{\phi}$ , since the larger the  $(1 - 2\beta_0)$  factor, the smaller  $(\ddot{\bar{\phi}} + 2\mathcal{H}\dot{\bar{\phi}})$  must be for a given  $a^2 V_{,\phi}$ . We predict, therefore, that  $\bar{\phi}$  and its derivatives scale as  $1/(1 - 2\beta_0)$ . This is confirmed by our numerical analysis using CLASS, as demonstrated in Fig. 4.2.

Thus one can see that for very large (negative) values of the coupling parameter  $\beta_0$ , the scalar field evolves more slowly, effectively playing the role of a cosmological constant.

### 4.3.2 Effect of the coupling on the CDM velocity divergence

The CDM velocity divergence  $\theta_c$  evolves according to Eq. (4.26). For a quadratic coupling one obtains

$$\dot{\theta}_c = -\mathcal{H}\theta_c + \frac{-2\beta_0(\ddot{\phi} + 2\mathcal{H}\dot{\phi})\delta\phi - 2\beta_0\dot{\phi}\dot{\delta}\phi}{(\bar{\rho}_c a^2 - 2\beta_0\dot{\phi}^2)}. \quad (4.30)$$

We will now use this equation as the basis for understanding how  $\theta_c$  depends on the coupling on both large and small scales. Figure 4.3 shows the present-day value of  $\theta_c$  as a function of  $\beta_0$  for a range of scales.

#### 4.3.2.1 Large scales

At large scales, small  $k$ , the present-day CDM velocity divergence rises and falls with  $\beta_0$ , with a peak at  $\beta_0 = -10^0$ . Equation (4.30) allows us to explain this behaviour. We established that  $\dot{\phi}$  scales with  $\beta_0$  like  $1/(1 - 2\beta_0)$  in Section 4.3.1. On large scales,  $\delta\phi$  and its derivatives also scale in this way. (See Fig. 4.4.) Thus, every term in the numerator of Eq. (4.30) depends on  $\beta_0$  as  $\beta_0/(1 - 2\beta_0)^2$ , and so does  $\theta_c$  itself. This is illustrated by the solid black line in Fig. 4.3, which is very similar in form to the cyan and magenta lines, demonstrating the scaling on large scales. The denominator of Eq. (4.30) does not play an important role, since the first term is always significantly larger than the second term.

#### 4.3.2.2 Small scales

On small scales, however,  $\delta\phi$  and its derivatives do not depend on  $\beta_0$  (apart from the background effect on the metric perturbation  $h$ , described in Section 4.3.3.2). This is illustrated by the blue line in Fig. 4.4. Thus, the terms in the numerator of Eq. (4.30) scale as  $\beta_0/(1 - 2\beta_0)$  as opposed to  $\beta_0/(1 - 2\beta_0)^2$  as they do for large scales. This scaling is illustrated by the dashed black line in Fig. 4.3, which closely

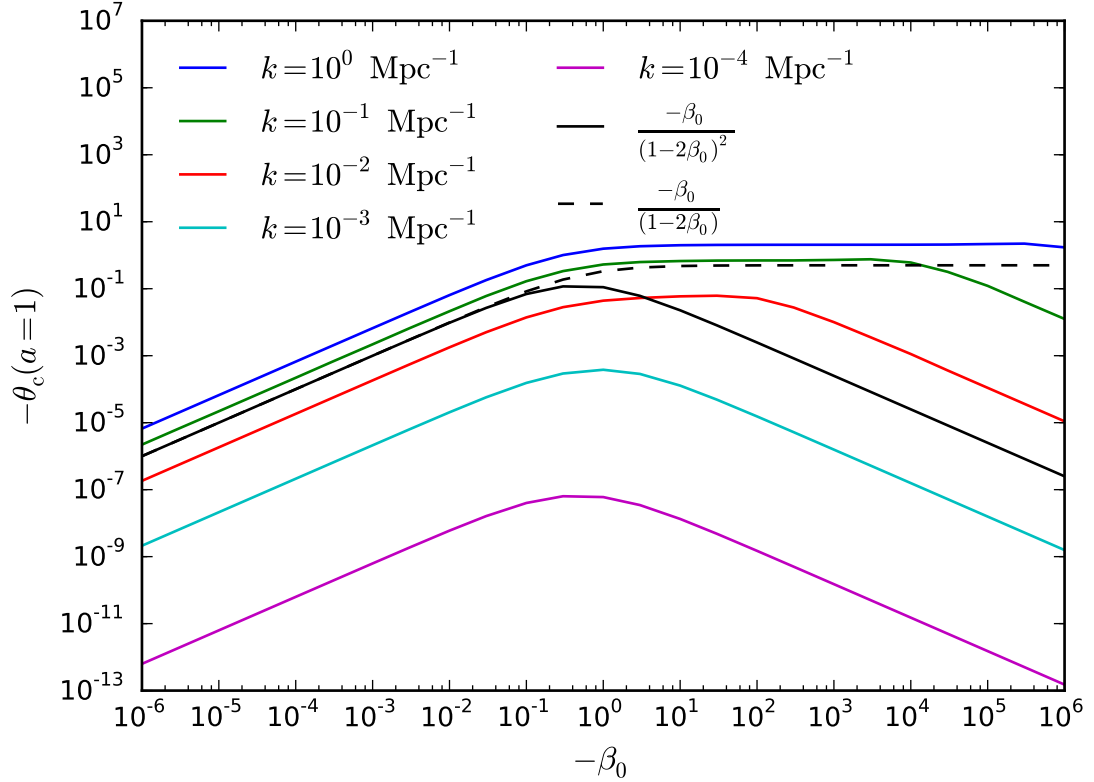


Figure 4.3: The present-day cold dark matter velocity divergence  $\theta_c$  as a function of the coupling parameter  $\beta_0$  for a range of scales  $k$ . For small  $k$  (large scales),  $\theta_c$  scales with  $\beta_0$  as  $\beta_0/(1 - 2\beta_0)^2$  (solid black line). As  $k$  increases, this dependence starts to tend towards  $\beta_0/(1 - 2\beta_0)$  (dashed black line).  $H_0$  and  $\lambda$  are held fixed as in Fig. 4.1.

matches the form of the blue line, which corresponds to very small scales. Note that we cannot necessarily trust the output from CLASS for such very small scales as  $k = 1 \text{ Mpc}^{-1}$  because at these scales perturbations grow large enough that the linear approximation, on which CLASS's calculations are based, breaks down. It is worthwhile to include it, however, because it demonstrates the small-scale limit which is approached even on larger scales where the output of CLASS can be trusted. See for example the green line in Fig. 4.4, which illustrates that for  $k = 10^{-1} \text{ Mpc}^{-1}$ , the scalar field perturbation  $\delta\phi$  is independent of  $\beta_0$  for all but very large values  $|\beta_0| > 10^4$ .

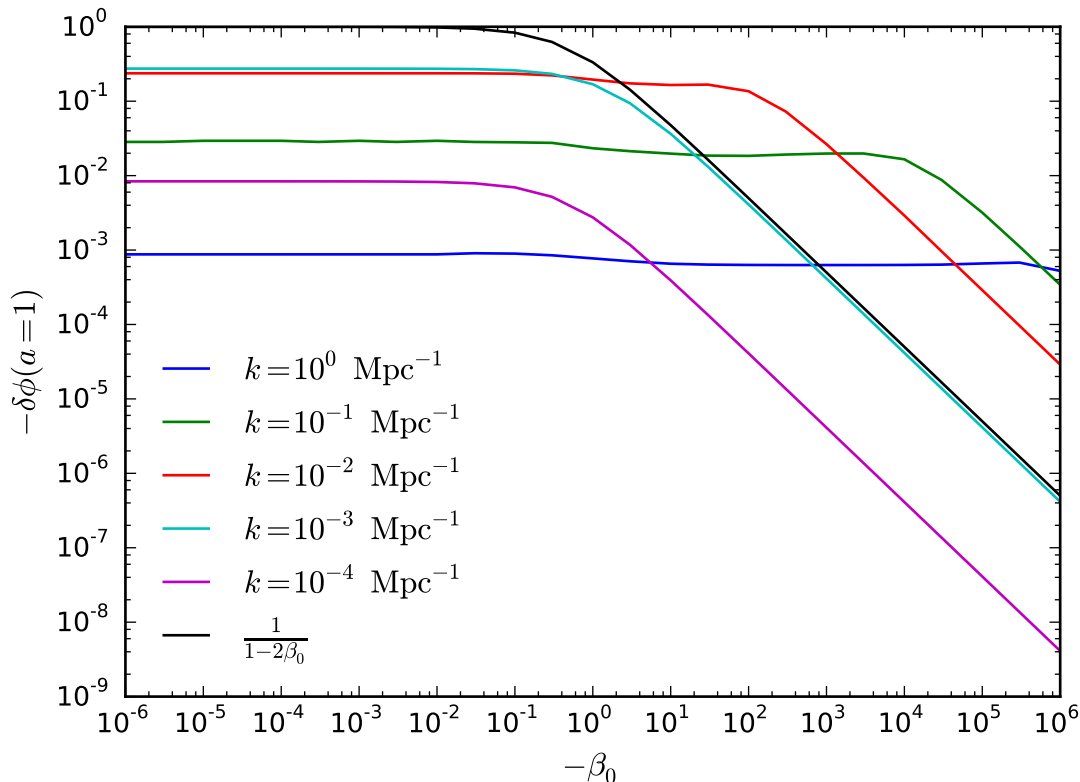


Figure 4.4: The present-day value of the scalar field perturbation  $\delta\phi$  as a function of the coupling parameter  $\beta_0$  for a range of scales  $k$ . For large scales (e.g. magenta line),  $\delta\phi$  scales with  $\beta_0$  as  $1/(1 - 2\beta_0)$  (black line), while for small scales (e.g. blue line),  $\delta\phi$  is approximately constant with  $\beta_0$  (with a very small sigmoid curve due to the effect of the background expansion rate on the metric perturbation  $h$ , described in Section 4.3.3.2).  $H_0$  and  $\lambda$  are held fixed as in Fig. 4.1.

### 4.3.3 Effect of the coupling on the CDM density contrast

As discussed in Section 4.2.4, the evolution equation for the CDM density contrast, Eq. (4.25) is not modified by adding a Type 3 coupling. Both terms in Eq. (4.25) contribute  $\beta_0$  dependence to the CDM density contrast, and for fixed  $H_0$ , as we consider here, the effects are of similar magnitudes. This subsection will demonstrate how the  $\beta_0$  dependence of  $\theta_c$  and  $h$  affects the behaviour of the CDM density contrast.

#### 4.3.3.1 Contribution from CDM velocity perturbations

It turns out that the two terms in Eq. (4.25) have opposite signs, and that the magnitude of the second term is always greater than that of the first (for all  $k$ ).

These two facts, combined with the fact that  $|\delta_c|$  grows with time, mean that the larger the value of  $|\theta_c|$ , the smaller  $|\delta_c|$  will be, because the first term partially cancels the second term. In Section 4.3.2 it was demonstrated that  $|\theta_c|$  took its largest values for moderate values of  $\beta_0$ , with  $\theta_c \rightarrow 0$  for both  $\beta_0 \rightarrow 0$  and  $\beta_0 \rightarrow -\infty$ .

This is the central mechanism by which Type 3 models of coupled quintessence bring about a reduction in the predicted structure formation. Models in which cold dark matter interacts only gravitationally have  $\theta_c = 0$  in the synchronous gauge [4] so the effect from the second term in Eq. (4.25) is maximal. This is true both in  $\Lambda$ CDM and uncoupled quintessence but not when a Type 3 coupling is present. However, before proceeding to show how this affects  $P(k)$  and  $\sigma_8$  it is necessary to discuss the other important mechanism by which the Type 3 coupling affects  $\delta_c$ , which is via the metric perturbation  $h$ .

### 4.3.3.2 Contribution from the metric perturbation

The evolution equation of the metric perturbation  $h$  is not modified by the introduction of a Type 3 coupling, but there is still an indirect dependence which comes about as a result of the modification to the evolution of the background scalar field  $\bar{\phi}$ . Here we will discuss the steps necessary to understand the dependence of  $h$  on the coupling.

**Energy density of the scalar field** The energy density and pressure of the scalar field are given by [114]

$$\bar{\rho}_\phi = \frac{1}{2}(1 - 2\beta_0)\frac{\dot{\bar{\phi}}^2}{a^2} + V(\phi), \quad (4.31)$$

and

$$\bar{p}_\phi = \frac{1}{2}(1 - 2\beta_0)\frac{\dot{\bar{\phi}}^2}{a^2} - V(\phi), \quad (4.32)$$

respectively. The energy density of the scalar field obeys the usual conservation equation

$$\dot{\bar{\rho}}_\phi + 3\mathcal{H}(\bar{\rho}_\phi + \bar{p}_\phi) = 0 \quad (4.33)$$

$$\Rightarrow \dot{\bar{\rho}}_\phi = -3\mathcal{H}(1 - 2\beta_0)\frac{\dot{\bar{\phi}}^2}{a^2}. \quad (4.34)$$

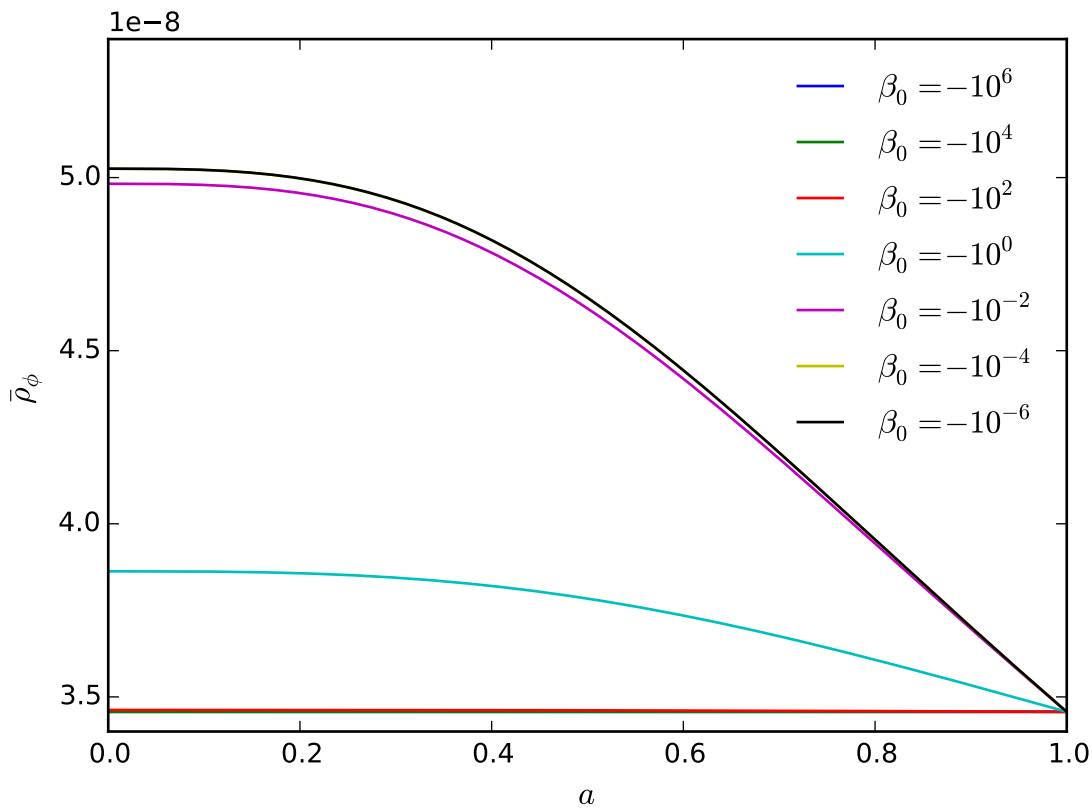


Figure 4.5: The evolution of the background energy density of the scalar field,  $\bar{\rho}_\phi$  for a range of values of the coupling parameter  $\beta_0$ . For large values of  $|\beta_0|$ , the background energy density of the scalar field is approximately constant, while for smaller values of  $|\beta_0|$ , the density drops with time, leading to larger  $\bar{\rho}_\phi$  in the past (assuming the present-day value is fixed). Both effects saturate, leading to a sigmoid curve in  $\beta$ -space.  $H_0$  and  $\lambda$  are held fixed as in Fig. 4.1.

As already established in Section 4.3.1,  $\dot{\phi}$  scales with  $\beta_0$  like  $1/(1 - 2\beta_0)$ , so it follows that  $\dot{\bar{\rho}}_\phi$  also scales as  $1/(1 - 2\beta_0)$ . Thus, for small values of  $|\beta_0|$ ,  $\bar{\rho}_\phi$  can fall with time (as any fluid with  $w > -1$  does as the universe expands), but for large values of  $|\beta_0|$ ,  $\dot{\bar{\rho}}_\phi$  is very small, and  $\bar{\rho}_\phi$  is approximately constant; as alluded to in Section 4.3.1, the scalar field acts like a cosmological constant for very large values of  $|\beta_0|$ . The way in which the evolution of  $\bar{\rho}_\phi$  depends on the coupling parameter  $\beta_0$  is illustrated by Fig. 4.5.

If one chooses to fix the Hubble parameter at the present epoch and assumes a spatially flat universe, then one effectively fixes the energy density of the scalar field at the present epoch (since the energy densities of matter and radiation are well constrained). Thus, if  $\bar{\rho}_\phi$  falls with time (for small  $|\beta_0|$ ), this means that in the

recent past  $\bar{\rho}_\phi$  was larger than it is today. Similarly, if  $\bar{\rho}_\phi$  is constant (for large  $|\beta_0|$ ) then trivially it took its present value in the recent past. Thus, a larger value of  $|\beta_0|$  entails a smaller value of  $\bar{\rho}_\phi$  in the recent past.

**Expansion rate** Via the Friedmann equation,  $\mathcal{H}^2 = \bar{\rho}a^2/(3M_{\text{P}}^2)$ , a larger  $\bar{\rho}_\phi$  gives a larger Hubble parameter. Thus, at some point in the recent past, say  $z = 1$ , small  $|\beta_0|$  gives rise to large  $\mathcal{H}(z = 1)$  and large  $|\beta_0|$  gives rise to small  $\mathcal{H}(z = 1)$ . However, it is not the case that one could in principle raise or lower  $\mathcal{H}(z = 1)$  as much as one wanted by changing the value of  $\beta_0$  because the effect saturates in both directions. As  $|\beta_0| \rightarrow 0$ , the 1 in  $(1 - 2\beta_0)$  becomes dominant and further decreasing  $|\beta_0|$  makes no further difference to  $\mathcal{H}$ . As  $|\beta_0| \rightarrow \infty$ , however,  $\dot{\bar{\rho}}_\phi \rightarrow 0$ ,  $\bar{\rho}_\phi \rightarrow \text{const}$  and increasing  $|\beta_0|$  further makes no difference to  $\mathcal{H}$ . In ‘ $\beta$ -space’,  $\mathcal{H}(z = 1)$  approximates a downwards sigmoid curve<sup>12</sup>.

**Metric perturbation** This small sigmoid curve in the background has a few effects, but the most important is on  $\delta_c$  through the metric perturbation  $h$ , which obeys the standard evolution equation:

$$\dot{h} = \frac{1}{\mathcal{H}} \left( \frac{a^2}{M_{\text{P}}^2} \sum_i \bar{\rho}^{(i)} \delta^{(i)} + 2k^2 \eta \right), \quad (4.35)$$

where the above equation is obtained by re-arranging Eq. (4.7). The conformal time  $\tau$  is not the best time variable to use here, because we wish to compare cases with different expansion histories at a fixed redshift. Working in terms of the scale factor, Eq. (4.35) becomes:

$$\frac{dh}{da} = \frac{1}{a} \frac{1}{\mathcal{H}} \left( \frac{a^2}{M_{\text{P}}^2} \sum_i \bar{\rho}^{(i)} \delta^{(i)} + 2k^2 \eta \right). \quad (4.36)$$

For the purposes of illustrating the effect of the coupling, it suffices to focus on  $\sum_i \bar{\rho}^{(i)} \delta^{(i)}$ , and in particular on the contribution from matter, which is the largest

---

<sup>12</sup>I employ the term ‘sigmoid curve’ in a few instances in this chapter. I use this as a concise way of describing behaviour where one variable depends on another in such a way that the dependent variable asymptotically approaches one value for very small values of the independent variable and another value for very large values of the independent variable. Between these two extremes it varies smoothly over a limited range of the independent variable with no apparent stationary points. I do not mean to imply that the results obey the precise mathematical definition for a sigmoid curve; the term should be taken instead as a qualitative description.

contribution. We then have:

$$\frac{dh}{da} \supset \frac{1}{\dot{a}} \frac{1}{\mathcal{H}} \frac{a^2}{M_{\text{P}}^2} \bar{\rho}_{\text{m}} \delta_{\text{m}}. \quad (4.37)$$

Finally, employing  $\bar{\rho}_{\text{m}} = \bar{\rho}_{\text{m}0} a^{-3}$ , Eq. (4.37) gives

$$\frac{dh}{da} \supset \frac{\bar{\rho}_{\text{m}0} \delta_{\text{m}}}{a^2 \mathcal{H}^2 M_{\text{P}}^2}, \quad (4.38)$$

from which we can conclude that, for a particular redshift in the recent past, a larger value of  $\mathcal{H}$  (which corresponds to small  $|\beta_0|$ ) entails a smaller rate of increase of  $h$ , and hence  $\dot{\delta}_{\text{c}}$  (see Eq. (4.25)). Since the absolute value of  $\delta_{\text{c}}$  grows with time, a smaller gradient in the recent past means a smaller value at the present epoch.

**Summary** Since the dependence of  $\mathcal{H}$  at a particular redshift on  $\beta_0$  was a sigmoid curve, it follows that the background contribution to  $\delta_{\text{c}}$  is also a sigmoid curve in  $\beta_0$ . Large values of  $|\beta_0|$  result in an enhancement of the size of the density contrast relative to uncoupled quintessence.

Figure 4.6 illustrates the two main effects on the evolution of  $\delta_{\text{c}}$  as described above, at a scale  $k = 0.12 \text{ Mpc}^{-1}$ , by displaying the terms in Eq. (4.25) and  $\delta_{\text{c}}/\tau$  itself for comparison. In the early universe both effects are small and none of the terms depend on  $\beta_0$ . However, in the late universe, the metric perturbation  $\dot{h}$  starts to evolve differently for different  $\beta_0$ , with large  $|\beta_0|$  resulting in slightly larger  $|\dot{h}|$ . This plot does not illustrate it, but both of these extremes are ‘plateaus’ in  $\beta$ -space, in the sense that increasing or decreasing  $|\beta_0|$  from its largest or smallest value plotted in Fig. 4.6 respectively does not further shift the extreme values of  $h$ .

At the same time, one can observe  $\theta_{\text{c}}$  starting to contribute at late times, with  $\mathcal{O}(1)$  values of  $\beta_0$  producing the largest effect. The combination of these two contributions can be seen appearing in the  $\delta_{\text{c}}/\tau$  evolution (solid lines), with  $\delta_{\text{c}}(\beta_0 = -10^{-6})$  slightly above  $\delta_{\text{c}}(\beta_0 = -10^6)$  due to the contribution from  $\dot{h}$ , and  $\delta_{\text{c}}(\beta_0 = -10^0)$  coming slightly above both of them due to the contribution from  $\theta_{\text{c}}$ . This ordering is also seen in Fig. 4.7, looking at  $k \approx 10^{-1} \text{ Mpc}^{-1}$ .

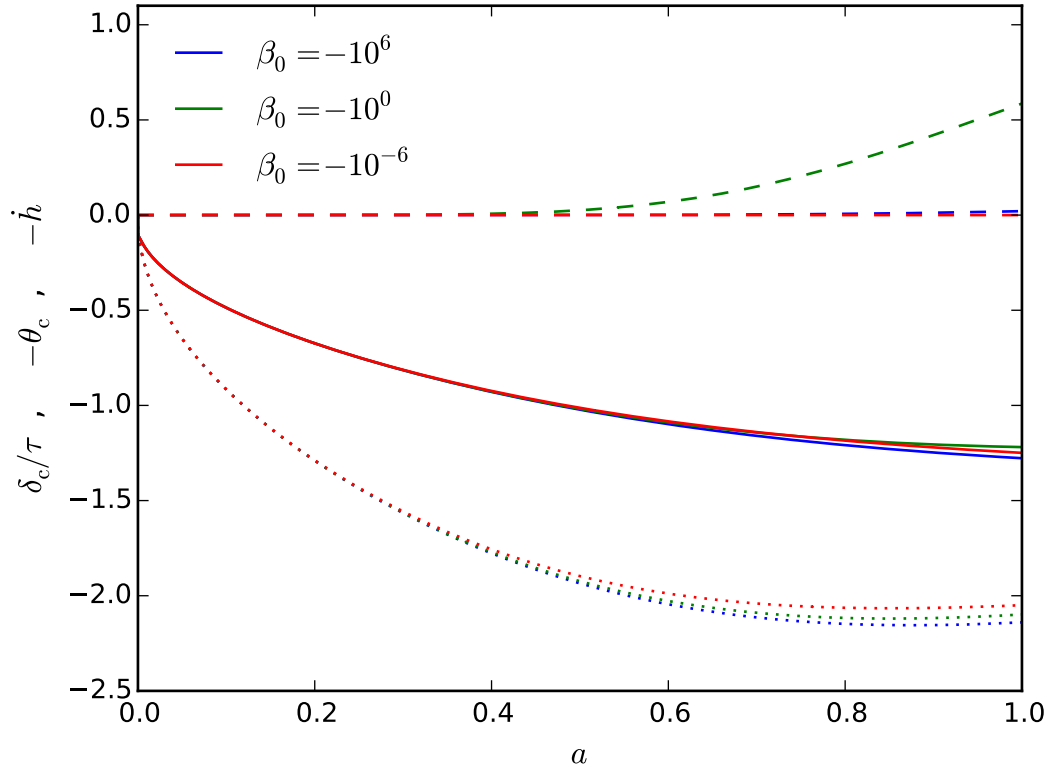


Figure 4.6: The terms of the evolution equation of the CDM density contrast, Eq. (4.25), along with the density contrast itself divided by the conformal time  $\tau$  for comparison (solid lines). The CDM velocity divergence  $\theta_c$  is given by dashed lines and the metric perturbation  $\dot{h}$  is given by dotted lines. In each case we fix  $k = 0.12 \text{ Mpc}^{-1}$ .  $H_0$  and  $\lambda$  are held fixed as in Fig. 4.1.

#### 4.3.4 Effect of the coupling on the matter power spectrum

In order to compare models to observations it is useful to calculate the matter power spectrum  $P(k)$  and its amplitude on the scale of galaxy clusters  $\sigma_8$ .

The matter power spectrum at a time  $t$  is given by

$$P(k, t) = \frac{2\pi^2}{k^3} \delta_m(k, t)^2 \mathcal{P}(k) \quad (4.39)$$

$$= \frac{2\pi^2}{k^3} \delta_m(k, t)^2 A_s \left( \frac{k}{k_*} \right)^{n_s-1}, \quad (4.40)$$

where  $\mathcal{P}(k)$  is the primordial power spectrum  $\mathcal{P}(k) = A_s (k/k_*)^{n_s-1}$ . The present-day matter power spectrum  $P(k, t_0)$  is denoted by  $P(k)$  for compactness. Since the

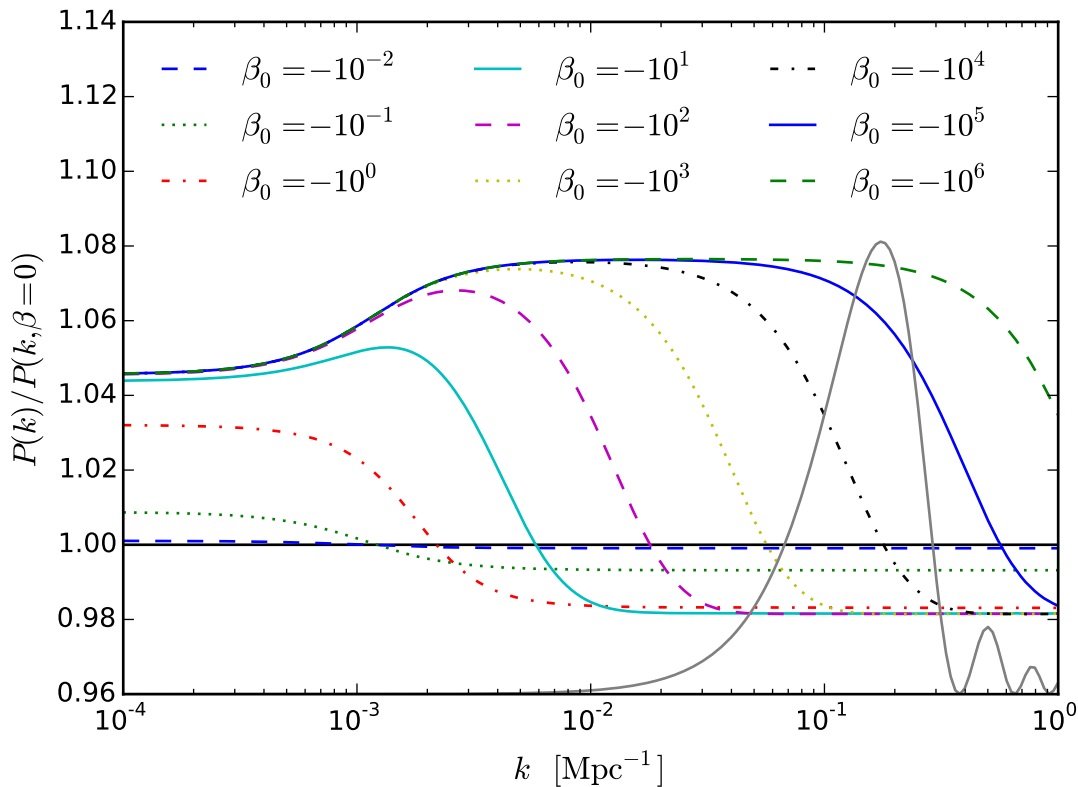


Figure 4.7: Linear matter power spectrum  $P(k)$  for a model with a coupling  $\gamma(Z) = \beta_0 Z^2$  relative to the power spectrum for uncoupled quintessence. The Fourier-transformed window function  $W_8(k)$  has been schematically superimposed as a grey solid line to illustrate the part of  $P(k)$  which is important for the calculation of  $\sigma_8$ . Note that the values on the y-axis do not pertain to the window function.  $H_0$  and  $\lambda$  are held fixed as in Fig. 4.1.

primordial power spectrum is close to being flat, with  $n_s \approx 1$  [6], the matter power spectrum  $P(k)$  derives all its interesting features from the matter density contrast  $\delta_m$ . In the previous section we presented an approximate analytic justification for the behaviour of the CDM density contrast  $\delta_c$ . Due to the gravitational interaction between dark matter and baryons (that is, the rest of the matter), their density contrasts obey  $\delta_c \approx \delta_b \approx \delta_m$  to a very good approximation. Thus, all the physics contained in the matter power spectrum has already been illustrated above. The matter power spectrum is plotted for a range of values of the coupling parameter  $\beta_0$  in Fig. 4.7.

The amplitude of matter fluctuations on the scale of clusters is characterised by

$\sigma_8$ , given by

$$\sigma_8^2 = \frac{1}{2\pi^2} \int P(k)W_8(k)^2 k^2 dk, \quad (4.41)$$

where  $W_8(k)$  is the window function  $W_R(k)$  introduced in Chapter 1, on a scale  $R = 8h^{-1}$  Mpc. This function has been superimposed on the matter power spectrum in Fig. 4.7 to illustrate which parts of  $P(k)$  contribute to the integral in Eq. (4.41).  $\sigma_8$  contains no physical information not already contained in  $P(k)$  but it is a convenient way to quantify structure formation on a physically relevant scale, and is helpful for comparison to observation.

The result found in Ref. [106] that  $\sigma_8$  is suppressed in Type 3 models can now be intuitively understood. Two main effects contribute to the form of the matter power spectrum for Type 3 models. The first is a general enhancement for large  $|\beta_0|$  relative to small  $|\beta_0|$  resulting from the dependence of the metric perturbation  $h$  on the background evolution. The second is a scale-dependent effect due to the CDM velocity divergence  $\theta_c$  that suppresses  $P(k)$  most strongly for intermediate magnitudes of the coupling parameter. These two effects are seen in Fig. 4.7, where the curves corresponding to large  $|\beta_0|$  are above those corresponding to small  $|\beta_0|$  for low  $k$ , but as  $k$  increases each one drops below uncoupled quintessence at a  $k$  that is larger the larger  $|\beta_0|$  is. Thus, any  $|\beta_0|$  that gives suppression of  $P(k)$  on the scales which  $\sigma_8$  samples (i.e. around  $k = 0.1 \text{ Mpc}^{-1}$ ), results in a corresponding suppression of  $\sigma_8$  as shown in Fig. 4.1.

## 4.4 Generalisation of the coupling

Previously we have considered a coupling function of the form  $\gamma(Z) = \beta_0 Z^2$ . One can easily generalise this to couplings of the form  $\gamma(Z) = \beta_{n-2} Z^n$ . Type 3 models with cubic couplings  $\gamma(Z) = \beta_1 Z^3$  have already been considered in Ref. [225], in which the authors demonstrate that Type 3 models in general lead to a varying speed of sound of dark energy, with the  $n = 2$  case discussed in Ref. [106] and above being an exception. However, they also conclude that the impact of the varying sound speed on any cosmological observables is negligible compared to the effects due to the coupling with dark matter. They note that previous work has found that the sound speed of dark energy does not leave any observable fingerprints unless it becomes very small indeed,  $c_s^2 \sim \mathcal{O}(10^{-3})$  [234–237], while the sound speed for a model with a

coupling  $\gamma(Z) = \beta_{n-2}Z^n$  never becomes smaller than  $c_s^2 \rightarrow 1/(n-1)$ . They find that the  $n = 3$  coupling gives qualitatively similar results to the  $n = 2$  case as studied in Ref. [106].

Before embarking on a detailed discussion of the behaviour of general  $n$  couplings, it is worth saying a few words about the dimensions and sign of  $\beta_{n-2}$ . As the coupling function  $\gamma(Z)$  appears as a term in the Lagrangian it must have mass dimension 4. The dimensions of  $Z = u^\mu \nabla_\mu \phi$  are mass-squared, so we can see that for  $\gamma(Z) = \beta_{n-2}Z^n$ ,  $\beta_{n-2}$  must have mass dimension  $-2(n-2)$ . In the CLASS code, the scalar field is in units of the Planck mass and time is in units of Mpc. Thus, in what follows,  $\beta_{n-2}$  will carry units of  $[\text{Mpc}/M_{\text{P}}]^{n-2}$ . Because of the way the coupling adds  $\beta$ -dependent terms to the kinetic part of the Lagrangian, there is always one sign of  $\beta_{n-2}$  that, for large enough  $|\beta_{n-2}|$ , gives rise to a wrong-sign kinetic term and resulting instability. To avoid this, we always choose to only consider  $\beta_{n-2}$  with a sign such that  $\gamma(Z)$  is negative. Since  $Z$  is always negative, this means that if  $n$  is even, we consider negative  $\beta_{n-2}$  and if  $n$  is odd, we consider positive  $\beta_{n-2}$ . In what follows we will for the most part discuss the coupling parameter in terms of its absolute value  $|\beta_{n-2}|$ .

#### 4.4.1 Effect of the coupling on the scalar field evolution

As with the  $n = 2$  case, the CDM density contrast evolves according to Eq. (4.25). The Type 3 coupling impacts the CDM density contrast via both  $\theta_c$  and  $h$ . As with  $n = 2$ , to understand how  $\theta_c$  and  $h$  depend on the coupling, one must understand the scalar field evolution. For a power-law coupling  $\gamma(Z) = \beta_{n-2}Z^n$ , the scalar field equation, Eq. (4.27), is given by

$$[1 - n(n-1)\beta_{n-2}\bar{Z}^{n-2}](\ddot{\bar{\phi}} - \mathcal{H}\dot{\bar{\phi}}) + 3a\mathcal{H}(n\beta_{n-2}\bar{Z}^{n-1} - \bar{Z}) + a^2V_{,\phi} = 0. \quad (4.42)$$

Writing everything in terms of  $\bar{\phi}$  and its derivatives, using  $\bar{Z} = -\dot{\bar{\phi}}/a$ , one obtains

$$\left[1 - n(n-1)\beta_{n-2}\left(-\frac{\dot{\bar{\phi}}}{a}\right)^{n-2}\right]\ddot{\bar{\phi}} + 2\mathcal{H}\dot{\bar{\phi}} + n(4-n)a\mathcal{H}\beta_{n-2}\left(-\frac{\dot{\bar{\phi}}}{a}\right)^{n-1} + a^2V_{,\phi} = 0. \quad (4.43)$$

To understand the way in which the scalar field evolves, it is instructive to consider two limits. First, we take the limit in which  $\dot{\bar{\phi}}$  is very small. The second term in the square bracket becomes negligible, as does the third term of the equation. One finds:

$$\ddot{\bar{\phi}} + 2\mathcal{H}\dot{\bar{\phi}} + a^2V_{,\phi} = 0, \quad (4.44)$$

which is simply the scalar field equation for uncoupled quintessence. For a decaying exponential potential, a scalar field obeying this equation will grow with time, as will its first derivative. Hence, for early times,  $\dot{\bar{\phi}}$  is small and the Type 3 coupling is negligible. As this effectively uncoupled scalar field evolves, however, the coupling will become important and one cannot neglect the two terms omitted above. From Eq. (4.43) it is clear that this will occur earlier in time the larger  $|\beta_{n-2}|$  is. For now let us ignore the intermediate regime in which all terms are important and make the assumption that  $\dot{\bar{\phi}}$  is large, such that  $-n(n-1)\beta_{n-2}(-\dot{\bar{\phi}}/a)^{n-2} \gg 1$ . In this regime, Eq. (4.43) becomes

$$-n(n-1)\beta_{n-2} \left(-\frac{\dot{\bar{\phi}}}{a}\right)^{n-2} \ddot{\bar{\phi}} + n(4-n)a\mathcal{H}\beta_{n-2} \left(-\frac{\dot{\bar{\phi}}}{a}\right)^{n-1} + a^2V_{,\phi} = 0. \quad (4.45)$$

Note that for  $n = 4$  the second term in Eq. (4.45) is equal to zero and therefore one would not neglect the  $2\mathcal{H}\dot{\bar{\phi}}$  term in Eq. (4.43). For our present purposes, however, this distinction is not vital. What is important to note is that, since we are considering the regime where  $-n(n-1)\beta_{n-2}(-\dot{\bar{\phi}}/a)^{n-2} \gg 1$ , Eq. (4.45) predicts a slower evolution of  $\dot{\bar{\phi}}$  and hence  $\bar{\phi}$  due to the large factor multiplying  $\ddot{\bar{\phi}}$ . This is similar to the argument for  $n = 2$ , where the factor multiplying  $\ddot{\bar{\phi}}$  was simply  $-2\beta_0$ , the crucial difference being the time dependence introduced by allowing  $n > 2$ .

Thus, a scalar field coupled to cold dark matter by a Type 3 coupling of the form  $\gamma(Z) = \beta_{n-2}Z^n$  will evolve like an uncoupled quintessence field at early times when  $\dot{\bar{\phi}}$  is small, and then at later times will evolve somewhat slower than an uncoupled field. The time at which this transition takes place is earlier the larger  $|\beta_{n-2}|$  is, and the suppression of the evolution of  $\bar{\phi}$  is larger the larger  $|\beta_{n-2}|$  is. This behaviour is demonstrated in Fig. 4.8, for the  $n = 3$  and  $n = 4$  cases. As with  $n = 2$ , very large values for  $|\beta_{n-2}|$  lead to behaviour that mimics a cosmological constant.

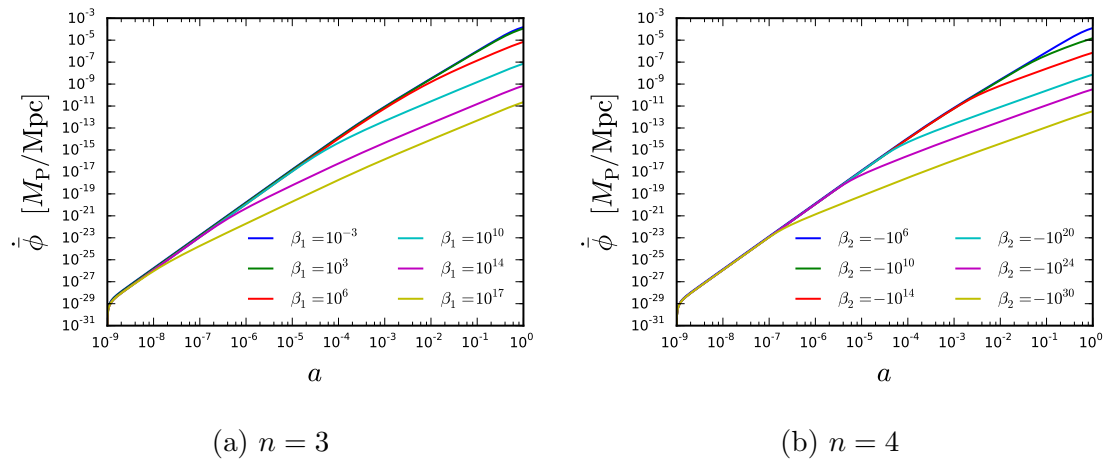


Figure 4.8: The evolution of the conformal time derivative of the scalar field with the scale factor  $a$  for a Type 3 coupling of the form  $\gamma(Z) = \beta_{n-2}Z^n$ , for different values of the coupling parameter  $|\beta_{n-2}|$ . At early times the effect of the coupling is negligible with  $\dot{\phi}$  evolving like an uncoupled scalar field. At later times, sooner the larger  $|\beta_{n-2}|$  is, the coupling becomes important and the scalar field evolves more slowly for large  $|\beta_{n-2}|$ . The slope of the potential is held fixed at  $\lambda = 1.22$  and the sound horizon at recombination is held fixed at  $\theta_s = 0.0104$ . The units of  $\beta_{n-2}$  are  $(\text{Mpc}/M_{\text{P}})^{n-2}$ .

#### 4.4.2 Effect of the coupling on the metric perturbation

The way in which the coupling affects the metric perturbation  $h$  is almost exactly the same for general  $n$  as it was for  $n = 2$  already discussed (see Section 4.3.3.2). To see why this should be the case, recall that the evolution of the metric perturbation is impacted via the scalar field background energy density  $\bar{\rho}_\phi$ . The general  $n$  couplings behave similarly to  $n = 2$  in the late universe, with the differences appearing in the early universe where even large values of the coupling parameter lead to uncoupled quintessence behaviour. Because the scalar field energy density  $\bar{\rho}_\phi$  is only important in the late universe, the Type 3 coupling only affects the metric perturbation  $h$  in the late universe. Hence, the argument presented in Section 4.3.3.2 is valid here.

#### 4.4.3 Effect of the coupling on the CDM velocity divergence

The other important way in which the Type 3 coupling affects the CDM density contrast is via the CDM velocity divergence  $\theta_c$ . For a power-law coupling  $\gamma(Z) =$

$\beta_{n-2}Z^n$ , Eq. (4.26) can be written as:

$$\dot{\theta}_c + \mathcal{H}\theta_c = \frac{n\beta_{n-2}(a^3\bar{Z}^{n-1}\delta\phi)}{a^4(\bar{\rho}_c - n\beta_{n-2}\bar{Z}^n)}. \quad (4.46)$$

As with the  $n = 2$  case, the dependence of the denominator on  $\beta_{n-2}$  is not crucial because  $\bar{\rho}_c$  is always significantly larger than  $n\beta_{n-2}\bar{Z}^n$ . To understand how  $\theta_c$  depends on the coupling parameter, then, it suffices to consider only the numerator.

Recall (Section 4.3.1) the way in which  $\dot{\phi}$  depends on  $\beta_0$  in the  $n = 2$  case:

$$\dot{\phi} \sim \frac{1}{1 - 2\beta_0}. \quad (4.47)$$

In analogy to this one might expect the scaling for general  $n$  to look like

$$\dot{\phi} \sim \frac{1}{1 - n(n-1)\beta_{n-2}\bar{Z}^{n-2}}. \quad (4.48)$$

This relation is of limited use because it contains  $\dot{\phi}$  on both sides (recall  $\bar{Z} = -\dot{\phi}/a$ ). However, as in Section 4.4.1, one can take Eq. (4.48) to two limits. The first is the  $n(n-1)\beta_{n-2}\bar{Z}^{n-2} \ll 1$  limit, where the model behaves like uncoupled quintessence and  $\dot{\phi}$  evolves independently of  $\beta_{n-2}$ . The second is the  $n(n-1)\beta_{n-2}\bar{Z}^{n-2} \gg 1$  limit, where

$$\dot{\phi} \sim \frac{1}{-n(n-1)\beta_{n-2}\bar{Z}^{n-2}}. \quad (4.49)$$

Employing  $\bar{Z} = -\dot{\phi}/a$ , and rearranging,

$$\dot{\phi} \sim |\beta_{n-2}|^{-\frac{1}{n-1}}. \quad (4.50)$$

The derivation of this relation was not at all rigorous, but it turns out to be correct. Numerical evolution of the equations as presented in Fig. 4.8 reveals that for sufficiently large  $|\beta_{n-2}|$  and sufficiently late times,  $\dot{\phi}$  depends on  $\beta_{n-2}$  in a way consistent with Eq. (4.50).

Returning to the  $\theta_c$  equation, Eq. (4.46), it can now be seen that, for sufficiently large  $|\beta_{n-2}|$  and sufficiently late times, the factor  $\beta_{n-2}\bar{Z}^{n-1}$ , should be independent of the coupling parameter  $|\beta_{n-2}|$ . Thus the  $|\beta_{n-2}|$ -dependence of  $\theta_c$  should come primarily from  $\delta\phi$ . However, for sufficiently small values of  $|\beta_{n-2}|$ , Eq. (4.48) tells us that  $\dot{\phi}$  should be independent of  $\beta_{n-2}$  such that the term  $\beta_{n-2}\bar{Z}^{n-1}$  is proportional

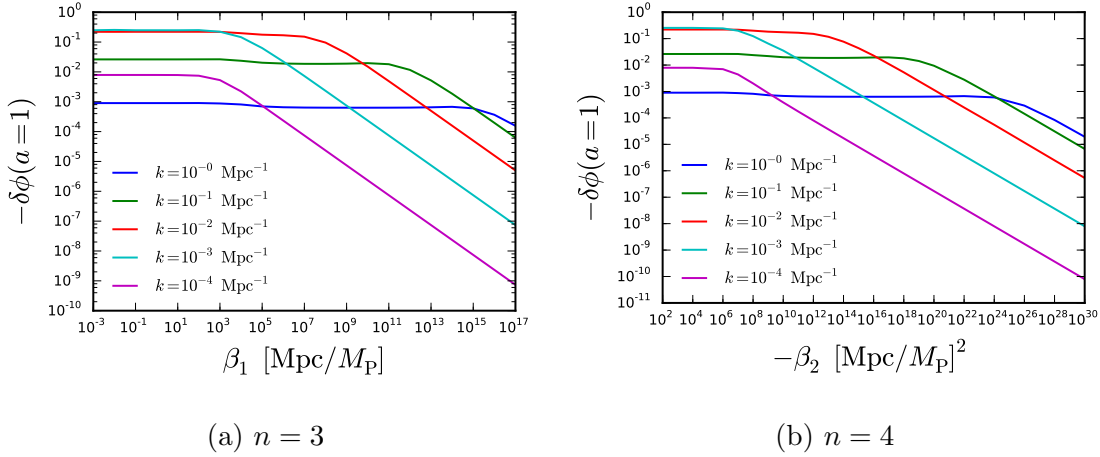


Figure 4.9: The present-day value of the scalar field perturbation  $\delta\phi$  for a Type 3 coupling  $\gamma(Z) = \beta_{n-2}Z^n$  as a function of  $\beta_{n-2}$  for several scales  $k$ . As with the  $n = 2$  case,  $\delta\phi$  is independent of  $|\beta_{n-2}|$  for small  $|\beta_{n-2}|$  and falls with  $|\beta_{n-2}|$  for large  $|\beta_{n-2}|$ . The value of  $|\beta_{n-2}|$  at which the crossover from one regime to the other occurs is larger for small scales.  $\theta_s$  and  $\lambda$  are held fixed as in Fig. 4.8. See Fig. 4.4 for comparison to the  $n = 2$  case.

to to  $\beta_{n-2}$  as the latter becomes small.

To complete the discussion of the dependence of  $\theta_c$  on  $\beta_{n-2}$ , it is necessary to consider the scalar field perturbation  $\delta\phi$ . As with  $n = 2$ , the way in which  $\delta\phi$  depends on  $\beta_{n-2}$  is scale-dependent. Figure 4.9a shows  $\delta\phi$  at the present epoch for  $n = 3$ , as a function of  $\beta_1$  for a range of scales  $k$ . For small  $\beta_1$ ,  $\delta\phi$  is approximately independent of  $\beta_1$ , while for large  $\beta_1$ ,  $\delta\phi \sim \beta_1^{-1/2}$ . For large scales (small  $k$ ) this transition occurs for very small  $\beta_1$  while for small scales (large  $k$ ) the transition occurs for large  $\beta_1$ . Figure 4.9b shows how  $\delta\phi$  depends on  $\beta_2$  for an  $n = 4$  coupling. Again, for small  $|\beta_2|$ ,  $\delta\phi$  is approximately constant with  $\beta_2$ , but for large  $|\beta_2|$ ,  $\delta\phi$  falls as  $|\beta_2|^{-1/3}$ , again, with the transition occurring later in  $|\beta_2|$  on small scales. Note that this is qualitatively similar to how  $\delta\phi$  depends on  $\beta_0$  for the  $n = 2$  coupling as illustrated in Fig. 4.4. For general  $n$ , the scalar field perturbation in the large  $|\beta_{n-2}|$  limit obeys

$$\delta\phi \sim |\beta_{n-2}|^{-\frac{1}{n-1}}, \quad (4.51)$$

which is the same as the late-universe, large  $|\beta_{n-2}|$  dependence of  $\dot{\bar{\phi}}$  as shown in Eq. (4.50).

The discussions above can be combined to explain how the CDM velocity divergence  $\theta_c$  depends on the coupling parameter  $\beta_{n-2}$  for general  $n$ . The general features

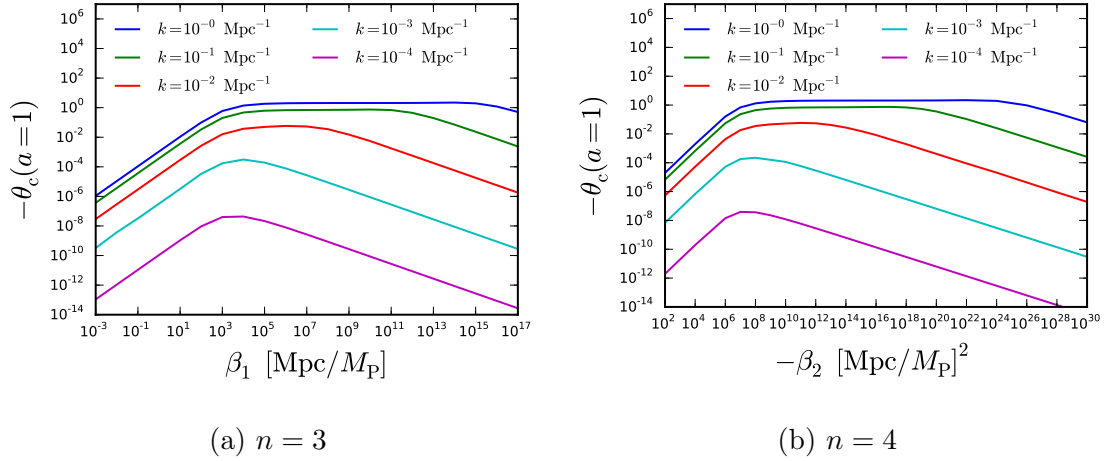


Figure 4.10: The present-day CDM velocity divergence  $\theta_c$  for a Type 3 coupling  $\gamma(Z) = \beta_{n-2}Z^n$  as a function of  $\beta_{n-2}$  for several scales  $k$ . As with the  $n = 2$  case (see Fig. 4.3),  $|\theta_c|$  drops off for both very large and very small values of  $|\beta_{n-2}|$  with a peak at around  $\beta_1 \sim 10^4 \text{ Mpc}/M_P$  for  $n = 3$  and  $\beta_2 \sim -10^8 [\text{Mpc}/M_P]^2$  for  $n = 4$ . As with the  $n = 2$  case, the peak is broader and flatter on small scales.  $\theta_s$  and  $\lambda$  are held fixed as in Fig. 4.8.

are as follows: for very small  $|\beta_{n-2}|$ ,  $\theta_c$  will be approximately proportional to  $\beta_{n-2}$  due to both  $\dot{\phi}$  and  $\delta\phi$  being approximately constant with  $\beta_{n-2}$  in this regime. For very large  $\beta_{n-2}$ ,  $\theta_c$  will fall as  $\beta_{n-2}^{-1/(n-1)}$ , since this is how  $\delta\phi$  depends on  $\beta_{n-2}$ , while the  $\beta$ -dependence of  $\dot{\phi}^{n-1}$  is cancelled out by the factor of  $\beta_{n-2}$  on the numerator of Eq. (4.46). Between these two regimes,  $\theta_c$  will have a broad peak whose breadth will be larger for small scales than for large scales due to the scale-dependence of the crossover in  $\delta\phi(\beta)$ . These features can be seen in Fig. 4.10 for the  $n = 3$  and  $n = 4$  cases. Again, the  $\theta_c$  dependence on  $\beta_{n-2}$  is qualitatively similar to the  $n = 2$  case, but it should be noted that there is an extra time dependence present for  $n > 2$  couplings due to the  $\beta$ -dependence of the time at which the coupling effectively ‘switches on’ described in Section 4.4.1 and illustrated in Fig. 4.8. In terms of  $\theta_c$ , the position of the peak in Fig. 4.10 moves to the left with time. In other words, in the early universe, large values of  $\beta_1$  produce maximal  $\theta_c$ , while in the late universe, relatively small  $\beta_1$  maximise  $\theta_c$ . It turns out that this time dependence does not significantly affect cosmological observables, however, because the impact of the Type 3 coupling is only manifest on late-universe features, such as large-scale structure.

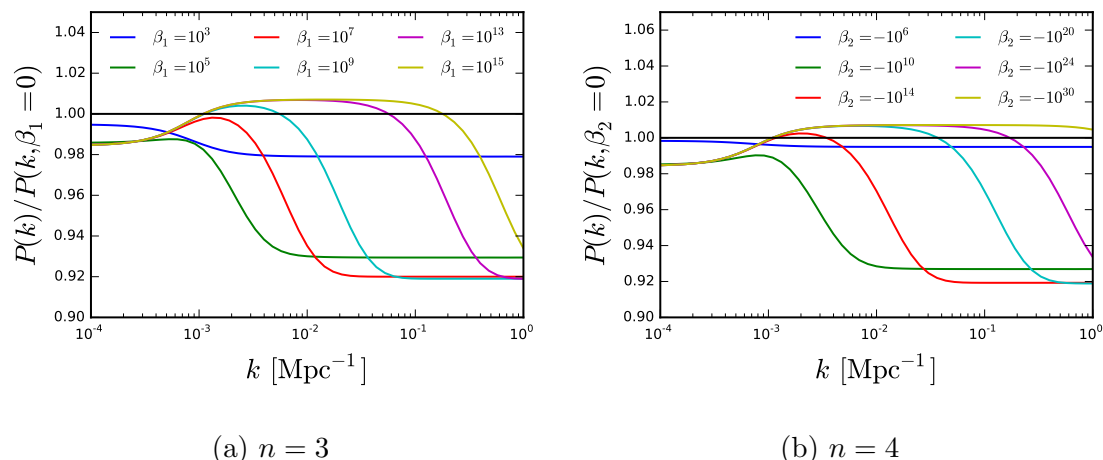


Figure 4.11: The linear matter power spectrum  $P(k)$  for a Type 3 model with a coupling  $\gamma(Z) = \beta_{n-2}Z^n$  normalised to the matter power spectrum of uncoupled quintessence. The units of  $\beta_{n-2}$  are  $(\text{Mpc}/M_{\text{P}})^{n-2}$ . As with the  $n = 2$  case (Fig. 4.7), small values of the coupling parameter  $|\beta_{n-2}|$  give rise to small suppression of  $P(k)$ , while large values result in enhancement that extends to smaller scales the larger  $|\beta_{n-2}|$  is.  $\theta_s$  and  $\lambda$  are held fixed as in Fig. 4.8.

#### 4.4.4 Summary

In this section we have considered more general power-law Type 3 couplings than the simple quadratic case explored in Section 4.3. Qualitatively, the impact of the coupling on structure formation is the same for general  $n$  as for  $n = 2$ . This is confirmed by the results illustrated in Figs. 4.11 and 4.12; large  $|\beta_{n-2}|$  gives rise to behaviour similar to  $\Lambda\text{CDM}$ , with a large value of  $\sigma_8$ , while intermediate values of  $|\beta_{n-2}|$  result in  $\sigma_8$  being even smaller than the uncoupled quintessence case, seen in the  $|\beta_{n-2}| \rightarrow 0$  limit.

We can conclude from this that the tendency for Type 3 coupled quintessence models to give rise to a reduction in the late-universe structure formation is a rather generic one, applying for all power-law couplings  $\gamma(Z) = \beta_{n-2}Z^n$ . This section has omitted discussion of any couplings not of this power-law form. One reason for this is that the more contrived the coupling we wish to consider the harder it may be to physically motivate. As we have seen, there is no necessity to contrive a particular form of the coupling, since even the simplest, quadratic coupling gives rise to interesting physical behaviour.

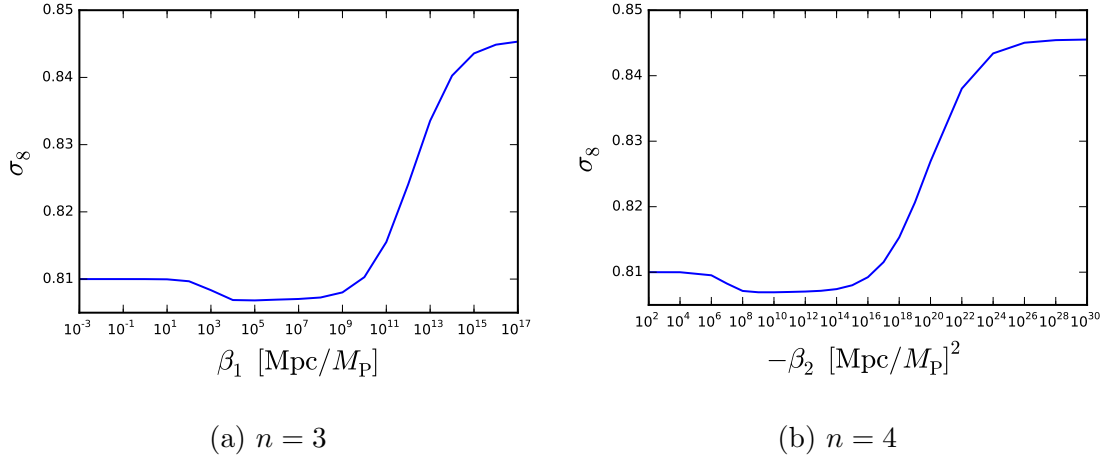


Figure 4.12: The amplitude of matter fluctuations  $\sigma_8$  for a Type 3 coupling with  $\gamma(Z) = \beta_{n-2}Z^n$  as a function of  $\beta_{n-2}$ . As with  $n = 2$  (Fig. 4.1), there is slight suppression relative to uncoupled quintessence for intermediate values of  $|\beta_{n-2}|$ , while large values give rise to enhancement.  $\theta_s$  and  $\lambda$  are held fixed as in Fig. 4.8.

## 4.5 The role of the scalar field potential

The preceding sections have focused on investigating the effect of changing the coupling function  $\gamma(Z)$ , while keeping the potential  $V(\phi) = Ae^{-\lambda\phi/M_P}$  fixed. This section considers the potential in more detail. In the interest of clarity, we shall return to a quadratic coupling:  $\gamma(Z) = \beta_0 Z^2$ .

As discussed in Chapter 2, the parameter  $\lambda$  is constrained in uncoupled quintessence by  $\lambda^2 < 2$  in order to give rise to accelerated expansion [113]. If  $\lambda$  is too large, the potential is so steep that  $\dot{\phi}$  becomes large and the equation of state of the universe is significantly larger than  $-1$ . However, for Type 3 couplings, this requirement is relaxed. As demonstrated in Section 4.3.1, a large value of  $|\beta_0|$  acts somewhat like a friction term, limiting how quickly  $\bar{\phi}$  can evolve.

In this section we shall demonstrate that larger values of  $\lambda$  can give rise to even greater suppression of structure growth than has already been demonstrated. Combined with the possibility of using the Type 3 coupling to slow the evolution of the scalar field, this hints at even greater prospects for Type 3 models to ease the  $\sigma_8$  tension than has previously been realised.

### 4.5.1 Field redefinition relating potential and coupling

Type 3 couplings of the form  $\gamma(Z) = \beta_0 Z^2$  have the property that, at the background level, the coupling simply gives rise to a modified kinetic term in the scalar field equation. For a single exponential potential, the background scalar field obeys

$$(1 - 2\beta_0)(\ddot{\bar{\phi}} + 2\mathcal{H}\dot{\bar{\phi}}) - a^2 A \lambda e^{-\lambda\bar{\phi}/M_{\text{P}}} = 0. \quad (4.52)$$

The dependence on the coupling can be recast from the kinetic term to the potential term by a field redefinition:

$$\psi = (1 - 2\beta_0)^{\frac{1}{2}} \phi, \quad (4.53)$$

giving

$$(1 - 2\beta_0)^{\frac{1}{2}}(\ddot{\psi} + 2\mathcal{H}\dot{\psi}) - a^2 A \lambda \exp\left[-\frac{\lambda\bar{\psi}}{(1 - 2\beta_0)^{\frac{1}{2}} M_{\text{P}}}\right] = 0. \quad (4.54)$$

Defining a new potential constant

$$\tilde{\lambda} = \lambda(1 - 2\beta_0)^{-\frac{1}{2}}, \quad (4.55)$$

Eq. (4.54) takes the form of an uncoupled scalar field:

$$\ddot{\bar{\psi}} + 2\mathcal{H}\dot{\bar{\psi}} - a^2 A \tilde{\lambda} e^{-\tilde{\lambda}\bar{\psi}/M_{\text{P}}} = 0, \quad (4.56)$$

where the slope of the potential is reduced by a factor of  $(1 - 2\beta_0)^{1/2}$  compared to the case with no coupling,  $\beta_0 = 0$ . Thus one can see that potentials with a slope  $\lambda$  so large as to cause problems in the background evolution for uncoupled quintessence can be ‘saved’ by a Type 3 coupling with sufficiently large  $|\beta_0|$ . The usual quintessence constraint that  $\lambda^2 < 2$  here applies not to  $\lambda$  but to  $\tilde{\lambda}$ .

As discussed in Section 4.4, there is a qualitatively similar picture for couplings with  $n > 2$ , with larger  $|\beta_{n-2}|$  slowing the background scalar field evolution. However, when  $n > 2$  the scalar field equation is non-linear in  $\dot{\bar{\phi}}$ , so the above field redefinition argument does not apply. Increasing  $|\beta_{n-2}|$  does indeed slow the evolution of  $\bar{\phi}$  but it is not obviously equivalent at the background level to a reduction of the slope of the potential as in the  $n = 2$  case.

## 4.5.2 Effect of changing the slope of a single exponential potential

In Section 4.5.1 we demonstrated a simple relationship between the coupling parameter  $\beta_0$  and the potential parameter  $\lambda$  at the level of the background scalar field equation. However, that argument revealed nothing about the behaviour of the perturbations. We ran CLASS for a range of values of  $\lambda$  and  $\beta_0$  in order to analyse this.

Figure 4.13 shows the value of  $\sigma_8$  as a function of  $\beta_0$  for a range of  $\lambda$ . It can be seen that steeper potentials can give rise to very large suppression of structure growth. Note that for very large  $|\beta_0|$  all potentials give rise to the same  $\sigma_8$  as they all approach the  $\Lambda$ CDM limit. For very small  $|\beta_0|$ , uncoupled quintessence is approached and the steeper potentials are not viable as they give rise to too rapid an evolution of  $\bar{\phi}$ . This is the reason for the lines corresponding to large  $\lambda$  stopping as  $|\beta_0|$  is reduced. Figure 4.14 shows the present-day value of the Hubble parameter  $H_0$  dropping rapidly as  $|\beta_0|$  is reduced. The CLASS code returns an error if  $H_0 < 30 \text{ km s}^{-1} \text{ Mpc}^{-1}$ .

Even small decreases in  $H_0$  are problematic. I discussed in Chapter 1 that late-universe probes of the present-day Hubble parameter give a larger value than early-universe probes (see Ref. [88] and references therein), so if  $H_0$  is reduced the tension is exacerbated. However, looking at both Figs. 4.13 and 4.14 together, one can see that there is a region of parameter space where  $\sigma_8$  can be reduced without paying the price of reducing  $H_0$ , for example  $\lambda = 3$ ,  $\beta_0 = -10^2$ .

This result tentatively suggests that the prospects for Type 3 models to reconcile early- and late-universe measurements of structure formation may be even greater than previously realised. The remainder of this section will explore the mechanism by which this behaviour comes about.

### 4.5.2.1 Background

The way in which  $\lambda$  and  $\beta_0$  affect the Hubble parameter is straightforward. It has already been argued in Section 4.3.3.2 that a larger  $|\beta_0|$  gives rise to a smaller  $\dot{\bar{\phi}}$  and hence a more constant  $\bar{\rho}_\phi$ , whereas a smaller  $|\beta_0|$  allows  $\bar{\phi}$  to evolve and hence  $\bar{\rho}_\phi$  do drop to smaller values. Via the Friedmann equation this results in a smaller

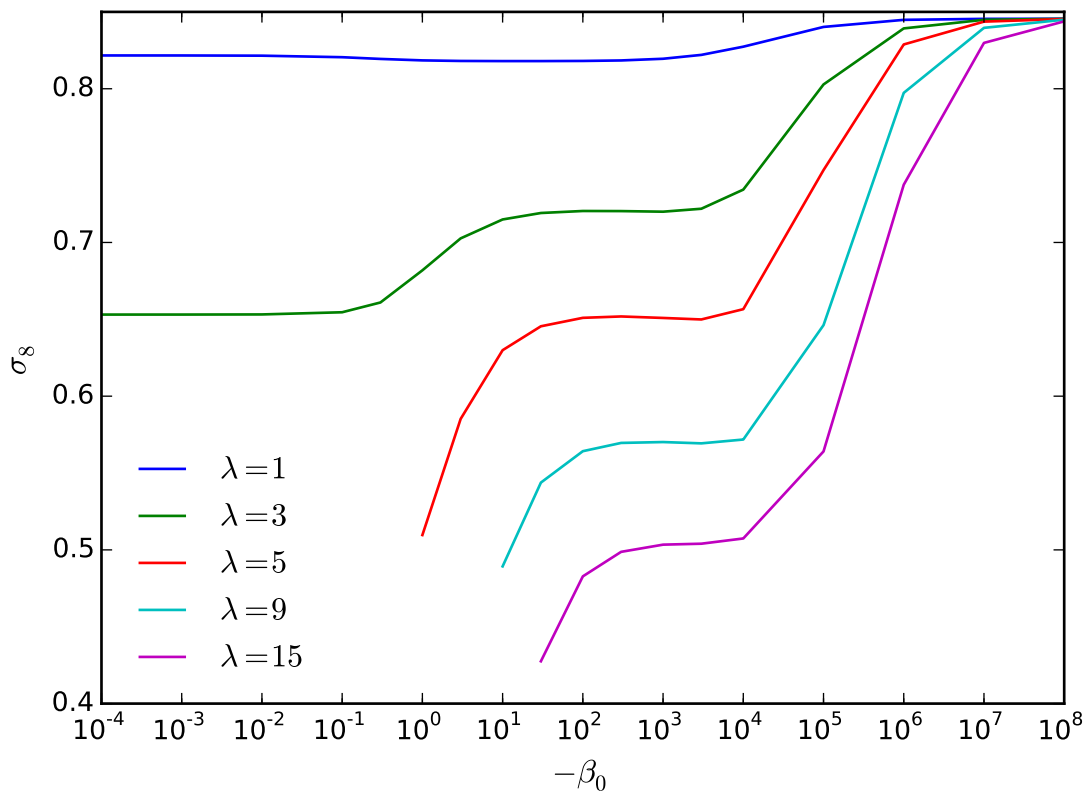


Figure 4.13: The amplitude of matter fluctuations  $\sigma_8$  as a function of the coupling parameter  $|\beta_0|$  for a range of potential parameters  $\lambda$  for a quadratic coupling function  $\gamma(Z) = \beta_0 Z^2$  and an exponential potential  $V(\phi) = Ae^{-\lambda\phi/M_{\text{Pl}}}$ . The sound horizon at recombination is held fixed at  $\theta_s = 0.0104$ .

value of the Hubble parameter in the present epoch<sup>13</sup>. Increasing  $\lambda$  has a similar effect to decreasing  $|\beta_0|$ ; increasing the slope of the potential results in a more rapid evolution of  $\bar{\phi}$  and so a drop in the energy density  $\bar{\rho}_\phi$  and a smaller present-day Hubble parameter. The reduction in  $H_0$  shown in Fig. 4.14 for small  $|\beta_0|$  and large  $\lambda$  is entirely due to this effect. Figure 4.15 illustrates that the present-day value of the energy density  $\bar{\rho}_\phi$  is decreased both for large  $\lambda$  and small  $|\beta_0|$ .

<sup>13</sup>In Section 4.3.3.2 the present-day Hubble parameter was fixed and we considered changes to  $\mathcal{H}$  in the recent past. Here we fix the sound horizon at recombination,  $\theta_s$  so the present-day Hubble parameter is affected by the choice of  $\beta_0$ .

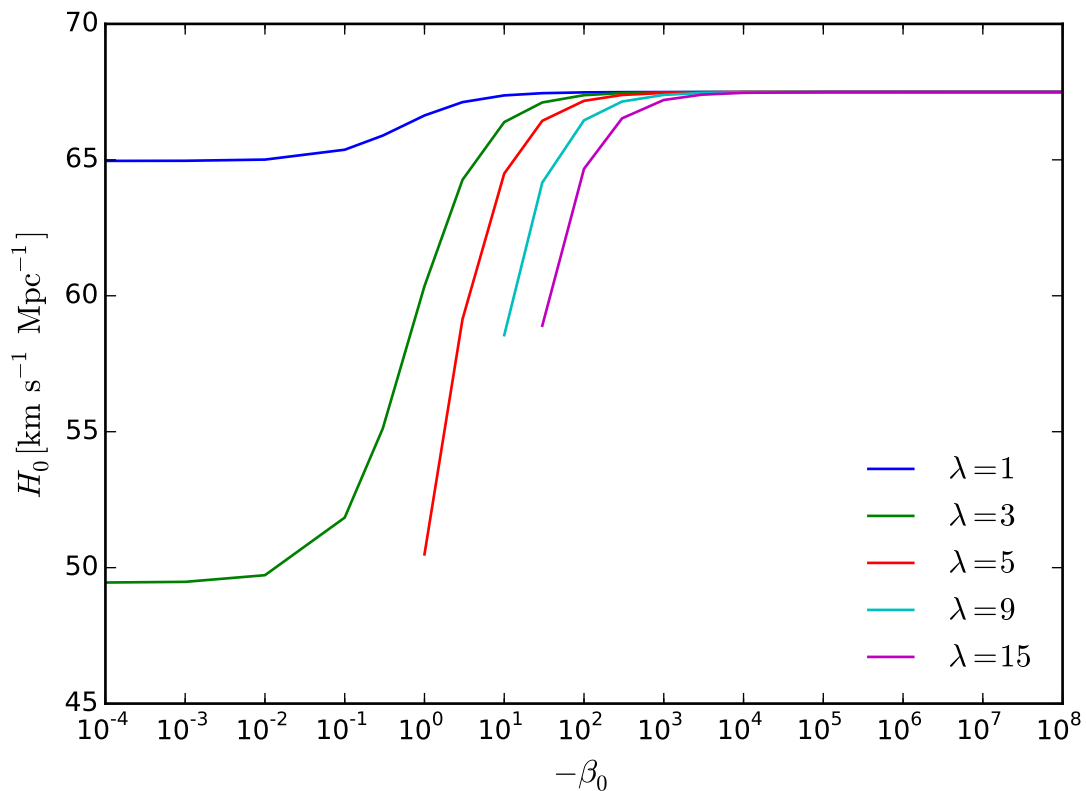


Figure 4.14: The present-day value of the Hubble parameter  $H_0$  as a function of the coupling parameter  $|\beta_0|$  for a range of potential parameters  $\lambda$  for a quadratic coupling function  $\gamma(Z) = \beta_0 Z^2$  and an exponential potential  $V(\phi) = Ae^{-\lambda\phi/M_{\text{P}}}$ . The sound horizon at recombination is held fixed at  $\theta_s = 0.0104$ .

#### 4.5.2.2 Structure formation

To understand how structure growth is affected by the potential parameter  $\lambda$  one needs to consider the CDM velocity divergence. Figure 4.16 shows how the evolution of  $\theta_c$  is affected by the potential parameter  $\lambda$ : larger  $\lambda$ , corresponding to a steeper potential, results in  $|\theta_c|$  rising more rapidly. Larger  $\theta_c$  at a given time reduces the time derivative of the CDM density contrast  $\delta_c$  (see Eq. (4.25)), resulting in a smaller  $|\delta_c|$  at the present epoch and hence a reduction of  $\sigma_8$  for large  $\lambda$  as seen in Fig. 4.13. The  $\lambda$ -dependence of  $\theta_c$  can be seen in the  $\theta_c$  equation. Substituting for  $\ddot{\phi}$  using Eq. (4.29), Eq. (4.30) becomes

$$\dot{\theta}_c = -\mathcal{H}\theta_c + \frac{\frac{2\beta_0}{1-2\beta_0}a^2V_{,\phi}\delta\phi - 2\beta_0\dot{\phi}\dot{\delta}\phi}{(\bar{\rho}_c a^2 - 2\beta_0\dot{\phi}^2)}, \quad (4.57)$$

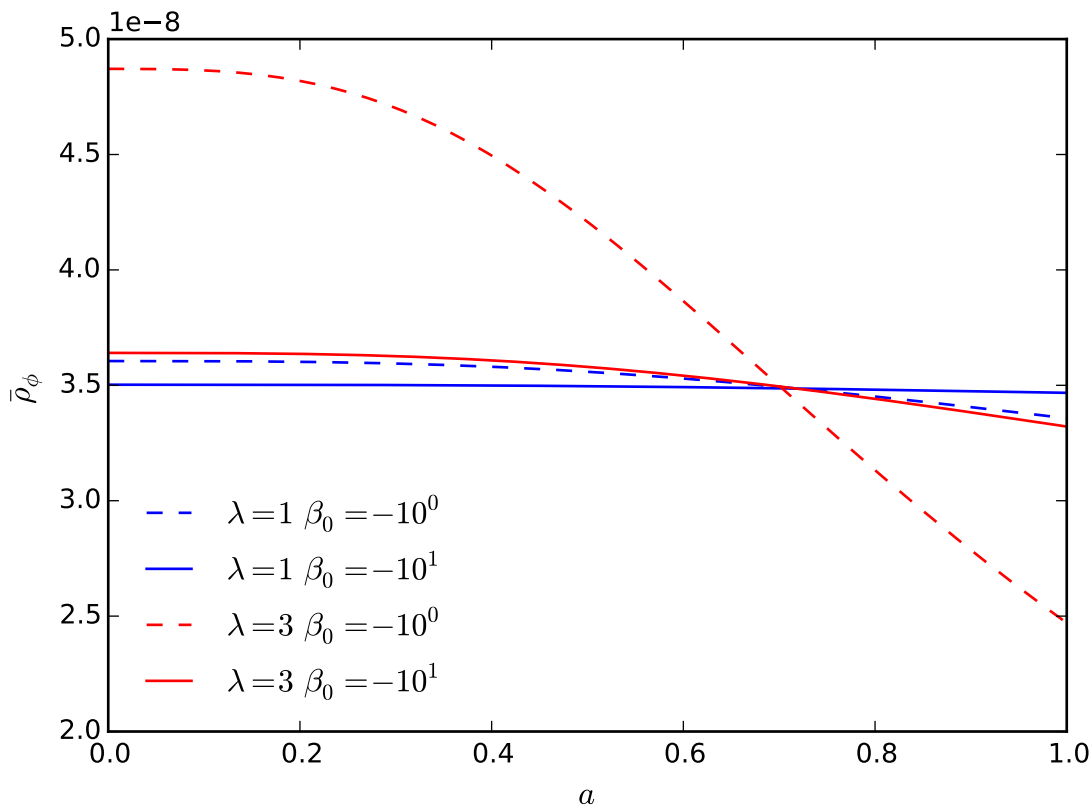


Figure 4.15: The evolution of the background energy density of the scalar field  $\bar{\rho}_\phi$  for two values of the coupling parameter  $\beta_0$  and the potential parameter  $\lambda$ . Larger values of  $\lambda$  and smaller values of  $|\beta_0|$  both result in a smaller present-day value of  $\bar{\rho}_\phi$ . The sound horizon at recombination is held fixed at  $\theta_s = 0.0104$ .

which, for an exponential potential  $V(\phi) = Ae^{-\lambda\phi/M_P}$ , yields

$$\dot{\theta}_c = -\mathcal{H}\theta_c + \frac{-\frac{2\beta_0}{1-2\beta_0}a^2 A\lambda e^{-\lambda\phi/M_P}\delta\phi - 2\beta_0\dot{\phi}\delta\dot{\phi}}{(\bar{\rho}_c a^2 - 2\beta_0\dot{\phi}^2)}. \quad (4.58)$$

Both of the terms in the numerator become larger in magnitude when  $\lambda$  is large. In the first term this is obvious; in the second it is a consequence of the  $V_{,\phi\phi}$  term in Eq. (4.28). Hence, a large slope  $\lambda$  results in a large (negative)  $\theta_c$  leading to a reduction in  $\delta_c$  and a suppression of structure growth.

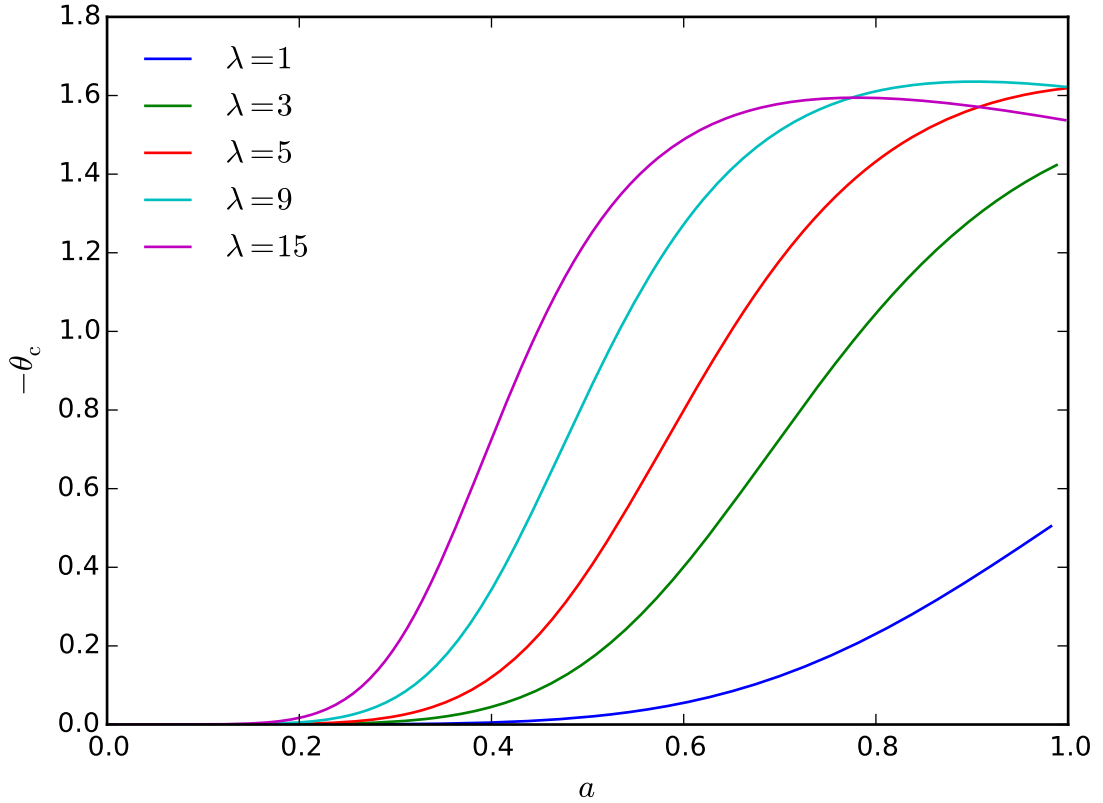


Figure 4.16: The evolution of the CDM velocity divergence  $\theta_c$  as a function of the scale factor  $a$  for a range of different potential parameters  $\lambda$  with a coupling parameter  $\beta_0 = -10^2$ , at a scale  $k = 0.1 \text{ Mpc}^{-1}$ . Larger values of  $\lambda$  give rise to larger  $|\theta_c|$ , with the effect saturating in the late universe for  $\lambda \geq 5$ . The sound horizon at recombination is held fixed at  $\theta_s = 0.0104$ .

### 4.5.3 Double exponential potentials

Double exponential potentials of the form  $V(\phi) = A_1 e^{-\lambda_1 \phi/M_{\text{P}}} + A_2 e^{-\lambda_2 \phi/M_{\text{P}}}$  can provide interesting behaviour for uncoupled quintessence, as discussed in Chapter 2. In this section I discuss double exponential potentials in the context of Type 3 models. In particular, I argue that in Type 3 models, only the gradient of the potential at a particular  $\phi$  value is crucial, and not the overall shape of the potential.

We have already seen that Type 3 models with a large coupling parameter  $|\beta_0|$  result in a ‘slowing’ effect on the scalar field evolution, with extremely large values giving rise to cosmological constant-like behaviour. This can be seen in our numerical results in Figs. 4.2 and 4.8 and in the analytic argument laid out in Section 4.5.1. The consequence of this is that, for sufficiently large  $|\beta_0|$ , the scalar field  $\phi$  does

not explore a wide range of its potential, and instead is limited to a small region, even if the potential is very steep. Based on this argument, one can predict that considering other potential functions, such as double exponentials, will not introduce any interesting behaviour that is not present in the single exponential case already considered. We have tested this by investigating several double exponential potentials. Figure 4.17 shows the evolution of the derivative of the scalar field for three example potentials. The first is the single exponential case already considered. The second has  $\lambda_1$  and  $\lambda_2$  of the same sign, similar to the potential proposed in Ref. [116] and discussed in Chapter 2. The third has  $\lambda_1$  and  $\lambda_2$  of opposite sign similar to the models discussed in Ref. [238], giving rise to a global minimum into which the scalar field can fall. For simplicity we have set  $A_1 = A_2$  in both of the double exponential cases. It can be seen in Fig. 4.17 that, while the uncoupled scalar field is able to evolve relatively quickly and is sensitive to the form of the potential, the coupling effectively stops the scalar field from evolving irrespective of the form of the potential.

The gradient of the scalar field potential certainly plays a key role; this was demonstrated in Sections 4.5.1 and 4.5.2. However, for sufficiently large  $|\beta_0|$ , only the gradient in the vicinity of the initial value of  $\phi$  is relevant. The rest of the potential is never explored by the scalar field and so has no cosmological consequences. There is a wide range of possibilities for the form of the scalar field potential, which we have only explored a small part of. However, the argument that the Type 3 coupling stops the scalar field from evolving rapidly and so the overall form of the potential is not crucial seems to be a general one. We can conclude from this that the ability for Type 3 models to ease the  $\sigma_8$  tension is not unique to the single exponential potential studied in Ref. [106] but should be expected for any potential that is sufficiently steep.

## 4.6 Discussion

Unlike most coupled dark energy models that have been studied in the literature, Type 3 models, as classified at the Lagrangian level in Ref. [114], consist of a coupling between the momentum of the dark matter and the gradient of the scalar field of dark energy. It was demonstrated in Ref. [106] using MCMC methods that such models can ease the tension between early- and late-universe measurements of the degree of structure formation in the universe.

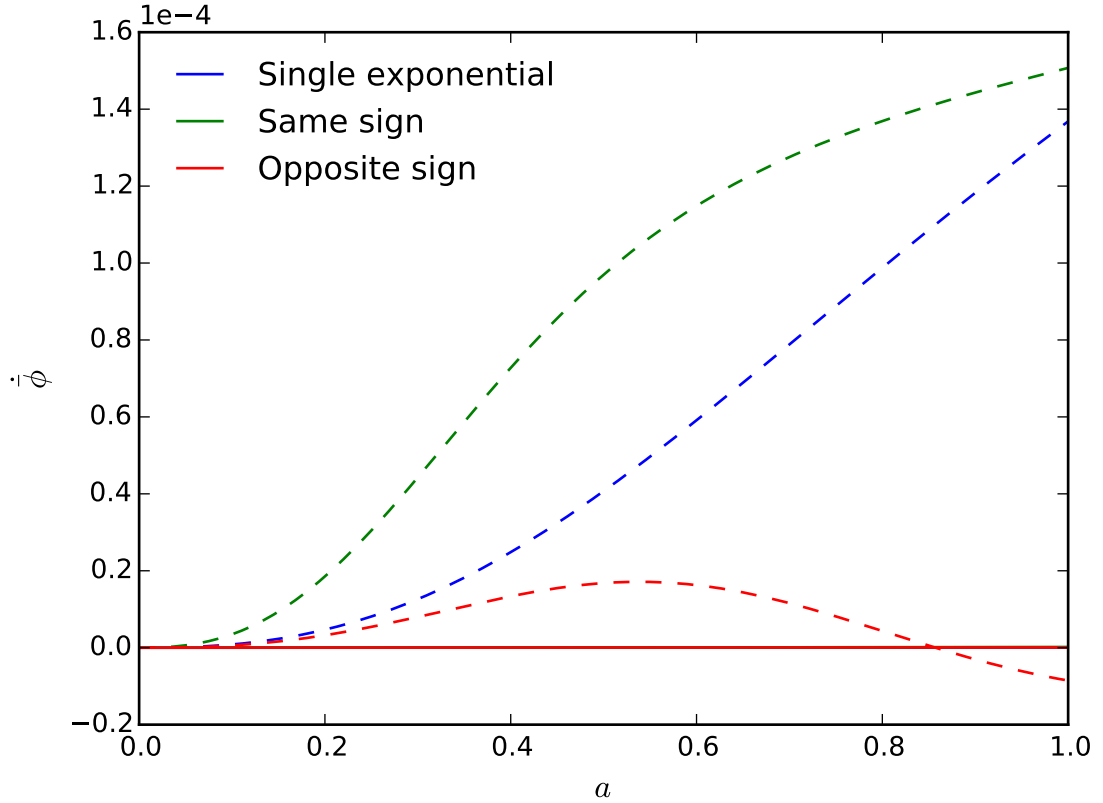


Figure 4.17: The evolution of the time derivative of the scalar field with the scale factor for three different scalar field potentials  $V(\phi)$ . Dashed lines correspond to the results of setting the coupling parameter  $\beta_0 = 0$ . Solid lines (there are three solid lines almost directly on top of one another) correspond to the results of allowing a Type 3 coupling with a large coupling parameter  $\beta_0 = -10^3$ . The single exponential case already studied, with  $V(\phi) = Ae^{\lambda\phi/M_{\text{P}}}$ ,  $\lambda = 1.22$ , is shown in blue, while two double exponential potentials of the form  $V(\phi) = A(e^{-\lambda_1\phi/M_{\text{P}}} + e^{-\lambda_2\phi/M_{\text{P}}})$  are shown in green and red, with green corresponding to  $\lambda_1 = 1$ ,  $\lambda_2 = 5$  and red corresponding to  $\lambda_1 = 5$ ,  $\lambda_2 = -3$ . It can be seen that the uncoupled cases allow the scalar field to evolve relatively rapidly, with behaviour highly sensitive to the form of the potential. When the Type 3 couplings are present, however, the scalar field is able to evolve only very slowly, with the form of the potential having very little impact. The sound horizon at recombination is held fixed at  $\theta_s = 0.0104$ .

In this chapter I have discussed two novel contributions to the study of Type 3 models. In Section 4.3 I presented a detailed approximate analytic approach to understand the underlying physics that gives rise to the resulting suppression of structure growth discovered by Ref. [106]. Then Sections 4.4 and 4.5 embarked on a generalisation of the model considered in Section 4.3 by considering couplings other than the quadratic one already considered, and potentials beyond the single exponential with a fixed slope that was the focus of Section 4.3.

The most interesting feature of Type 3 models that gives rise to their observed suppression of structure growth is that they exhibit a non-zero velocity divergence of CDM,  $\theta_c$ , which is normally equal to zero in the synchronous gauge. The CDM density contrast then has a small additional contribution that is not present in the uncoupled case. This contribution has a sign such that it always reduces the absolute value of the density contrast, which is equivalent to a suppression of structure growth. This mechanism was fleshed out in detail in Section 4.3.

A cubic coupling  $\gamma(Z) = \beta_1 Z^3$  has already been considered in the literature [225], with a focus on the variable sound speed of dark energy that is present in Type 3 models with  $\gamma(Z) = \beta_{n-2} Z^n$  for  $n > 2$ . Our focus, on the other hand, was on any implications such couplings might have for the growth of structure. We concluded that the key features are still present: very small couplings recover uncoupled quintessence, very large couplings mimic  $\Lambda$ CDM in the late universe, and coupling parameters in an intermediate range give rise to structure growth suppression relative to both extremes. The key difference is the time-dependence introduced by power-law couplings with  $n > 2$ , which results in the coupling ‘switching on’ at some time; later for small  $|\beta_{n-2}|$  and earlier for large  $|\beta_{n-2}|$ . Another manifestation of the time-dependence is the shifting profile of the CDM velocity divergence  $\theta_c$ . At early times,  $|\theta_c|$  is maximised for larger  $|\beta_{n-2}|$  while at later times it is maximised for smaller  $|\beta_{n-2}|$ . As far as we can tell, neither of these time-dependent effects are particularly important, since most of the interesting behaviour of Type 3 models is manifest in the late universe. A possible avenue for future research would be to carry out an MCMC analysis similar to that of Ref. [106] for more general couplings to investigate quantitatively whether such models have any advantages or disadvantages in terms of fitting the data compared to the  $n = 2$  case.

Of the two main tensions between early- and late-universe observations, the one we have considered here, the amount of structure growth, is the less severe. The

more severe tension is in measurements of the expansion rate of the universe, which according to our work cannot be addressed by Type 3 models. However, even if we cannot reduce the  $H_0$  tension, we should at least aspire to make it no worse, since ameliorating a mild tension at the expense of exacerbating a more extreme tension worsens the fit to the data overall. The results of Section 4.5 suggest that Type 3 models are able to imply a very large suppression of structure formation (at least down to the level found by presently available late-universe probes [102–105]) without making the  $H_0$  tension worse. The suppression of structure growth is achieved by setting  $\lambda$  to be large (e.g.  $\lambda \sim 3$ ), whilst any reduction in the expansion rate is prevented by setting  $|\beta_0|$  to be large ( $|\beta_0| \gtrsim 10^2$ ). Investigating whether such choices of the parameters  $\lambda$  and  $\beta_0$  are favoured by the data would require a more rigorous analysis such as that carried out in Ref. [106]. Indeed, the posterior distribution for  $\lambda$  found by Ref. [106] does not appear to be fully contained within the prior, which only extends as far as 2.1. Extending the prior range to include the larger values of  $\lambda$  that we have considered here may be an interesting aspect for future study.

As well as looking in more detail at the effect of varying  $\lambda$  for a single exponential potential, we have briefly considered more general potentials, in the form of double exponential potentials. Double exponential potentials are of interest for uncoupled quintessence in two main forms. If both exponents are of the same sign but of different magnitude then one can have a situation in which the scalar field rolls quickly down the steeper part in the early universe in the form of a scaling solution [61] before hitting the flatter part of the potential in the late universe, giving rise to slow roll and an equation of state close to the observed value of  $-1$  [116]. On the other hand, if the exponents are of opposite signs then the potential acquires a minimum about which the scalar field can oscillate, providing another basis for the equation of state to evolve close to the observationally preferred value [238]. Looking at these types of potential in the context of Type 3 models, however, we do not find any indication that their properties are as interesting as they are in uncoupled quintessence. The key reason for this is that Type 3 models provide a very natural way to slow the evolution of the scalar field without requiring a shallow slope or a minimum about which to oscillate. If the coupling parameter  $\beta_0$  has an absolute value that is significantly greater than unity it provides an effect similar to a friction term, that slows the scalar field evolution even for a steep potential. It appears simpler and more attractive, therefore, to content oneself with a single exponential potential than to introduce

extra degrees of freedom that do not necessarily add any interesting or useful physical behaviour to the model.

In this chapter I have explored the underlying physical mechanism for the interesting behaviour of Type 3 models and demonstrated the robustness of such behaviour to changing the form of the coupling function  $\gamma(Z)$  and the scalar field potential  $V(\phi)$ . I hope that a robust understanding of the underlying physics and its domain of applicability will help guide future study in this exciting and little-studied field.

# Chapter 5

## Conclusions

Understanding the cause of the current period of accelerated universal expansion is one of the great unanswered questions in cosmology. Assuming Einstein's general theory of relativity is the correct theory of gravity, the rate of expansion of the universe implies that 70% of its present-day energy density is in the form of a negative-pressure fluid known as dark energy. To improve our theoretical understanding of dark energy we construct models whose predictions we can test against the extraordinary wealth of observational data we now have access to. The standard model of cosmology,  $\Lambda$ CDM, was reviewed in Chapter 1 and describes dark energy as a cosmological constant. This model fits the data very well but suffers from serious theoretical issues such as the cosmological constant problem and the coincidence problem. In addition, there are tensions between early- and late-universe measurements of the present-day expansion rate  $H_0$  and the amplitude of matter fluctuations  $\sigma_8$  when  $\Lambda$ CDM is taken as the cosmological model. This motivates the study of alternative models of dark energy such as those I have discussed in this thesis. I have presented research on two types of dark energy, exploring the extent to which they can address the problems faced by  $\Lambda$ CDM and investigating whether they might encounter their own problems in trying to agree with observational data.

Both of the classes of models I have considered are examples of scalar field dark energy, in which the cosmological constant is assumed to be zero and dark energy is instead described by a single scalar field which dynamically acquires an appropriate energy density and pressure to give rise to the observed accelerated expansion. Both cases are examples of interacting dark energy; a coupling is introduced between the dark energy scalar field and either neutrinos or dark matter. The theoretical background for both types of model, as well as more general background on dynamical dark energy, was presented in Chapter 2.

The first type of dark energy I discussed was growing neutrino quintessence (GNQ), in which a coupling is introduced between the dark energy scalar field and

the neutrino sector. This study was the subject of Chapter 3. The motivation for such couplings is that they can solve the coincidence problem. During radiation and matter domination the scalar field  $\phi$  obeys a scaling solution in which it tracks the energy density of the dominant fluid species. Once the neutrinos become non-relativistic the coupling causes the scalar field to come to a halt, acquiring a negative equation of state and producing accelerated expansion. This mechanism produces early dark energy during the scaling regime, where the scalar field contributes an approximately constant fraction of the energy density of the universe. We used the Doran and Robbers parametrisation of early dark energy [117] and constraints from CMB experiments to constrain a class of GNQ models.

We focused in particular on a model proposed by Wetterich [216], which describes both inflation and dark energy by the same scalar field, employing the GNQ mechanism and embedding it in an approach to quantum gravity called crossover gravity. Wetterich used an approximate analytic treatment of the scaling regime to derive an upper bound on a model parameter  $\kappa$  that controls the size of the scalar field kinetic term. He pointed out that CMB constraints on early dark energy also provide a lower bound on  $\kappa$  such that more precise CMB measurements in the future may be able to rule out or support the model. Using a modified version of `CAMB`, we solved the background evolution equations, applied the most recent CMB measurements and did indeed find that the new lower bound on  $\kappa$  exceeds Wetterich's upper bound, apparently ruling out the model. However, we also repeated the analytic calculation in the scaling regime and found disagreement with Wetterich's results, such that the upper bound is not present. Thus we conclude that the model is not ruled out after all.

We broadened our analysis of the Wetterich model to include related GNQ models by considering various forms for the kinetic function, scalar field potential, and neutrino–scalar coupling function. In particular, we considered inverse power-law potentials both analytically and numerically using our modified version of `CAMB`. We found an analytic solution for the evolution of the scalar field energy density in the radiation- and matter-dominated eras which we were able to confirm with the numerical solution. We found that there was no early dark energy present and so the constraints we applied to the exponential potentials do not apply to the inverse power-law potentials.

In addition to the background analyses discussed above, we calculated for the

first time the equations of motion to linear order in perturbations for the Wetterich model. This was intended as the basis of an investigation using `CAMB` to study the model in more detail than the background analysis allowed. Ultimately this approach did not yield results, possibly due to the formation of non-linear neutrino lumps rendering the linear approximation invalid.

Most of the recent literature on GNQ has studied the neutrino lumps which form as a consequence of the coupling to the scalar field. While we have found novel results using a purely background analysis, it is my opinion that there is not much more to be gained by continuing in this direction, and N-body methods that can properly take account of the neutrino lumps may prove a more fruitful area for future research.

The formalism of Ref. [114] provides a powerful framework for building interacting dark energy models and there is no reason why it cannot be applied to couplings with the neutrinos rather than dark matter. The most widely studied GNQ models have neutrino–scalar couplings that are sub-cases of Type 1, while Type 2 and 3 couplings between dark energy and neutrinos are very little studied. Ref. [239] investigated a physically motivated neutrino–scalar coupling similar to a Type 3 coupling and found that such an interaction could solve the coincidence problem while avoiding the formation of neutrino ‘lumps’ that conventional GNQ models suffer from. It is clear that couplings other than the ‘standard’ GNQ form can have interesting cosmological consequences that deserve further study.

The second class of models we studied were Type 3 interacting dark energy models, introduced in Ref. [114]. This research was the subject of Chapter 4. The classification scheme of Ref. [114] divides interacting dark energy into three Types according to what couplings between dark energy and dark matter are present in the Lagrangian. Type 1 includes many previously studied models of interacting dark energy in which the coupling was introduced phenomenologically in the equations of motion, while Types 2 and 3 are much less studied. Type 3 models consist of a pure momentum coupling, resulting in them being less tightly constrained than Types 1 and 2. Furthermore, they have been shown to be able to alleviate the tension between early- and late-universe measurements of structure formation, making them a particularly interesting case to study.

We investigated the mechanism by which the growth of structure is suppressed

in Type 3 models and presented an explanation for this behaviour with reference to the underlying equations for a simple quintessence case with an exponential scalar field potential  $V(\phi) = Ae^{-\lambda\phi}$  and a quadratic coupling  $\gamma(Z) = \beta_0 Z^2$ . The velocity divergence of CDM is increased by the coupling to the gradient of the scalar field, which brings about a reduction in the density contrast of CDM, corresponding to less growth of structure. The particular value of the coupling parameter that maximises the suppression can be inferred from the CDM velocity divergence evolution equation using simple scaling arguments.

After developing this understanding of the physics of Type 3 models we used a modified version of **CLASS** to explore the effect of changing the form of the coupling function to higher powers of  $Z$ . This generalisation introduces some new time dependence into the behaviour of the coupling but does not significantly affect the consequences for structure formation. We conclude from this that structure growth suppression is a rather generic feature of Type 3 coupled quintessence. We demonstrated explicitly the results for cubic and quartic coupling functions.

We also focused on the role of the scalar field potential in the behaviour of Type 3 coupled quintessence. For a single exponential potential, we found that the slope,  $\lambda$ , of the potential plays a key role in structure growth suppression. Increasing  $\lambda$  decreases  $\sigma_8$  but also reduces the present-day expansion rate of the universe  $H_0$ . This latter result is to be avoided, since it exacerbates the already large tension with late-universe measurements of  $H_0$ . However, the Type 3 coupling can bring about a slowing effect on the scalar field evolution through a modification to the kinetic term of the scalar field equation. One can avoid the reduction in  $H_0$  by increasing the coupling parameter to increase the slowing effect on the scalar field. By varying the potential parameter  $\lambda$  and the coupling parameter  $\beta_0$  one can obtain solutions in which structure growth is substantially suppressed without bringing about a reduction in  $H_0$ . We considered more general scalar field potentials in the form of double exponential potentials. However, due to the fact that Type 3 couplings can slow the evolution of the scalar field even for steep potentials, the overall form of the scalar field potential is often not crucial, since the field will never ‘see’ the parts of the potential that are far from its initial conditions.

Type 3 interacting dark energy is a very young topic but it is one that holds great potential for future study. One unanswered question from our work is how natural are the choices we have made. In the course of our study we have allowed

the coupling parameter to vary over several orders of magnitude, at times finding that dimensionless values of  $|\beta_0| \sim 10^2$  yield useful or interesting results. We have not considered questions about how the models we have considered might arise from a more fundamental theory, so we cannot say definitively whether such values are reasonable, but the presence of large dimensionless parameters is somewhat unappealing. Similarly, the use of a large coupling to slow the scalar field evolution almost to a standstill is attractive from the point of view of obtaining a realistic present-day expansion rate, but may present a fine-tuning problem. If the scalar field remains at the same point of its potential for most of the universe's history, and this point gives just the right amount of dark energy to bring about the present rate of expansion, then the question arises as to why the field should have had that initial value rather than any other. (To be precise, in our analysis with CLASS any fine tuning would have been in finding the prefactor  $A$  of the scalar field potential rather than in the initial value of the scalar field itself, but the distinction is not crucial.) It may be the case that power-law couplings with higher order than quadratic might be useful here. We found that such couplings result in the scalar field evolving like uncoupled quintessence in the early universe before being slowed in the late universe. Whether a scenario along these lines could bring about the desired late-universe behaviour for generic initial conditions would be an interesting subject for future study.

Another limitation of our work is that we have not used MCMC methods to compare the predictions of the model to observational data in a rigorous way. Instead we have run a Boltzmann code for a few choices of parameters and compared the cosmological observables obtained to the best-fit values found by observations. The reason for our choice of approach was to illuminate the mechanism by which different parameter choices affect the output, but a more rigorous comparison with the data is desirable. Such an analysis for a quadratic coupling and single exponential potential was carried out in Ref. [106]; future study could build on this and our work by applying MCMC methods to more general choices of the Type 3 coupling parameter and scalar field potential.

The fundamental nature of dark energy is unlikely to be discovered in the immediate future. At present there are a great many proposed models whose cosmological consequences need to be investigated and compared against the increasingly precise cosmological data available to us. The coupled quintessence scenarios we have stud-

ied in this work have exciting prospects for resolving some of the issues with the standard cosmological paradigm, and reveal intriguing behaviour that I hope future study will further illuminate.

# Bibliography

- [1] A. Einstein, ‘The foundation of the general theory of relativity’, *Annalen der Physik*, vol. 49, pp. 769–822, 1916. DOI: 10.1002/andp.200590044.
- [2] S. M. Carroll, ‘Lecture notes on general relativity’, 1997. arXiv: [gr-qc/9712019](#) [gr-qc].
- [3] H. Stephani, D. Kramer, M. A. H. MacCallum *et al.*, *Exact solutions of Einstein’s field equations*. Cambridge, UK: Cambridge University Press, 2003, ISBN: 9780521467025. DOI: 10.1017/CB09780511535185.
- [4] C.-P. Ma and E. Bertschinger, ‘Cosmological perturbation theory in the synchronous and conformal Newtonian gauges’, *The Astrophysical Journal*, vol. 455, pp. 7–25, 1995. DOI: 10.1086/176550. arXiv: [astro-ph/9506072](#) [astro-ph].
- [5] L. Lehner, ‘Numerical relativity: A Review’, *Classical and Quantum Gravity*, vol. 18, R25–R86, 2001. DOI: 10.1088/0264-9381/18/17/202. arXiv: [gr-qc/0106072](#) [gr-qc].
- [6] N. Aghanim *et al.*, ‘Planck 2018 results. VI. Cosmological parameters’, 2018. arXiv: [1807.06209](#) [astro-ph.CO].
- [7] V. M. Slipher, ‘The radial velocity of the Andromeda Nebula’, *Lowell Observatory Bulletin*, vol. 2, pp. 56–57, 1913.
- [8] V. M. Slipher, ‘Spectrographic observations of nebulae’, *Popular Astronomy*, vol. 23, pp. 21–24, 1915.
- [9] A. Friedmann, ‘Über die Krümmung des Raumes’, *Zeitschrift für Physik*, vol. 10, pp. 377–386, 1922. DOI: 10.1007/BF01332580.
- [10] G. Lemaître, ‘Un univers homogène de masse constante et de rayon croissant rendant compte de la vitesse radiale des nébuleuses extra-galactiques’, *Annales de la Société Scientifique de Bruxelles*, vol. 47, pp. 49–59, 1927.
- [11] E. Hubble, ‘A relation between distance and radial velocity among extra-galactic nebulae’, *Proceedings of the National Academy of Science*, vol. 15, pp. 168–173, 1929. DOI: 10.1073/pnas.15.3.168.

- [12] A. G. Riess *et al.*, ‘Observational evidence from supernovae for an accelerating universe and a cosmological constant’, *The Astronomical Journal*, vol. 116, pp. 1009–1038, 1998. DOI: 10.1086/300499. arXiv: astro-ph/9805201 [astro-ph].
- [13] B. P. Schmidt *et al.*, ‘The High-Z Supernova Search: Measuring cosmic deceleration and global curvature of the universe using type Ia supernovae’, *The Astrophysical Journal*, vol. 507, pp. 46–63, 1998. DOI: 10.1086/306308. arXiv: astro-ph/9805200 [astro-ph].
- [14] E. W. Kolb and M. S. Turner, *The Early Universe*. Boulder, CO: Westview Press, 1990, ISBN: 9780201626742.
- [15] R. P. Woodard, ‘How far are we from the quantum theory of gravity?’, *Reports on Progress in Physics*, vol. 72, p. 126 002, 2009. DOI: 10.1088/0034-4885/72/12/126002. arXiv: 0907.4238 [gr-qc].
- [16] B. Schulz, ‘Review on the quantization of gravity’, 2014. arXiv: 1409.7977 [gr-qc].
- [17] K. C. Freeman, ‘On the disks of spiral and S0 galaxies’, *The Astrophysical Journal*, vol. 160, p. 811, 1970. DOI: 10.1086/150474.
- [18] V. C. Rubin and W. K. Ford Jr., ‘Rotation of the Andromeda Nebula from a spectroscopic survey of emission regions’, *The Astrophysical Journal*, vol. 159, p. 379, 1970. DOI: 10.1086/150317.
- [19] Y. Sofue and V. Rubin, ‘Rotation curves of spiral galaxies’, *Annual Review of Astronomy and Astrophysics*, vol. 39, pp. 137–174, 2001. DOI: 10.1146/annurev.astro.39.1.137.
- [20] F. Zwicky, ‘Die Rotverschiebung von extragalaktischen Nebeln’, *Helvetica Physica Acta*, vol. 6, pp. 110–127, 1933. DOI: 10.1007/s10714-008-0707-4.
- [21] M. Oguri, C. E. Rusu and E. E. Falco, ‘The stellar and dark matter distributions in elliptical galaxies from the ensemble of strong gravitational lenses’, *Monthly Notices of the Royal Astronomical Society*, vol. 439, pp. 2494–2504, 2014. DOI: 10.1093/mnras/stu106. arXiv: 1309.5408 [astro-ph.CO].

- [22] D. E. Applegate, A. Mantz, S. W. Allen *et al.*, ‘Cosmology and astrophysics from relaxed galaxy clusters – IV. Robustly calibrating hydrostatic masses with weak lensing’, *Monthly Notices of the Royal Astronomical Society*, vol. 457, pp. 1522–1534, 2016. DOI: 10.1093/mnras/stw005. arXiv: 1509.02162 [astro-ph.CO].
- [23] D. E. Applegate, A. von der Linden, P. L. Kelly *et al.*, ‘Weighing the Giants – III. Methods and measurements of accurate galaxy cluster weak-lensing masses’, *Monthly Notices of the Royal Astronomical Society*, vol. 439, pp. 48–72, 2014. DOI: 10.1093/mnras/stt2129. arXiv: 1208.0605 [astro-ph.CO].
- [24] A. Vikhlinin, A. Kravtsov, W. Forman *et al.*, ‘Chandra sample of nearby relaxed galaxy clusters: Mass, gas fraction, and mass–temperature relation’, *The Astrophysical Journal*, vol. 640, pp. 691–709, 2006. DOI: 10.1086/500288. arXiv: astro-ph/0507092 [astro-ph].
- [25] M. Markevitch, A. H. Gonzalez, D. Clowe *et al.*, ‘Direct constraints on the dark matter self-interaction cross section from the merging galaxy cluster 1E 0657-56’, *The Astrophysical Journal*, vol. 606, pp. 819–824, 2004. DOI: 10.1086/383178. arXiv: astro-ph/0309303 [astro-ph].
- [26] J. R. Bond, A. S. Szalay and M. S. Turner, ‘Formation of galaxies in a gravitino-dominated universe’, *Physical Review Letters*, vol. 48, pp. 1636–1639, 1982. DOI: 10.1103/PhysRevLett.48.1636.
- [27] G. R. Blumenthal, H. Pagels and J. R. Primack, ‘Galaxy formation by dissipationless particles heavier than neutrinos’, *Nature*, vol. 299, pp. 37–38, 1982. DOI: 10.1038/299037a0.
- [28] P. J. E. Peebles, ‘Large-scale background temperature and mass fluctuations due to scale-invariant primeval perturbations’, *The Astrophysical Journal Letters*, vol. 263, pp. L1–L5, 1982. DOI: 10.1086/183911.
- [29] G. R. Blumenthal, S. M. Faber, J. R. Primack and M. J. Rees, ‘Formation of galaxies and large scale structure with cold dark matter’, *Nature*, vol. 311, pp. 517–525, 1984. DOI: 10.1038/311517a0.
- [30] S. D. M. White, C. S. Frenk and M. Davis, ‘Clustering in a neutrino-dominated universe’, *The Astrophysical Journal Letters*, vol. 274, pp. L1–L5, 1983. DOI: 10.1086/184139.

- [31] M. Davis, G. Efstathiou, C. S. Frenk and S. D. M. White, ‘The evolution of large-scale structure in a universe dominated by cold dark matter’, *The Astrophysical Journal*, vol. 292, pp. 371–394, 1985. DOI: 10.1086/163168.
- [32] C. S. Frenk, S. D. M. White, G. Efstathiou and M. Davis, ‘Cold dark matter, the structure of galactic haloes and the origin of the Hubble sequence’, *Nature*, vol. 317, pp. 595–597, 1985. DOI: 10.1038/317595a0.
- [33] N. Menci, A. Grazian, M. Castellano and N. G. Sanchez, ‘A stringent limit on the warm dark matter particle masses from the abundance of  $z = 6$  galaxies in the Hubble Frontier Fields’, *The Astrophysical Journal*, vol. 825, p. L1, 2016. DOI: 10.3847/2041-8205/825/1/L1. arXiv: 1606.02530 [astro-ph.CO].
- [34] M. Safarzadeh, E. Scannapieco and A. Babul, ‘A limit on the warm dark matter particle mass from the redshifted 21 cm absorption line’, *The Astrophysical Journal*, vol. 859, p. L18, 2018. DOI: 10.3847/2041-8213/aac5e0. arXiv: 1803.08039 [astro-ph.CO].
- [35] S. Staggs, J. Dunkley and L. Page, ‘Recent discoveries from the cosmic microwave background: A review of recent progress’, *Reports on Progress in Physics*, vol. 81, p. 044901, 2018. DOI: 10.1088/1361-6633/aa94d5.
- [36] A. A. Penzias and R. W. Wilson, ‘A measurement of excess antenna temperature at 4080 Mc/s.’, *The Astrophysical Journal*, vol. 142, pp. 419–421, 1965. DOI: 10.1086/148307.
- [37] R. H. Dicke, P. J. E. Peebles, P. G. Roll and D. T. Wilkinson, ‘Cosmic black-body radiation.’, *The Astrophysical Journal*, vol. 142, pp. 414–419, 1965. DOI: 10.1086/148306.
- [38] P. A. R. Ade *et al.*, ‘Planck 2013 results. I. Overview of products and scientific results’, *Astronomy & Astrophysics*, vol. 571, A1, 2014. DOI: 10.1051/0004-6361/201321529. arXiv: 1303.5062 [astro-ph.CO].
- [39] Y. Rephaeli, ‘Comptonization of the cosmic microwave background: The Sunyaev–Zeldovich effect’, *Annual Review of Astronomy and Astrophysics*, vol. 33, pp. 541–579, 1995. DOI: 10.1146/annurev.aa.33.090195.002545.
- [40] A. A. Starobinsky, ‘A new type of isotropic cosmological models without singularity’, *Physics Letters*, vol. B91, pp. 99–102, 1980. DOI: 10.1016/0370-2693(80)90670-X.

- [41] A. H. Guth, ‘Inflationary universe: A possible solution to the horizon and flatness problems’, *Physical Review*, vol. D23, pp. 347–356, 1981. DOI: 10.1103/PhysRevD.23.347.
- [42] A. D. Linde, ‘Inflationary cosmology’, *Lecture Notes in Physics*, vol. 738, pp. 1–54, 2008. DOI: 10.1007/978-3-540-74353-8\_1. arXiv: 0705.0164 [hep-th].
- [43] L. Kofman, A. D. Linde and A. A. Starobinsky, ‘Reheating after inflation’, *Physical Review Letters*, vol. 73, pp. 3195–3198, 1994. DOI: 10.1103/PhysRevLett.73.3195. arXiv: hep-th/9405187 [hep-th].
- [44] Y. Akrami *et al.*, ‘Planck 2018 results. X. Constraints on inflation’, 2018. arXiv: 1807.06211 [astro-ph.CO].
- [45] V. Springel, C. S. Frenk and S. D. M. White, ‘The large-scale structure of the universe’, *Nature*, vol. 440, p. 1137, 2006. DOI: 10.1038/nature04805. arXiv: astro-ph/0604561 [astro-ph].
- [46] M. J. Geller and J. P. Huchra, ‘Mapping the universe’, *Science*, vol. 246, pp. 897–903, 1989. DOI: 10.1126/science.246.4932.897.
- [47] M. Colless *et al.*, ‘The 2dF Galaxy Redshift Survey: Final data release’, 2003. arXiv: astro-ph/0306581 [astro-ph].
- [48] S. Cole *et al.*, ‘The 2dF Galaxy Redshift Survey: Power-spectrum analysis of the final dataset and cosmological implications’, *Monthly Notices of the Royal Astronomical Society*, vol. 362, pp. 505–534, 2005. DOI: 10.1111/j.1365-2966.2005.09318.x. arXiv: astro-ph/0501174 [astro-ph].
- [49] D. G. York *et al.*, ‘The Sloan Digital Sky Survey: Technical summary’, *The Astronomical Journal*, vol. 120, pp. 1579–1587, 2000. DOI: 10.1086/301513. arXiv: astro-ph/0006396 [astro-ph].
- [50] T. Abbott *et al.*, ‘The dark energy survey’, 2005. arXiv: astro-ph/0510346 [astro-ph].
- [51] C. Heymans, L. Van Waerbeke, L. Miller *et al.*, ‘CFHTLenS: The Canada–France–Hawaii Telescope Lensing Survey’, *Monthly Notices of the Royal Astronomical Society*, vol. 427, pp. 146–166, 2012. DOI: 10.1111/j.1365-2966.2012.21952.x. arXiv: 1210.0032 [astro-ph.CO].

- [52] A. Lewis and S. Bridle, ‘Cosmological parameters from CMB and other data: A Monte Carlo approach’, *Physical Review*, vol. D66, p. 103511, 2002. DOI: 10.1103/PhysRevD.66.103511. arXiv: astro-ph/0205436 [astro-ph].
- [53] B. Audren, J. Lesgourgues, K. Benabed and S. Prunet, ‘Conservative constraints on early cosmology: An illustration of the Monte Python cosmological parameter inference code’, *Journal of Cosmology and Astroparticle Physics*, vol. 1302, p. 001, 2013. DOI: 10.1088/1475-7516/2013/02/001. arXiv: 1210.7183 [astro-ph.CO].
- [54] H. B. G. Casimir, ‘On the attraction between two perfectly conducting plates’, *Indagationes Mathematicae*, vol. 10, pp. 261–263, 1948.
- [55] A. Padilla, ‘Lectures on the cosmological constant problem’, 2015. arXiv: 1502.05296 [hep-th].
- [56] S. Weinberg, ‘The cosmological constant problem’, *Reviews of Modern Physics*, vol. 61, pp. 1–23, 1989. DOI: 10.1103/RevModPhys.61.1.
- [57] S. Nobbenhuis, ‘Categorizing different approaches to the cosmological constant problem’, *Foundations of Physics*, vol. 36, pp. 613–680, 2006. DOI: 10.1007/s10701-005-9042-8. arXiv: gr-qc/0411093 [gr-qc].
- [58] J. Polchinski, ‘The cosmological constant and the string landscape’, in *The Quantum Structure of Space and Time: Proceedings of the 23rd Solvay Conference on Physics, Brussels, Belgium. 1–3 December 2005*, 2006, pp. 216–236. arXiv: hep-th/0603249 [hep-th].
- [59] J. Martin, ‘Everything you always wanted to know about the cosmological constant problem (but were afraid to ask)’, *Comptes Rendus Physique*, vol. 13, pp. 566–665, 2012. DOI: 10.1016/j.crhy.2012.04.008. arXiv: 1205.3365 [astro-ph.CO].
- [60] C. P. Burgess, ‘The cosmological constant problem: Why it’s hard to get dark energy from micro-physics’, in *Proceedings, 100th Les Houches Summer School: Post-Planck Cosmology: Les Houches, France, July 8 – August 2, 2013*, 2015, pp. 149–197. DOI: 10.1093/acprof:oso/9780198728856.003.0004. arXiv: 1309.4133 [hep-th].
- [61] E. J. Copeland, A. R. Liddle and D. Wands, ‘Exponential potentials and cosmological scaling solutions’, *Physical Review*, vol. D57, pp. 4686–4690, 1998. DOI: 10.1103/PhysRevD.57.4686. arXiv: gr-qc/9711068 [gr-qc].

- [62] C. Wetterich, ‘Growing neutrinos and cosmological selection’, *Physics Letters*, vol. B655, pp. 201–208, 2007. DOI: 10.1016/j.physletb.2007.08.060. arXiv: 0706.4427 [hep-ph].
- [63] L. Amendola, M. Baldi and C. Wetterich, ‘Quintessence cosmologies with a growing matter component’, *Physical Review*, vol. D78, p. 023015, 2008. DOI: 10.1103/PhysRevD.78.023015. arXiv: 0706.3064 [astro-ph].
- [64] B. Paczynski, ‘Gravitational microlensing by the galactic halo’, *The Astrophysical Journal*, vol. 304, pp. 1–5, 1986. DOI: 10.1086/164140.
- [65] K. Griest, ‘Galactic microlensing as a method of detecting massive compact halo objects’, *The Astrophysical Journal*, vol. 366, pp. 412–421, 1991. DOI: 10.1086/169575.
- [66] B. J. Carr and S. W. Hawking, ‘Black holes in the early universe’, *Monthly Notices of the Royal Astronomical Society*, vol. 168, pp. 399–415, 1974.
- [67] B. J. Carr, ‘The primordial black hole mass spectrum’, *The Astrophysical Journal*, vol. 201, pp. 1–19, 1975. DOI: 10.1086/153853.
- [68] R. D. Peccei and H. R. Quinn, ‘CP conservation in the presence of pseudo-particles’, *Physical Review Letters*, vol. 38, pp. 1440–1443, 1977. DOI: 10.1103/PhysRevLett.38.1440.
- [69] L. D. Duffy and K. van Bibber, ‘Axions as dark matter particles’, *New Journal of Physics*, vol. 11, p. 105008, 2009. DOI: 10.1088/1367-2630/11/10/105008.
- [70] G. Jungman, M. Kamionkowski and K. Griest, ‘Supersymmetric dark matter’, *Physics Reports*, vol. 267, pp. 195–373, 1996. DOI: 10.1016/0370-1573(95)00058-5. arXiv: hep-ph/9506380 [hep-ph].
- [71] M. Tanabashi *et al.*, ‘Review of particle physics’, *Physical Review*, vol. D98, p. 030001, 2018. DOI: 10.1103/PhysRevD.98.030001.
- [72] B. J. Carr, K. Kohri, Y. Sendouda and J. Yokoyama, ‘New cosmological constraints on primordial black holes’, *Physical Review*, vol. D81, p. 104019, 2010. DOI: 10.1103/PhysRevD.81.104019. arXiv: 0912.5297 [astro-ph.CO].
- [73] P. W. Graham, S. Rajendran and J. Varela, ‘Dark matter triggers of supernovae’, *Physical Review*, vol. D92, p. 063007, 2015. DOI: 10.1103/PhysRevD.92.063007. arXiv: 1505.04444 [hep-ph].

- [74] P. Tisserand *et al.*, ‘Limits on the Macho content of the galactic halo from the EROS-2 survey of the Magellanic Clouds’, *Astronomy & Astrophysics*, vol. 469, pp. 387–404, 2007. DOI: 10.1051/0004-6361:20066017. arXiv: astro-ph/0607207 [astro-ph].
- [75] R. A. Allsman *et al.*, ‘MACHO Project limits on black hole dark matter in the 1–30 solar mass range’, *The Astrophysical Journal*, vol. 550, p. L169, 2001. DOI: 10.1086/319636. arXiv: astro-ph/0011506 [astro-ph].
- [76] H. Niikura *et al.*, ‘Microlensing constraints on primordial black holes with Subaru/HSC Andromeda observations’, *Nature Astronomy*, vol. 3, pp. 524–534, 2019. DOI: 10.1038/s41550-019-0723-1. arXiv: 1701.02151 [astro-ph.CO].
- [77] H. Niikura, M. Takada, S. Yokoyama *et al.*, ‘Constraints on Earth-mass primordial black holes from OGLE 5-year microlensing events’, *Physical Review*, vol. D99, p. 083503, 2019. DOI: 10.1103/PhysRevD.99.083503. arXiv: 1901.07120 [astro-ph.CO].
- [78] M. Zumalacarregui and U. Seljak, ‘Limits on stellar-mass compact objects as dark matter from gravitational lensing of type Ia supernovae’, *Physical Review Letters*, vol. 121, p. 141101, 2018. DOI: 10.1103/PhysRevLett.121.141101. arXiv: 1712.02240 [astro-ph.CO].
- [79] K. Schutz and A. Liu, ‘Pulsar timing can constrain primordial black holes in the LIGO mass window’, *Physical Review*, vol. D95, p. 023002, 2017. DOI: 10.1103/PhysRevD.95.023002. arXiv: 1610.04234 [astro-ph.CO].
- [80] Y. Ali-Haïmoud, E. D. Kovetz and M. Kamionkowski, ‘Merger rate of primordial black-hole binaries’, *Physical Review*, vol. D96, p. 123523, 2017. DOI: 10.1103/PhysRevD.96.123523. arXiv: 1709.06576 [astro-ph.CO].
- [81] M. Raidal, V. Vaskonen and H. Veermäe, ‘Gravitational waves from primordial black hole mergers’, *Journal of Cosmology and Astroparticle Physics*, vol. 1709, p. 037, 2017. DOI: 10.1088/1475-7516/2017/09/037. arXiv: 1707.01480 [astro-ph.CO].
- [82] Y. Ali-Haïmoud and M. Kamionkowski, ‘Cosmic microwave background limits on accreting primordial black holes’, *Physical Review*, vol. D95, p. 043534, 2017. DOI: 10.1103/PhysRevD.95.043534. arXiv: 1612.05644 [astro-ph.CO].

- [83] G. Sato-Polito, E. D. Kovetz and M. Kamionkowski, ‘Constraints on the primordial curvature power spectrum from primordial black holes’, 2019. arXiv: 1904.10971 [astro-ph.CO].
- [84] S. J. Asztalos, G. Carosi, C. Hagmann *et al.*, ‘SQUID-based microwave cavity search for dark-matter axions’, *Physical Review Letters*, vol. 104, 041301, p. 041 301, 2010. DOI: 10.1103/PhysRevLett.104.041301. arXiv: 0910.5914 [astro-ph.CO].
- [85] D. G. Cerdeno and A. M. Green, ‘Direct detection of WIMPs’, in *Particle Dark Matter: Observations, Models and Searches*, G. Bertone, Ed. Cambridge: Cambridge University Press, 2010, pp. 347–369, ISBN: 9781107653924. DOI: 10.1017/CB09780511770739. arXiv: 1002.1912 [astro-ph.CO].
- [86] J. Conrad, ‘Indirect detection of WIMP dark matter: A compact review’, in *Interplay between Particle and Astroparticle physics (IPA2014) London, United Kingdom, August 18–22, 2014*, 2014. arXiv: 1411.1925 [hep-ph].
- [87] J. Goodman, M. Ibe, A. Rajaraman *et al.*, ‘Constraints on dark matter from colliders’, *Physical Review*, vol. D82, p. 116 010, 2010. DOI: 10.1103/PhysRevD.82.116010. arXiv: 1008.1783 [hep-ph].
- [88] L. Verde, T. Treu and A. G. Riess, ‘Tensions between the early and the late universe’, 2019. arXiv: 1907.10625 [astro-ph.CO].
- [89] T. M. C. Abbott *et al.*, ‘Dark Energy Survey Year 1 results: A precise H0 estimate from DES Y1, BAO, and D/H data’, *Monthly Notices of the Royal Astronomical Society*, vol. 480, pp. 3879–3888, 2018. DOI: 10.1093/mnras/sty1939. arXiv: 1711.00403 [astro-ph.CO].
- [90] A. G. Riess, S. Casertano, W. Yuan *et al.*, ‘Large Magellanic Cloud Cepheid standards provide a 1% foundation for the determination of the Hubble constant and stronger evidence for physics beyond  $\Lambda$ CDM’, *The Astrophysical Journal*, vol. 876, p. 85, 2019. DOI: 10.3847/1538-4357/ab1422. arXiv: 1903.07603 [astro-ph.CO].
- [91] W. L. Freedman, B. F. Madore, D. Hatt *et al.*, ‘The Carnegie-Chicago Hubble Program. VIII. An independent determination of the Hubble constant based on the tip of the red giant branch’, *The Astrophysical Journal*, vol. 882, p. 34, 2019. DOI: 10.3847/1538-4357/ab2f73. arXiv: 1907.05922 [astro-ph.CO].

- [92] K. C. Wong *et al.*, ‘H0LiCOW XIII. A 2.4% measurement of  $H_0$  from lensed quasars:  $5.3\sigma$  tension between early and late-universe probes’, 2019. arXiv: 1907.04869 [astro-ph.CO].
- [93] B. Czerny, R. Beaton, M. Bejger *et al.*, ‘Astronomical distance determination in the Space Age. Secondary distance indicators’, *Space Science Review*, vol. 214, 32, p. 32, 2018. DOI: 10.1007/s11214-018-0466-9. arXiv: 1801.00598 [astro-ph.GA].
- [94] S. Refsdal, ‘On the possibility of determining Hubble’s parameter and the masses of galaxies from the gravitational lens effect’, *Monthly Notices of the Royal Astronomical Society*, vol. 128, p. 307, 1964. DOI: 10.1093/mnras/128.4.307.
- [95] M. J. Reid, J. A. Braatz, J. J. Condon *et al.*, ‘The Megamaser Cosmology Project. I. Very long baseline interferometric observations of UGC 3789’, *The Astrophysical Journal*, vol. 695, pp. 287–291, 2009. DOI: 10.1088/0004-637x/695/1/287.
- [96] J. L. Tonry, J. P. Blakeslee, E. A. Ajhar and A. Dressler, ‘The SBF survey of galaxy distances. I. Sample selection, photometric calibration, and the Hubble constant’, *The Astrophysical Journal*, vol. 475, pp. 399–413, 1997. DOI: 10.1086/303576. arXiv: astro-ph/9609113 [astro-ph].
- [97] J. B. Jensen, J. L. Tonry, R. I. Thompson *et al.*, ‘The infrared surface brightness fluctuation Hubble constant’, *The Astrophysical Journal*, vol. 550, p. 503, 2001. DOI: 10.1086/319819. arXiv: astro-ph/0011288 [astro-ph].
- [98] B. P. Abbott *et al.*, ‘Observation of gravitational waves from a binary black hole merger’, *Physical Review Letters*, vol. 116, p. 061102, 2016. DOI: 10.1103/PhysRevLett.116.061102. arXiv: 1602.03837 [gr-qc].
- [99] B. P. Abbott *et al.*, ‘GW170817: Observation of gravitational waves from a binary neutron star inspiral’, *Physical Review Letters*, vol. 119, p. 161101, 2017. DOI: 10.1103/PhysRevLett.119.161101. arXiv: 1710.05832 [gr-qc].
- [100] B. P. Abbott *et al.*, ‘A gravitational-wave standard siren measurement of the Hubble constant’, *Nature*, vol. 551, pp. 85–88, 2017. DOI: 10.1038/nature24471. arXiv: 1710.05835 [astro-ph.CO].

- [101] P. A. R. Ade *et al.*, ‘Planck 2015 results. XIV. Dark energy and modified gravity’, *Astronomy & Astrophysics*, vol. 594, A14, 2016. DOI: 10.1051/0004-6361/201525814. arXiv: 1502.01590 [astro-ph.CO].
- [102] P. A. R. Ade *et al.*, ‘Planck 2013 results. XX. Cosmology from Sunyaev–Zeldovich cluster counts’, *Astronomy & Astrophysics*, vol. 571, A20, 2014. DOI: 10.1051/0004-6361/201321521. arXiv: 1303.5080 [astro-ph.CO].
- [103] H. Hildebrandt *et al.*, ‘KiDS-450: Cosmological parameter constraints from tomographic weak gravitational lensing’, *Monthly Notices of the Royal Astronomical Society*, vol. 465, p. 1454, 2017. DOI: 10.1093/mnras/stw2805. arXiv: 1606.05338 [astro-ph.CO].
- [104] F. Köhlinger, M. Viola, B. Joachimi *et al.*, ‘KiDS-450: The tomographic weak lensing power spectrum and constraints on cosmological parameters’, *Monthly Notices of the Royal Astronomical Society*, vol. 471, pp. 4412–4435, 2017. DOI: 10.1093/mnras/stx1820. arXiv: 1706.02892 [astro-ph.CO].
- [105] J. Alsing, A. Heavens and A. H. Jaffe, ‘Cosmological parameters, shear maps and power spectra from CFHTLenS using Bayesian hierarchical inference’, *Monthly Notices of the Royal Astronomical Society*, vol. 466, pp. 3272–3292, 2016. DOI: 10.1093/mnras/stw3161. arXiv: 1607.00008 [astro-ph.CO].
- [106] A. Pourtsidou and T. Tram, ‘Reconciling CMB and structure growth measurements with dark energy interactions’, *Physical Review*, vol. D94, p. 043518, 2016. DOI: 10.1103/PhysRevD.94.043518. arXiv: 1604.04222 [astro-ph.CO].
- [107] T. Clifton, P. G. Ferreira, A. Padilla and C. Skordis, ‘Modified gravity and cosmology’, *Physics Reports*, vol. 513, pp. 1–189, 2012. DOI: 10.1016/j.physrep.2012.01.001. arXiv: 1106.2476 [astro-ph.CO].
- [108] G. Obied, H. Ooguri, L. Spodyneiko and C. Vafa, ‘De Sitter space and the swampland’, 2018. arXiv: 1806.08362 [hep-th].
- [109] P. Agrawal, G. Obied, P. J. Steinhardt and C. Vafa, ‘On the cosmological implications of the string swampland’, *Physics Letters*, vol. B784, pp. 271–276, 2018. DOI: 10.1016/j.physletb.2018.07.040. arXiv: 1806.09718 [hep-th].

- [110] B. Ratra and P. J. E. Peebles, ‘Cosmological consequences of a rolling homogeneous scalar field’, *Physical Review*, vol. D37, pp. 3406–3427, 1988. DOI: 10.1103/PhysRevD.37.3406.
- [111] C. Armendariz-Picon, V. Mukhanov and P. J. Steinhardt, ‘Dynamical solution to the problem of a small cosmological constant and late-time cosmic acceleration’, *Physical Review Letters*, vol. 85, pp. 4438–4441, 2000. DOI: 10.1103/PhysRevLett.85.4438.
- [112] C. Armendariz-Picon, T. Damour and V. F. Mukhanov, ‘k-Inflation’, *Physics Letters*, vol. B458, pp. 209–218, 1999. DOI: 10.1016/S0370-2693(99)00603-6. arXiv: hep-th/9904075 [hep-th].
- [113] E. J. Copeland, M. Sami and S. Tsujikawa, ‘Dynamics of dark energy’, *International Journal of Modern Physics*, vol. D15, pp. 1753–1936, 2006. DOI: 10.1142/S021827180600942X. arXiv: hep-th/0603057 [hep-th].
- [114] A. Pourtsidou, C. Skordis and E. J. Copeland, ‘Models of dark matter coupled to dark energy’, *Physical Review*, vol. D88, p. 083505, 2013. DOI: 10.1103/PhysRevD.88.083505. arXiv: 1307.0458 [astro-ph.CO].
- [115] R. Fardon, A. E. Nelson and N. Weiner, ‘Dark energy from mass varying neutrinos’, *Journal of Cosmology and Astroparticle Physics*, vol. 0410, p. 005, 2004. DOI: 10.1088/1475-7516/2004/10/005. arXiv: astro-ph/0309800 [astro-ph].
- [116] T. Barreiro, E. J. Copeland and N. J. Nunes, ‘Quintessence arising from exponential potentials’, *Physical Review*, vol. D61, p. 127301, 2000. DOI: 10.1103/PhysRevD.61.127301. arXiv: astro-ph/9910214 [astro-ph].
- [117] M. Doran and G. Robbers, ‘Early dark energy cosmologies’, *Journal of Cosmology and Astroparticle Physics*, vol. 0606, p. 026, 2006. DOI: 10.1088/1475-7516/2006/06/026. arXiv: astro-ph/0601544 [astro-ph].
- [118] L. P. Chimento, A. S. Jakubi, D. Pavon and W. Zimdahl, ‘Interacting quintessence solution to the coincidence problem’, *Physical Review*, vol. D67, p. 083513, 2003. DOI: 10.1103/PhysRevD.67.083513. arXiv: astro-ph/0303145 [astro-ph].
- [119] G. R. Farrar and P. J. E. Peebles, ‘Interacting dark matter and dark energy’, *The Astrophysical Journal*, vol. 604, pp. 1–11, 2004. DOI: 10.1086/381728. arXiv: astro-ph/0307316 [astro-ph].

- [120] J. D. Barrow and T. Clifton, ‘Cosmologies with energy exchange’, *Physical Review*, vol. D73, p. 103520, 2006. DOI: 10.1103/PhysRevD.73.103520. arXiv: gr-qc/0604063 [gr-qc].
- [121] S. Lee, G.-C. Liu and K.-W. Ng, ‘Constraints on the coupled quintessence from cosmic microwave background anisotropy and matter power spectrum’, *Physical Review*, vol. D73, p. 083516, 2006. DOI: 10.1103/PhysRevD.73.083516. arXiv: astro-ph/0601333 [astro-ph].
- [122] H. M. Sadjadi and M. Alimohammadi, ‘Cosmological coincidence problem in interactive dark energy models’, *Physical Review*, vol. D74, p. 103007, 2006. DOI: 10.1103/PhysRevD.74.103007. arXiv: gr-qc/0610080 [gr-qc].
- [123] L. Amendola, G. Camargo Campos and R. Rosenfeld, ‘Consequences of dark matter-dark energy interaction on cosmological parameters derived from SNIa data’, *Physical Review*, vol. D75, p. 083506, 2007. DOI: 10.1103/PhysRevD.75.083506. arXiv: astro-ph/0610806 [astro-ph].
- [124] B. Wang, J. Zang, C.-Y. Lin *et al.*, ‘Interacting dark energy and dark matter: Observational constraints from cosmological parameters’, *Nuclear Physics*, vol. B778, pp. 69–84, 2007. DOI: 10.1016/j.nuclphysb.2007.04.037. arXiv: astro-ph/0607126 [astro-ph].
- [125] R. Mainini and S. Bonometto, ‘Limits on coupling between dark components’, *Journal of Cosmology and Astroparticle Physics*, vol. 0706, p. 020, 2007. DOI: 10.1088/1475-7516/2007/06/020. arXiv: astro-ph/0703303 [astro-ph].
- [126] A. W. Brookfield, C. van de Bruck and L. M. H. Hall, ‘New interactions in the dark sector mediated by dark energy’, *Physical Review*, vol. D77, p. 043006, 2008. DOI: 10.1103/PhysRevD.77.043006. arXiv: 0709.2297 [astro-ph].
- [127] C. G. Boehmer, G. Caldera-Cabral, R. Lazkoz and R. Maartens, ‘Dynamics of dark energy with a coupling to dark matter’, *Physical Review*, vol. D78, p. 023505, 2008. DOI: 10.1103/PhysRevD.78.023505. arXiv: 0801.1565 [gr-qc].
- [128] J. Valiviita, E. Majerotto and R. Maartens, ‘Instability in interacting dark energy and dark matter fluids’, *Journal of Cosmology and Astroparticle Physics*, vol. 0807, p. 020, 2008. DOI: 10.1088/1475-7516/2008/07/020. arXiv: 0804.0232 [astro-ph].

- [129] J.-H. He and B. Wang, ‘Effects of the interaction between dark energy and dark matter on cosmological parameters’, *Journal of Cosmology and Astroparticle Physics*, vol. 0806, p. 010, 2008. DOI: 10.1088/1475-7516/2008/06/010. arXiv: 0801.4233 [astro-ph].
- [130] M. Quartin, M. O. Calvao, S. E. Joras *et al.*, ‘Dark interactions and cosmological fine-tuning’, *Journal of Cosmology and Astroparticle Physics*, vol. 0805, p. 007, 2008. DOI: 10.1088/1475-7516/2008/05/007. arXiv: 0802.0546 [astro-ph].
- [131] V. Pettorino and C. Baccigalupi, ‘Coupled and extended quintessence: Theoretical differences and structure formation’, *Physical Review*, vol. D77, p. 103003, 2008. DOI: 10.1103/PhysRevD.77.103003. arXiv: 0802.1086 [astro-ph].
- [132] R. Bean, E. E. Flanagan, I. Laszlo and M. Trodden, ‘Constraining interactions in cosmology’s dark sector’, *Physical Review*, vol. D78, p. 123514, 2008. DOI: 10.1103/PhysRevD.78.123514. arXiv: 0808.1105 [astro-ph].
- [133] S. H. Pereira and J. F. Jesus, ‘Can dark matter decay in dark energy?’, *Physical Review*, vol. D79, p. 043517, 2009. DOI: 10.1103/PhysRevD.79.043517. arXiv: 0811.0099 [astro-ph].
- [134] M. Baldi, V. Pettorino, G. Robbers and V. Springel, ‘Hydrodynamical N-body simulations of coupled dark energy cosmologies’, *Monthly Notices of the Royal Astronomical Society*, vol. 403, pp. 1684–1702, 2010. DOI: 10.1111/j.1365-2966.2009.15987.x. arXiv: 0812.3901 [astro-ph].
- [135] M. B. Gavela, D. Hernandez, L. Lopez Honorez *et al.*, ‘Dark coupling’, *Journal of Cosmology and Astroparticle Physics*, vol. 0907, p. 034, 2009. DOI: 10.1088/1475-7516/2010/05/E01, 10.1088/1475-7516/2009/07/034. arXiv: 0901.1611 [astro-ph.CO].
- [136] G. Caldera-Cabral, R. Maartens and B. M. Schaefer, ‘The growth of structure in interacting dark energy models’, *Journal of Cosmology and Astroparticle Physics*, vol. 0907, p. 027, 2009. DOI: 10.1088/1475-7516/2009/07/027. arXiv: 0905.0492 [astro-ph.CO].
- [137] J. Valiviita, R. Maartens and E. Majerotto, ‘Observational constraints on an interacting dark energy model’, *Monthly Notices of the Royal Astronomical Society*, vol. 402, pp. 2355–2368, 2010. DOI: 10.1111/j.1365-2966.2009.16115.x. arXiv: 0907.4987 [astro-ph.CO].

- [138] J.-Q. Xia, ‘Constraint on coupled dark energy models from observations’, *Physical Review*, vol. D80, 103514, p. 103514, 2009. DOI: 10.1103/PhysRevD.80.103514. arXiv: 0911.4820 [astro-ph.CO].
- [139] E. Majerotto, J. Valiviita and R. Maartens, ‘Adiabatic initial conditions for perturbations in interacting dark energy models’, *Monthly Notices of the Royal Astronomical Society*, vol. 402, pp. 2344–2354, 2010. DOI: 10.1111/j.1365-2966.2009.16140.x. arXiv: 0907.4981 [astro-ph.CO].
- [140] E. Abdalla, L. R. Abramo and J. C. C. de Souza, ‘Signature of the interaction between dark energy and dark matter in observations’, *Physical Review*, vol. D82, p. 023508, 2010. DOI: 10.1103/PhysRevD.82.023508. arXiv: 0910.5236 [gr-qc].
- [141] L. Lopez Honorez, B. A. Reid, O. Mena *et al.*, ‘Coupled dark matter-dark energy in light of near universe observations’, *Journal of Cosmology and Astroparticle Physics*, vol. 1009, 029, p. 029, 2010. DOI: 10.1088/1475-7516/2010/09/029. arXiv: 1006.0877 [astro-ph.CO].
- [142] T. Clemson, K. Koyama, G.-B. Zhao *et al.*, ‘Interacting dark energy: Constraints and degeneracies’, *Physical Review*, vol. D85, p. 043007, 2012. DOI: 10.1103/PhysRevD.85.043007. arXiv: 1109.6234 [astro-ph.CO].
- [143] E. R. M. Tarrant, C. van de Bruck, E. J. Copeland and A. M. Green, ‘Coupled quintessence and the halo mass function’, *Physical Review*, vol. D85, 023503, p. 023503, 2012. DOI: 10.1103/PhysRevD.85.023503. arXiv: 1103.0694 [astro-ph.CO].
- [144] F. Marulli, M. Baldi and L. Moscardini, ‘Clustering and redshift-space distortions in interacting dark energy cosmologies’, *Monthly Notices of the Royal Astronomical Society*, vol. 420, pp. 2377–2386, 2012. DOI: 10.1111/j.1365-2966.2011.20199.x. arXiv: 1110.3045 [astro-ph.CO].
- [145] V. Salvatelli, A. Marchini, L. Lopez-Honorez and O. Mena, ‘New constraints on coupled dark energy from the Planck satellite experiment’, *Physical Review*, vol. D88, p. 023531, 2013. DOI: 10.1103/PhysRevD.88.023531. arXiv: 1304.7119 [astro-ph.CO].

- [146] W. Yang and L. Xu, ‘Testing coupled dark energy with large scale structure observation’, *Journal of Cosmology and Astroparticle Physics*, vol. 1408, p. 034, 2014. DOI: 10.1088/1475-7516/2014/08/034. arXiv: 1401.5177 [astro-ph.CO].
- [147] W. Yang and L. Xu, ‘Cosmological constraints on interacting dark energy with redshift-space distortion after Planck data’, *Physical Review*, vol. D89, p. 083517, 2014. DOI: 10.1103/PhysRevD.89.083517. arXiv: 1401.1286 [astro-ph.CO].
- [148] R. C. Nunes and E. M. Barboza, ‘Dark matter-dark energy interaction for a time-dependent EoS parameter’, *General Relativity and Gravitation*, vol. 46, p. 1820, 2014. DOI: 10.1007/s10714-014-1820-1. arXiv: 1404.1620 [astro-ph.CO].
- [149] V. Faraoni, J. B. Dent and E. N. Saridakis, ‘Covariantizing the interaction between dark energy and dark matter’, *Physical Review*, vol. D90, p. 063510, 2014. DOI: 10.1103/PhysRevD.90.063510. arXiv: 1405.7288 [gr-qc].
- [150] S. Pan and S. Chakraborty, ‘A cosmographic analysis of holographic dark energy models’, *International Journal of Modern Physics*, vol. D23, p. 1450092, 2014. DOI: 10.1142/S0218271814500928. arXiv: 1410.8281 [gr-qc].
- [151] K. Tzanni and J. Miritzis, ‘Coupled quintessence with double exponential potentials’, *Physical Review*, vol. D89, p. 103540, 2014. DOI: 10.1103/PhysRevD.89.103540, 10.1103/PhysRevD.89.129902. arXiv: 1403.6618 [gr-qc].
- [152] S. Pan, S. Bhattacharya and S. Chakraborty, ‘An analytic model for interacting dark energy and its observational constraints’, *Monthly Notices of the Royal Astronomical Society*, vol. 452, pp. 3038–3046, 2015. DOI: 10.1093/mnras/stv1495. arXiv: 1210.0396 [gr-qc].
- [153] N. Tamanini, ‘Phenomenological models of dark energy interacting with dark matter’, *Physical Review*, vol. D92, p. 043524, 2015. DOI: 10.1103/PhysRevD.92.043524. arXiv: 1504.07397 [gr-qc].
- [154] Y.-H. Li, J.-F. Zhang and X. Zhang, ‘Testing models of vacuum energy interacting with cold dark matter’, *Physical Review*, vol. D93, p. 023002, 2016. DOI: 10.1103/PhysRevD.93.023002. arXiv: 1506.06349 [astro-ph.CO].

- [155] R. Murgia, S. Gariazzo and N. Fornengo, ‘Constraints on the coupling between dark energy and dark matter from CMB data’, *Journal of Cosmology and Astroparticle Physics*, vol. 1604, p. 014, 2016. DOI: 10.1088/1475-7516/2016/04/014. arXiv: 1602.01765 [astro-ph.CO].
- [156] R. C. Nunes, S. Pan and E. N. Saridakis, ‘New constraints on interacting dark energy from cosmic chronometers’, *Physical Review*, vol. D94, p. 023508, 2016. DOI: 10.1103/PhysRevD.94.023508. arXiv: 1605.01712 [astro-ph.CO].
- [157] W. Yang, H. Li, Y. Wu and J. Lu, ‘Cosmological constraints on coupled dark energy’, *Journal of Cosmology and Astroparticle Physics*, vol. 1610, p. 007, 2016. DOI: 10.1088/1475-7516/2016/10/007. arXiv: 1608.07039 [astro-ph.CO].
- [158] S. Pan and G. S. Sharov, ‘A model with interaction of dark components and recent observational data’, *Monthly Notices of the Royal Astronomical Society*, vol. 472, pp. 4736–4749, 2017. DOI: 10.1093/mnras/stx2278. arXiv: 1609.02287 [gr-qc].
- [159] E. G. M. Ferreira, J. Quintin, A. A. Costa *et al.*, ‘Evidence for interacting dark energy from BOSS’, *Physical Review*, vol. D95, p. 043520, 2017. DOI: 10.1103/PhysRevD.95.043520. arXiv: 1412.2777 [astro-ph.CO].
- [160] G. S. Sharov, S. Bhattacharya, S. Pan *et al.*, ‘A new interacting two-fluid model and its consequences’, *Monthly Notices of the Royal Astronomical Society*, vol. 466, pp. 3497–3506, 2017. DOI: 10.1093/mnras/stw3358. arXiv: 1701.00780 [gr-qc].
- [161] R. An, C. Feng and B. Wang, ‘Constraints on the dark matter and dark energy interactions from weak lensing bispectrum tomography’, *Journal of Cosmology and Astroparticle Physics*, vol. 1710, p. 049, 2017. DOI: 10.1088/1475-7516/2017/10/049. arXiv: 1706.02845 [astro-ph.CO].
- [162] L. Santos, W. Zhao, E. G. M. Ferreira and J. Quintin, ‘Constraining interacting dark energy with CMB and BAO future surveys’, *Physical Review*, vol. D96, p. 103529, 2017. DOI: 10.1103/PhysRevD.96.103529. arXiv: 1707.06827 [astro-ph.CO].
- [163] J. Mifsud and C. Van De Bruck, ‘Probing the imprints of generalized interacting dark energy on the growth of perturbations’, *Journal of Cosmology and Astroparticle Physics*, vol. 1711, p. 001, 2017. DOI: 10.1088/1475-7516/2017/11/001. arXiv: 1707.07667 [astro-ph.CO].

- [164] S. Kumar and R. C. Nunes, ‘Observational constraints on dark matter–dark energy scattering cross section’, *The European Physical Journal*, vol. C77, p. 734, 2017. DOI: 10.1140/epjc/s10052-017-5334-3. arXiv: 1709.02384 [astro-ph.CO].
- [165] J.-J. Guo, J.-F. Zhang, Y.-H. Li *et al.*, ‘Probing the sign-changeable interaction between dark energy and dark matter with current observations’, *Science China Physics, Mechanics and Astronomy*, vol. 61, p. 030011, 2018. DOI: 10.1007/s11433-017-9131-9. arXiv: 1710.03068 [astro-ph.CO].
- [166] S. Pan, A. Mukherjee and N. Banerjee, ‘Astronomical bounds on a cosmological model allowing a general interaction in the dark sector’, *Monthly Notices of the Royal Astronomical Society*, vol. 477, pp. 1189–1205, 2018. DOI: 10.1093/mnras/sty755. arXiv: 1710.03725 [astro-ph.CO].
- [167] R. An, C. Feng and B. Wang, ‘Relieving the tension between weak lensing and cosmic microwave background with interacting dark matter and dark energy models’, *Journal of Cosmology and Astroparticle Physics*, vol. 1802, p. 038, 2018. DOI: 10.1088/1475-7516/2018/02/038. arXiv: 1711.06799 [astro-ph.CO].
- [168] A. A. Costa, R. C. G. Landim, B. Wang and E. Abdalla, ‘Interacting dark energy: Possible explanation for 21-cm absorption at cosmic dawn’, *The European Physical Journal*, vol. C78, p. 746, 2018. DOI: 10.1140/epjc/s10052-018-6237-7. arXiv: 1803.06944 [astro-ph.CO].
- [169] Y. Wang and G.-B. Zhao, ‘Constraining the dark matter–vacuum energy interaction using the EDGES 21-cm absorption signal’, *The Astrophysical Journal*, vol. 869, p. 26, 2018. DOI: 10.3847/1538-4357/aaeb9c. arXiv: 1805.11210 [astro-ph.CO].
- [170] R. von Marttens, L. Casarini, D. F. Mota and W. Zimdahl, ‘Cosmological constraints on parametrized interacting dark energy’, *Physics of the Dark Universe*, vol. 23, p. 100248, 2019. DOI: 10.1016/j.dark.2018.10.007. arXiv: 1807.11380 [astro-ph.CO].
- [171] W. Yang, N. Banerjee, A. Paliathanasis and S. Pan, ‘Reconstructing the dark matter and dark energy interaction scenarios from observations’, 2018. arXiv: 1812.06854 [astro-ph.CO].

- [172] A. A. Costa *et al.*, ‘J-PAS: forecasts on interacting dark energy from baryon acoustic oscillations and redshift-space distortions’, *Monthly Notices of the Royal Astronomical Society*, vol. 488, pp. 78–88, 2019. DOI: 10.1093/mnras/stz1675. arXiv: 1901.02540 [astro-ph.CO].
- [173] M. Martinelli, N. B. Hogg, S. Peirone *et al.*, ‘Constraints on the interacting vacuum–geodesic CDM scenario’, *Monthly Notices of the Royal Astronomical Society*, vol. 488, pp. 3423–3438, 2019. DOI: 10.1093/mnras/stz1915. arXiv: 1902.10694 [astro-ph.CO].
- [174] C. Li, X. Ren, M. Khurshudyan and Y.-F. Cai, ‘Implications of the possible 21-cm line excess at cosmic dawn on dynamics of interacting dark energy’, 2019. arXiv: 1904.02458 [astro-ph.CO].
- [175] W. Yang, S. Vagnozzi, E. Di Valentino *et al.*, ‘Listening to the sound of dark sector interactions with gravitational wave standard sirens’, *Journal of Cosmology and Astroparticle Physics*, vol. 1907, p. 037, 2019. DOI: 10.1088/1475-7516/2019/07/037. arXiv: 1905.08286 [astro-ph.CO].
- [176] R. R. A. Bacheaga, E. Abdalla and K. S. F. Fornazier, ‘Forecasting the interaction in dark matter-dark energy models with standard sirens from the Einstein Telescope’, 2019. arXiv: 1906.08909 [astro-ph.CO].
- [177] H.-L. Li, D.-Z. He, J.-F. Zhang and X. Zhang, ‘Quantifying the impacts of future gravitational-wave data on constraining interacting dark energy’, 2019. arXiv: 1908.03098 [astro-ph.CO].
- [178] E. Di Valentino, A. Melchiorri, O. Mena and S. Vagnozzi, ‘Interacting dark energy after the latest Planck, DES, and  $H_0$  measurements: An excellent solution to the  $H_0$  and cosmic shear tensions’, 2019. arXiv: 1908.04281 [astro-ph.CO].
- [179] B. Wang, E. Abdalla, F. Atrio-Barandela and D. Pavon, ‘Dark matter and dark energy interactions: Theoretical challenges, cosmological implications and observational signatures’, *Reports on Progress in Physics*, vol. 79, p. 096 901, 2016. DOI: 10.1088/0034-4885/79/9/096901. arXiv: 1603.08299 [astro-ph.CO].
- [180] C. Wetterich, ‘The cosmon model for an asymptotically vanishing time-dependent cosmological “constant”’, *Astronomy & Astrophysics*, vol. 301, pp. 321–328, 1995. arXiv: hep-th/9408025 [hep-th].

- [181] L. Amendola, ‘Scaling solutions in general nonminimal coupling theories’, *Physical Review*, vol. D60, p. 043 501, 1999. DOI: 10 . 1103 / PhysRevD . 60 . 043501. arXiv: astro-ph/9904120 [astro-ph].
- [182] L. Amendola, ‘Coupled quintessence’, *Physical Review*, vol. D62, p. 043 511, 2000. DOI: 10 . 1103 / PhysRevD . 62 . 043511. arXiv: astro - ph / 9908023 [astro-ph].
- [183] D.-J. Liu and X.-Z. Li, ‘Dynamics of quintessence with thermal interactions’, *Physics Letters*, vol. B611, pp. 8–14, 2005. DOI: 10.1016/j.physletb.2005.02.048. arXiv: astro-ph/0501596 [astro-ph].
- [184] L. Lopez Honorez, O. Mena and G. Panotopoulos, ‘Higher-order coupled quintessence’, *Physical Review*, vol. D82, 123525, p. 123 525, 2010. DOI: 10 . 1103 / PhysRevD . 82 . 123525. arXiv: 1009.5263 [astro-ph.CO].
- [185] A. P. Billyard and A. A. Coley, ‘Interactions in scalar field cosmology’, *Physical Review*, vol. D61, p. 083 503, 2000. DOI: 10 . 1103 / PhysRevD . 61 . 083503. arXiv: astro-ph/9908224 [astro-ph].
- [186] J. P. Mimoso, A. Nunes and D. Pavon, ‘Asymptotic behavior of the warm inflation scenario with viscous pressure’, *Physical Review*, vol. D73, p. 023 502, 2006. DOI: 10 . 1103 / PhysRevD . 73 . 023502. arXiv: gr-qc/0512057 [gr-qc].
- [187] X.-m. Chen and Y. Gong, ‘Fixed points in interacting dark energy models’, *Physics Letters*, vol. B675, pp. 9–13, 2009. DOI: 10.1016/j.physletb.2009.03.064. arXiv: 0811.1698 [gr-qc].
- [188] C. Skordis, A. Pourtsidou and E. J. Copeland, ‘Parametrized post-Friedmannian framework for interacting dark energy theories’, *Physical Review*, vol. D91, p. 083 537, 2015. DOI: 10 . 1103 / PhysRevD . 91 . 083537. arXiv: 1502.07297 [astro-ph.CO].
- [189] W. Hu and I. Sawicki, ‘A parameterized post-Friedmann framework for modified gravity’, *Physical Review*, vol. D76, p. 104 043, 2007. DOI: 10 . 1103 / PhysRevD . 76 . 104043. arXiv: 0708.1190 [astro-ph].
- [190] C. Skordis, ‘Consistent cosmological modifications to the Einstein equations’, *Physical Review*, vol. D79, p. 123 527, 2009. DOI: 10 . 1103 / PhysRevD . 79 . 123527. arXiv: 0806.1238 [astro-ph].

- [191] T. Baker, P. G. Ferreira, C. Skordis and J. Zuntz, ‘Towards a fully consistent parameterization of modified gravity’, *Physical Review*, vol. D84, p. 124018, 2011. DOI: 10.1103/PhysRevD.84.124018. arXiv: 1107.0491 [astro-ph.CO].
- [192] T. Baker, P. G. Ferreira and C. Skordis, ‘The parameterized post-Friedmann framework for theories of modified gravity: Concepts, formalism and examples’, *Physical Review*, vol. D87, p. 024015, 2013. DOI: 10.1103/PhysRevD.87.024015. arXiv: 1209.2117 [astro-ph.CO].
- [193] F. Simpson, ‘Scattering of dark matter and dark energy’, *Physical Review*, vol. D82, p. 083505, 2010. DOI: 10.1103/PhysRevD.82.083505. arXiv: 1007.1034 [astro-ph.CO].
- [194] N. Afshordi, M. Zaldarriaga and K. Kohri, ‘On the stability of dark energy with mass-varying neutrinos’, *Physical Review*, vol. D72, p. 065024, 2005. DOI: 10.1103/PhysRevD.72.065024. arXiv: astro-ph/0506663 [astro-ph].
- [195] D. B. Kaplan, A. E. Nelson and N. Weiner, ‘Neutrino oscillations as a probe of dark energy’, *Physical Review Letters*, vol. 93, p. 091801, 2004. DOI: 10.1103/PhysRevLett.93.091801. arXiv: hep-ph/0401099 [hep-ph].
- [196] X.-J. Bi, B. Feng, H. Li and X. Zhang, ‘Cosmological evolution of interacting dark energy models with mass varying neutrinos’, *Physical Review*, vol. D72, p. 123523, 2005. DOI: 10.1103/PhysRevD.72.123523. arXiv: hep-ph/0412002 [hep-ph].
- [197] A. W. Brookfield, C. van de Bruck, D. F. Mota and D. Tocchini-Valentini, ‘Cosmology of mass-varying neutrinos driven by quintessence: Theory and observations’, *Physical Review*, vol. D73, p. 083515, 2006. DOI: 10.1103/PhysRevD.73.083515. arXiv: astro-ph/0512367 [astro-ph].
- [198] C. Spitzer, ‘Stability in MaVaN Models’, 2006. arXiv: astro-ph/0606034 [astro-ph].
- [199] R. Takahashi and M. Tanimoto, ‘Speed of sound in the mass varying neutrinos scenario’, *Journal of High Energy Physics*, vol. 2006, pp. 021–021, 2006. DOI: 10.1088/1126-6708/2006/05/021. arXiv: astro-ph/0601119 [astro-ph].

- [200] G. La Vacca and D. F. Mota, ‘Mass-varying neutrino in light of cosmic microwave background and weak lensing’, *Astronomy & Astrophysics*, vol. 560, A53, A53, 2013. DOI: 10.1051/0004-6361/201220971. arXiv: 1205.6059 [astro-ph.CO].
- [201] P. Adamson *et al.*, ‘Measurement of the neutrino mass splitting and flavor mixing by MINOS’, *Physical Review Letters*, vol. 106, p. 181801, 2011. DOI: 10.1103/PhysRevLett.106.181801. arXiv: 1103.0340 [hep-ex].
- [202] D. F. Mota, V. Pettorino, G. Robbers and C. Wetterich, ‘Neutrino clustering in growing neutrino quintessence’, *Physics Letters*, vol. B663, pp. 160–164, 2008. DOI: 10.1016/j.physletb.2008.03.060. arXiv: 0802.1515 [astro-ph].
- [203] N. Wintergerst, V. Pettorino, D. F. Mota and C. Wetterich, ‘Very large scale structures in growing neutrino quintessence’, *Physical Review*, vol. D81, p. 063525, 2010. DOI: 10.1103/PhysRevD.81.063525. arXiv: 0910.4985 [astro-ph.CO].
- [204] N. Wintergerst and V. Pettorino, ‘Clarifying spherical collapse in coupled dark energy cosmologies’, *Physical Review*, vol. D82, p. 103516, 2010. DOI: 10.1103/PhysRevD.82.103516. arXiv: 1005.1278 [astro-ph.CO].
- [205] V. Pettorino, N. Wintergerst, L. Amendola and C. Wetterich, ‘Neutrino lumps and the cosmic microwave background’, *Physical Review*, vol. D82, p. 123001, 2010. DOI: 10.1103/PhysRevD.82.123001. arXiv: 1009.2461 [astro-ph.CO].
- [206] N. J. Nunes, L. Schrempp and C. Wetterich, ‘Mass freezing in growing neutrino quintessence’, *Physical Review*, vol. D83, p. 083523, 2011. DOI: 10.1103/PhysRevD.83.083523. arXiv: 1102.1664 [astro-ph.CO].
- [207] N. Brouzakis, V. Pettorino, N. Tetradis and C. Wetterich, ‘Nonlinear matter spectra in growing neutrino quintessence’, *Journal of Cosmology and Astroparticle Physics*, vol. 1103, pp. 049–049, 2011. DOI: 10.1088/1475-7516/2011/03/049. arXiv: 1012.5255 [astro-ph.CO].
- [208] M. Baldi, V. Pettorino, L. Amendola and C. Wetterich, ‘Oscillating non-linear large-scale structures in growing neutrino quintessence’, *Monthly Notices of the Royal Astronomical Society*, vol. 418, pp. 214–229, 2011. DOI: 10.1111/j.1365-2966.2011.19477.x. arXiv: 1106.2161.

- [209] Y. Ayaita, M. Weber and C. Wetterich, ‘Structure formation and backreaction in growing neutrino quintessence’, *Physical Review*, vol. D85, p. 123 010, 2012. DOI: 10.1103/PhysRevD.85.123010. arXiv: 1112.4762 [astro-ph.CO].
- [210] Y. Ayaita, M. Weber and C. Wetterich, ‘Neutrino lump fluid in growing neutrino quintessence’, *Physical Review*, vol. D87, p. 043 519, 2013. DOI: 10.1103/PhysRevD.87.043519. arXiv: 1211.6589 [astro-ph.CO].
- [211] F. Fühner and C. Wetterich, ‘Backreaction in growing neutrino quintessence’, *Physical Review*, vol. D91, p. 123 542, 2015. DOI: 10.1103/PhysRevD.91.123542. arXiv: 1503.07995 [astro-ph.CO].
- [212] Y. Ayaita, M. Baldi, F. Fühner *et al.*, ‘Nonlinear growing neutrino cosmology’, *Physical Review*, vol. D93, p. 063 511, 2016. DOI: 10.1103/PhysRevD.93.063511. arXiv: 1407.8414 [astro-ph.CO].
- [213] S. Casas, V. Pettorino and C. Wetterich, ‘Dynamics of neutrino lumps in growing neutrino quintessence’, *Physical Review*, vol. D94, p. 103 518, 2016. DOI: 10.1103/PhysRevD.94.103518. arXiv: 1608.02358 [astro-ph.CO].
- [214] J. Lesgourgues and S. Pastor, ‘Massive neutrinos and cosmology’, *Physics Reports*, vol. 429, pp. 307–379, 2006. DOI: 10.1016/j.physrep.2006.04.001. arXiv: astro-ph/0603494 [astro-ph].
- [215] C. Wetterich, ‘Can structure formation influence the cosmological evolution?’, *Physical Review*, vol. D67, p. 043 513, 2003. DOI: 10.1103/PhysRevD.67.043513. arXiv: astro-ph/0111166 [astro-ph].
- [216] C. Wetterich, ‘Inflation, quintessence, and the origin of mass’, *Nuclear Physics*, vol. B897, pp. 111–178, 2015. DOI: 10.1016/j.nuclphysb.2015.05.019. arXiv: 1408.0156 [hep-th].
- [217] A. Barreira, P. Brax, S. Clesse *et al.*, ‘Linear perturbations in K-mouflage cosmologies with massive neutrinos’, *Physical Review*, vol. D91, 063528, p. 063 528, 2015. DOI: 10.1103/PhysRevD.91.063528. arXiv: 1411.5965.
- [218] A. Lewis, A. Challinor and A. Lasenby, ‘Efficient computation of CMB anisotropies in closed FRW models’, *The Astrophysical Journal*, vol. 538, pp. 473–476, 2000. DOI: 10.1086/309179. arXiv: astro-ph/9911177 [astro-ph].
- [219] B. Li, *Private communication*.

- [220] P. A. R. Ade *et al.*, ‘Planck 2015 results. XIII. Cosmological parameters’, *Astronomy & Astrophysics*, vol. 594, A13, 2016. DOI: 10.1051/0004-6361/201525830. arXiv: 1502.01589 [astro-ph.CO].
- [221] P. A. R. Ade *et al.*, ‘Planck 2013 results. XVII. Gravitational lensing by large-scale structure’, *Astronomy & Astrophysics*, vol. 571, A17, 2014. DOI: 10.1051/0004-6361/201321543. arXiv: 1303.5077 [astro-ph.CO].
- [222] L. Anderson *et al.*, ‘The clustering of galaxies in the SDSS-III Baryon Oscillation Spectroscopic Survey: Baryon acoustic oscillations in the Data Releases 10 and 11 galaxy samples’, *Monthly Notices of the Royal Astronomical Society*, vol. 441, pp. 24–62, 2014. DOI: 10.1093/mnras/stu523. arXiv: 1312.4877 [astro-ph.CO].
- [223] M. Betoule *et al.*, ‘Improved cosmological constraints from a joint analysis of the SDSS-II and SNLS supernova samples’, *Astronomy & Astrophysics*, vol. 568, A22, 2014. DOI: 10.1051/0004-6361/201423413. arXiv: 1401.4064 [astro-ph.CO].
- [224] P. A. R. Ade *et al.*, ‘Planck 2015 results. XXIV. Cosmology from Sunyaev–Zeldovich cluster counts’, *Astronomy & Astrophysics*, vol. 594, A24, 2016. DOI: 10.1051/0004-6361/201525833. arXiv: 1502.01597 [astro-ph.CO].
- [225] M. S. Linton, A. Poursidou, R. Crittenden and R. Maartens, ‘Variable sound speed in interacting dark energy models’, *Journal of Cosmology and Astroparticle Physics*, vol. 1804, p. 043, 2018. DOI: 10.1088/1475-7516/2018/04/043. arXiv: 1711.05196 [astro-ph.CO].
- [226] E. Bertschinger, ‘COSMICS: Cosmological initial conditions and microwave anisotropy codes’, 1995. arXiv: astro-ph/9506070 [astro-ph].
- [227] U. Seljak and M. Zaldarriaga, ‘A line of sight integration approach to cosmic microwave background anisotropies’, *The Astrophysical Journal*, vol. 469, pp. 437–444, 1996. DOI: 10.1086/177793. arXiv: astro-ph/9603033 [astro-ph].
- [228] M. Doran, ‘CMBEASY: An object oriented code for the cosmic microwave background’, *Journal of Cosmology and Astroparticle Physics*, vol. 0510, p. 011, 2005. DOI: 10.1088/1475-7516/2005/10/011. arXiv: astro-ph/0302138 [astro-ph].

- [229] J. Lesgourgues, ‘The Cosmic Linear Anisotropy Solving System (CLASS) I: Overview’, 2011. arXiv: 1104.2932 [astro-ph.IM].
- [230] D. Blas, J. Lesgourgues and T. Tram, ‘The Cosmic Linear Anisotropy Solving System (CLASS). Part II: Approximation schemes’, *Journal of Cosmology and Astroparticle Physics*, vol. 1107, 034, p. 034, 2011. DOI: 10.1088/1475-7516/2011/07/034. arXiv: 1104.2933.
- [231] J. Lesgourgues, ‘The Cosmic Linear Anisotropy Solving System (CLASS) III: Comparison with CAMB for LambdaCDM’, 2011. arXiv: 1104.2934.
- [232] J. Lesgourgues and T. Tram, ‘The Cosmic Linear Anisotropy Solving System (CLASS) IV: Efficient implementation of non-cold relics’, *Journal of Cosmology and Astroparticle Physics*, vol. 1109, 032, p. 032, 2011. DOI: 10.1088/1475-7516/2011/09/032. arXiv: 1104.2935.
- [233] S. Seager, D. D. Sasselov and D. Scott, ‘A new calculation of the recombination epoch’, *The Astrophysical Journal*, vol. 523, pp. L1–L5, 1999. DOI: 10.1086/312250. arXiv: astro-ph/9909275 [astro-ph].
- [234] J.-Q. Xia, Y.-F. Cai, T.-T. Qiu *et al.*, ‘Constraints on the sound speed of dynamical dark energy’, *International Journal of Modern Physics*, vol. D17, pp. 1229–1243, 2008. DOI: 10.1142/S0218271808012784. arXiv: astro-ph/0703202 [astro-ph].
- [235] G. Ballesteros and J. Lesgourgues, ‘Dark energy with non-adiabatic sound speed: Initial conditions and detectability’, *Journal of Cosmology and Astroparticle Physics*, vol. 1010, p. 014, 2010. DOI: 10.1088/1475-7516/2010/10/014. arXiv: 1004.5509 [astro-ph.CO].
- [236] R. de Putter, D. Huterer and E. V. Linder, ‘Measuring the speed of dark: Detecting dark energy perturbations’, *Physical Review*, vol. D81, 103513, p. 103 513, 2010. DOI: 10.1103/PhysRevD.81.103513. arXiv: 1002.1311 [astro-ph.CO].
- [237] T. Basse, O. Eggers Bjaelde, S. Hannestad and Y. Y. Y. Wong, ‘Confronting the sound speed of dark energy with future cluster surveys’, 2012. arXiv: 1205.0548 [astro-ph.CO].

- [238] S. Dutta, E. N. Saridakis and R. J. Scherrer, ‘Dark energy from a quintessence (phantom) field rolling near a potential minimum (maximum)’, *Physical Review*, vol. D79, p. 103 005, 2009. DOI: 10.1103/PhysRevD.79.103005. arXiv: 0903.3412 [astro-ph.CO].
- [239] F. Simpson, R. Jimenez, C. Pena-Garay and L. Verde, ‘Dark energy from the motions of neutrinos’, *Physics of the Dark Universe*, vol. 20, pp. 72–77, 2018. DOI: 10.1016/j.dark.2018.04.002. arXiv: 1607.02515 [astro-ph.CO].